CONTROLLED RELEASE OF ANTIBACTERIAL COMPOUNDS BASED ON MULTIPARAMETRIC ANALYSIS OF MESOPOROUS SILICON CARRIERS

by

MENGJIA WANG

Bachelor of Science, 2004
Beijing University of Agriculture
Beijing, China

Submitted to the Graduate Faculty of
College of Science and Engineering
Texas Christian University
in partial fulfillment of the requirements
for the degree of

Doctor of Philosophy

August, 2012

ACKNOWLEDGEMENTS

I would like to express my deep and sincere gratitude to my advisor and mentor, Dr. Jeffery L. Coffer. I thank him for his inspiration, guidance, encouragements, and great effort throughout my graduate study. I would also like to thank the members of the Coffer research group for their help, discussions, and suggestions in our lab. I express sincere gratitude to Dr. Philip S. Hartman of the Department of Biology for all of his training in bacteria culture techniques and antibacterial assays. I thank Dr. Onofrio Annunziata for providing the UV/Vis Spectrophometer and training for my research. I am grateful to Dr. Leigh T. Canham and Dr. Armando Loni from Inrinsiq™ Materials. Ltd. for the kind provision of mesoporous silicon powder.

Financial support by the Robert A. Welch Foundation is gratefully acknowledged.

TABLE OF CONTENTS

LIST OF FIGURES

LIST OF TABLES

I. Introduction

1.1 The Challenge of Drug Development

1.1.1 Drug Discovery in Modern Pharmaceutical Industry

Drug discovery is complex, time consuming, and expensive. Bringing a new drug from idea to market can be roughly broken down into two phases: 1) discovery and identification; 2) optimization and final selection.[1] Each of these two phases has many parts. In the early stages, many new molecules are synthesized and screened against the identified biological target, with subsequent narrowing of this library to a few promising compounds. Variants of these selected molecules are then synthesized, optimized, and screened further for best activity. An even smaller number of molecules are then identified for testing in pharmacological models *in vitro* and *in vivo*. In the end, only one or two drug candidates are chosen for further development. The drug discovery and development path, originally illustrated by Han *et al.*, is shown in Figure 1.[1]

In spite of this rigorous process, only ten percent of all compounds tested in humans end up as commercial products. An analysis of common failures is instructive (Figure 2). The reasons are diverse: unsuitable pharmacokinetics, 39%; lack of clinical efficacy, 30%; toxicity, 21% and commercial limitations, 5%. [1-3]

Since most failure is not presumably due to a lack of "biological activities", it is necessary to evaluate other major factors mentioned above that may potentially lead to developmental failures in drug candidate selection.

1.1.2 Main Factors Leading to Failures of Drug Selection

Moving beyond the identification of compounds with the desired biological activity, the major and interrelated factors in candidate selection may include certain

physicochemical properties of drugs such as molecular weight / size, solubility, stability, polarity, acid-base properties, etc.[1] However, the main challenge is to overcome the low solubility of drugs.[4, 5]

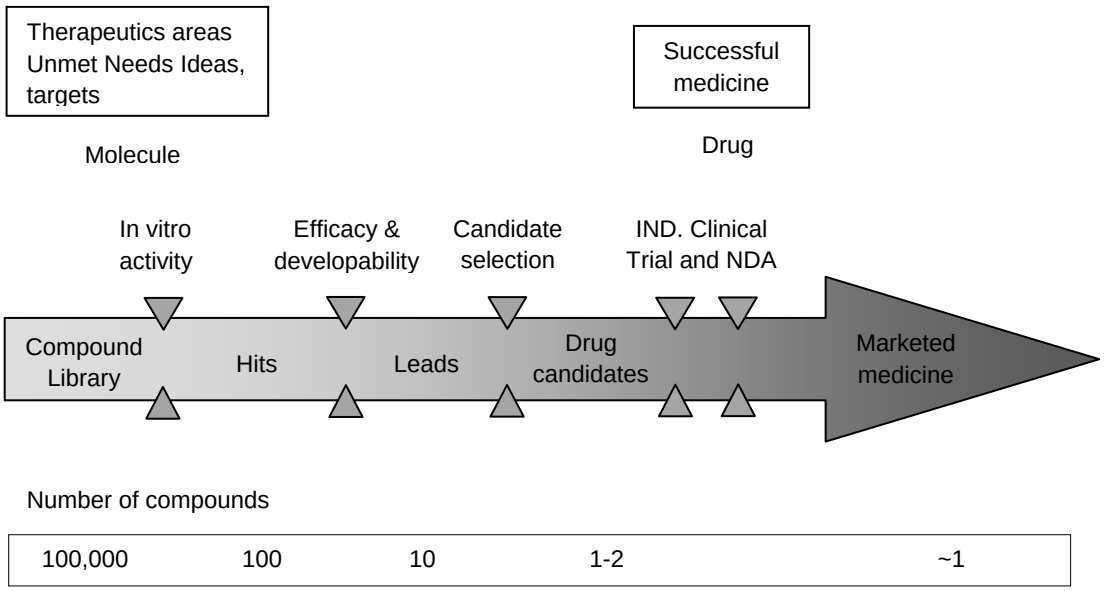

Figure 1. A schematic illustration of the drug discovery and development process with the estimated number of compounds shown for each step.[1]

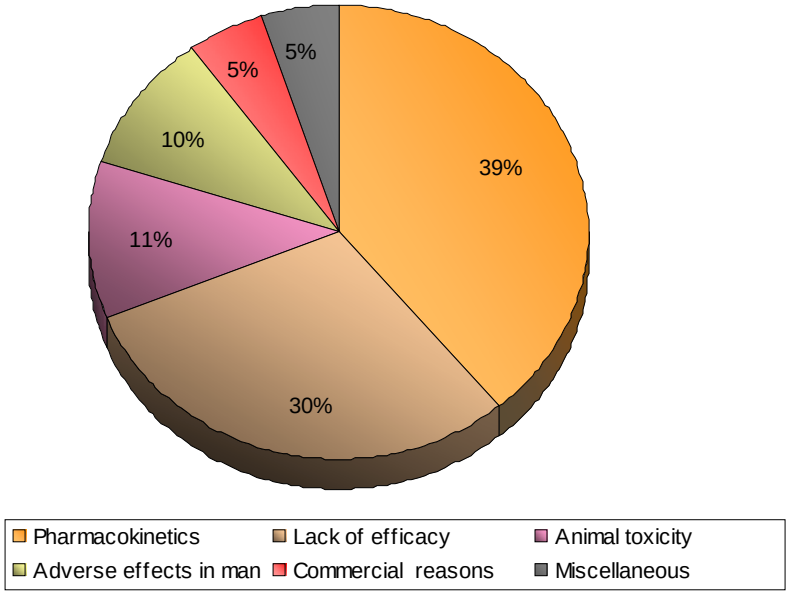

Figure 2. Major Factors for Project Failure in the Clinic.[3]

As mentioned earlier in the analysis of failures, 30% of drug candidates have poor pharmacokinetics due to poor solubility. Therefore, it is important to enhance solubility and keep drugs stable until they reach the site of action. In fact, drugs prefer the solid-state form, which are more stable and more convenient to administer compared to liquid formulations. However, such solids must dissolve before they can be absorbed by the human body. In many cases, the solubility of the drug cannot reach the required concentration at a given active site, and the drug loses its effectiveness.[1, 6]

Several methods to improve the solubility of drug molecules have been demonstrated. For example, reducing the particle size or amorphization to decrease the crystallinity degree of a drug are both helpful. Amorphous solids can enhance the solubility to 2–4 times higher than the crystalline forms.[7] However, some drugs with the amorphous state are less stable than the crystalline forms.[8]

Extensive research[5, 9] on solubility and stability has been done in order to reveal the role of aqueous solubility of drug in the process of drug absorption, and eventually, to enhance the bioavailability of drugs.

If one considers conventional drugs as “free”, that is without the use of a carrier, many of the pharmacological properties of “free” drugs can be improved through the use of drug delivery systems.[10]

The use of drug delivery systems is not only useful for absorption of drugs having very low solubility in water and / or stabilization of an amorphous drug, but also provides other benefits; for instance, reduced side effects, sustained and targeted release etc., which will be detailed in the following section.

1.2 Drug Delivery Systems (DDS) and Nanotechnology

Drug delivery has become the key issue in the development of a drug candidate. This method can be used to deliver drugs with a significant effect on its efficacy.

Drug delivery systems can overcome some limitations of drugs (short half-life, poor solubility, and stability), optimize therapeutic activity, and decrease toxicity.[10] Some drugs achieve their full therapeutic effect only within a certain range of concentration. Beyond this range, the drugs may be toxic or lose therapeutic effect. On the other hand, for some severe diseases, a sustained release of a drug with some requirement, such as a specific rate, is needed. As a result, drug delivery systems have been developed. They provide new strategies on controlling the pharmacodynamics (the biochemical and physiological effects of drugs and the mechanisms of their actions), pharmacokinetics, non-specific toxicity, biorecognition, immunogenicity (the property enabling a substance to provoke an immune response, or the degree to which a substance possesses this property), and efficacy.[11] Allen *et al.* have identified the following problems for free drugs that can be improved by the use of DDS:[10]

- Poor solubility;
- Tissue damage on extravasation
- Rapid break down of the drug *in vivo*
- Unfavorable pharmacokinetics
- Poor biodistribution
- Lack of selectivity for target tissue

Various drug delivery systems are currently under development. Soluble polymers,[12] microparticles made of insoluble or biodegradable natural and synthetic

polymers,[13, 14] microcapsules,[15] liposomes,[16] and micelles[17] are commonly used materials for drug carriers. The carriers can be made slowly degradable,[14] stimuli-reactive (e.g., pH- or temperature-sensitive),[18] and even targeted.[19] Some of these materials are structured at the microscale and, more recently, in nanoscale form. Drug delivery at the nanoscale, with potential applications in the areas of cancer,[20, 21] infectious disease,[22, 23] and a broad range of genetic disorders[24, 25] have been intensively investigated.

1.2.1 Introduction of Nanotechnology

Nanotechnology has become a popular term, by which it is possible to fabricate materials, devices, or systems at the nanoscale or molecular level. As defined by the National Nanotechnology Initiative (NNI), the strictest definition of nanotechnology is the study of materials where at least one dimension of the structure is in the range of 1-100 nm.[26]

Nanotechnology is not unique to one specific area. It represents a very wide range of subjects, from basic materials science to a variety of applications, including "nanomedicine". "Nanomedicine" is the use of nanotechnology to the areas of diagnosis and disease treatment.[27] Drug delivery nanosystems are one of the most important parts of nanomedicine. In practice, nanomedicine is not only limited to the nanoscale, but also includes micro-scale systems. Thus, nanotechnology also includes aspects of microtechnology as well.[28]

1.2.2 Materials for Drug Delivery Nanovehicles

To date, a variety of organic / inorganic nanomaterials and devices have been employed as delivery carriers. So far, over two dozen nanotechnology-based therapeutic

products have been approved by Food and Drug Administration (FDA) for clinical use, and more are in clinical trials.[29] Figure 3 highlights some nanoscale delivery systems which serve as important milestones throughout the development history of drug delivery.[30] The following parts will give a brief explanation of some typical drug delivery carriers.

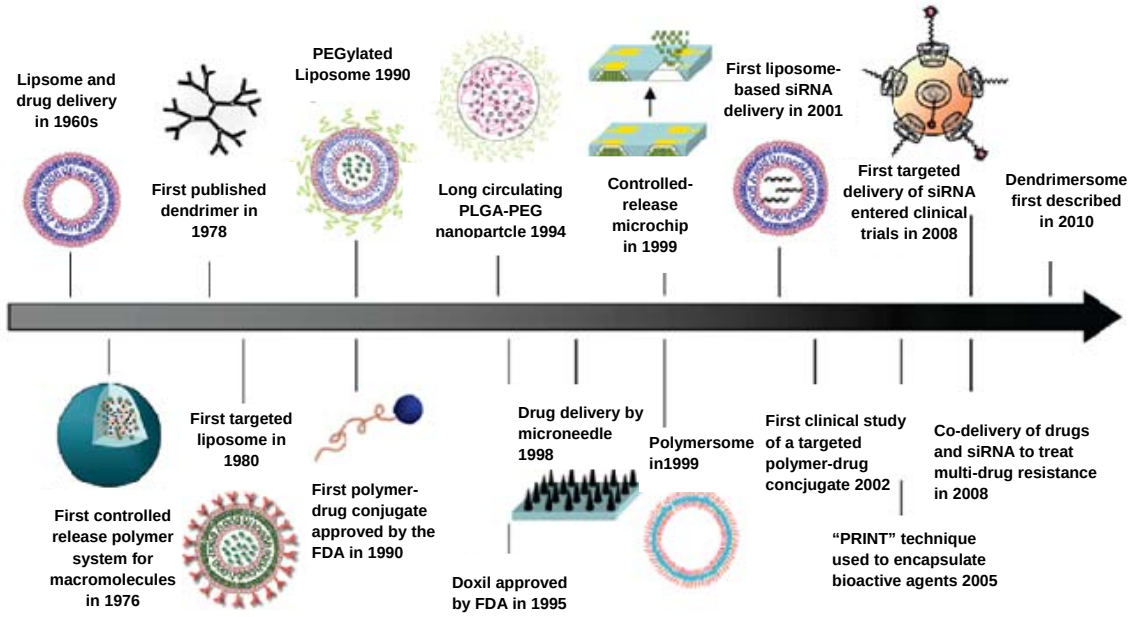

Figure 3. Timeline of nanotechnology-based drug delivery development.[30]

1.2.2.1 Polymer and Lipid based Drug Delivery System

Polymer and lipid employed drug delivery systems including polymer-drug or protein conjugates, liposomes, micelles, dendrimers, nano / micro polymeric particles, etc.[31, 32] have drawn a lot of attention in drug development. Liposomes are spherical lipid vesicles with a bilayered membrane structure composed of natural or synthetic amphiphilic lipid molecules, which were first described by Bangham in 1961 (his work was published in 1964).[31, 33, 34] The unique characteristics of a liposome are its capability

to encapsulate both hydrophilic and hydrophobic therapeutic agents with high efficiency, and to achieve easily any desired formulation with different sizes, surface charges or composition.[31, 34] Delivery of Doxil is a typical application of liposomes, approved by the FDA for the treatment of AIDS associated with Kaposi's sarcoma in 1995.[35]

First prepared in the 1960's, a micelle is an aggregate of amphiphilic molecules in water. There are two portions in a micelle: the inside is nonpolar, and the outside is polar. With this structure, hydrophobic drugs are allowed to be encapsulated in the inner core, and at the same time the outer hydrophilic layer stabilizes hydrophobic core and the external aqueous environment. Compared to classic surfactant micelles with microscale sizes, polymeric micelles fall into the nanosize range of 10-100 nm.[36] Polymeric micelles are formed by block copolymers which consist of two or more polymer chains with different hydrophobicities. These copolymers spontaneously assemble into a core–shell micellar structure, which is called "core-shell nanoparticles". Due to its nanoscale size, the structure of polymeric micelles offers some unique characteristics, compared with surfactant micelles, such as better stability, slower dissociation rate, narrower drug distribution and longer drug retaining time.[31, 36, 37]

Dendrimers have become one of the most rapidly expanding areas of drug delivery systems. Since their first synthesis by Vögtle in 1978, dendrimers have drawn explosive attention and been studied around the world.[38] A typical dendrimer consists of an initiator core and multiple layers with active terminal groups symmetrically surrounding the core-like branches.[31] The unique structure of a dendrimer makes it a versatile polymer because: 1) the internal cavities between branches can isolate a drug from its surroundings; 2) one dendrimer molecule has hundreds of possible sites to

couple with active species. Various functional agents, such as detecting agents or targeting components, can couple with the specific terminal groups of the outer surface,[31, 38, 39] as shown in Figure 4. Recently, researchers have developed a fifth generation polyamidoamine dendrimer (G5-PAMAM), the diameter of which is about 5 nm. There are more than 100 functional primary amines on the surface of this dendrimer. By attaching folate as the targeting molecule and methotrexate as the therapeutic agent, the G5 dendrimer was about 10 times more effective than methotrexate alone in inhibiting tumor growth.[40]

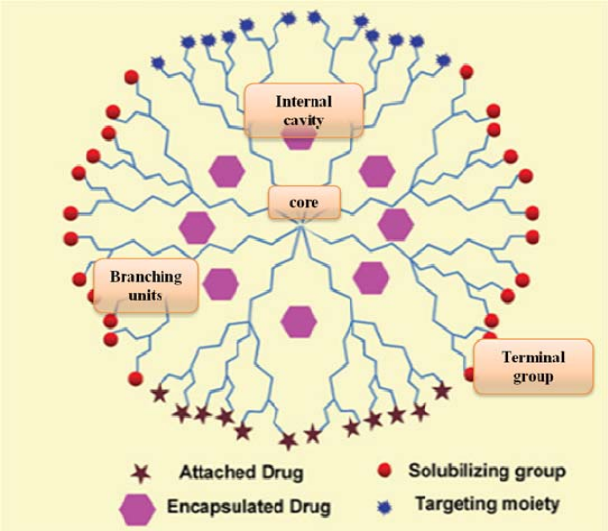

Figure 4. Possible sites for covalent attachment of drugs, encapsulation of drugs, and targeting moieties.

1.2.2.2 Inorganic Drug Delivery Systems

As mentioned above, organic systems like liposomes, micelles, dendrimers, and polymeric conjugates have made significant contributions to drug delivery. However, these organic systems have limitations, including poor thermal and chemical stability and rapid elimination by the immune system of the human body.[41] In contrast, inorganic

systems offer a biocompatible and stable alternative. Inorganic bioceramic materials especially provide an invaluable option in applications such as bone-like scaffolds.

Inorganic materials involved in drug delivery systems can be classified into two categories: 1) metallic nanoparticles, such as iron oxide, gold, and silver; and 2) bioceramic nanoparticles, such as silica, titania, alumina, carbon, zirconia, and calcium phosphate-based materials.

As a typical magnetic mateiral, iron oxide nanoparticles are very suitable for drug delivery materials. Iron oxide nanoparticles, which have been used as magnetic resonance imaging (MRI), drug-targeting or hyperthermia agents through intravenous or extravenous injection, offer a wide range of diagnosis and therapeutic options.[31, 42, 43] Magnetic hyperthermia is a cancer treatment modality, like radiotherapy and chemotherapy, which is based on the fact that magnetic materials produce heat when subjected to an alternating magnetic field. The ferromagnetic resonance of iron's unpaired electrons is a physical mechanism that can produce heat. When the temperature increases to the range of 39 °C to 42 °C, the heat can kill the tumor.[44] As an application of this method, Zhao and his colleagues injected a tiny amount (around 0.5 mL) of magnetic iron oxide nanoparticle solution directly into the tumor site of a mouse xenograft model of human HNSCC (head and neck squamous cell carcinoma). Under an alternating magnetic field, the temperature of the tumor center was rapidly elevated from around the room temperature to about 40 °C in the first 5-10 minutes, causing hyperthermia-mediated cell death.[45]

As another important inorganic material, colloidal gold particles were first prepared by Michael Faraday more than 150 years ago. However, colloidal gold particles

have never been associated with the term "nano" until about three decades ago.[28] Gold nanoparticles possess unique optical, electronic and chemical properties, which allow ligands and other moieties that contain functional groups (e.g., thiols, phosphines, amines, etc.) to be readily anchored on their surfaces.[1, 46] These moieties, including proteins and antibodies, therefore can serve as linking agents for further binding of biomolecules and targeting.

Bioceramics have gained acceptance in many therapeutic areas including ear implants, eye implants, and spinal fusion. Ceramic materials normally possess characteristics of biocompatibility, high hardness, and resorbability.[47] These properties satisfy the requirements for bone substitutes by temporarily supporting the bone defect region, conducting tissue regeneration in three dimensions, and eliminating the need for a second operation for implants' removal. At the same time, the porous structure of ceramic materials such as calcium phosphates are able to load drugs, hormones, growth factors, peptides and nucleic acids in their pores, and subsequently release them in a controlled fashion. In particular, since the introduction and the presence of an implant device within the body are known to increase the risk of infections, these devices made of ceramic materials with mesoporous structure are compatible with antibiotics, thereby preventing the formation of bacterial biofilms.[48,49] So far, many types of ceramic materials have been employed in these applications, e.g., hydroxyapatite (HA),[50] calcium phosphates,[51] and mesoporous silica.[52] Additionally, the low cost and ease of manufacture make ceramic materials a good candidate for drug delivery applications.[49]

1.3 Mesoporous Silicon (PSi): Introduction

As addressed before, although a wide variety of organic and inorganic porous carriers are available, inorganic drug carriers possess high stability, a major advantage over polymeric ones. The applications of siliceous materials (silica related) in drug delivery have been intensively studied, especially for ordered mesoporous silica.[53] Compared with mesoporous silica, mesoporous silicon can degrade completely in aqueous solutions into silicic acid, which is a major form of bio-available silicon in human body.[54] Thus, biodegradability and non-toxicity are main advantages of mesoporous silicon. In my research, mesoporous silicon (PSi) and its relevance to drug delivery have been investigated.

Porous silicon (PSi) was discovered by Arthur and Ingeborg Uhlir at Bell Laboratories accidentally in 1956.[55] In their study, they observed black, brown or red silicon surfaces, presumably with fine pores, while trying to electropolish crystalline silicon in a solution of hydrofluoric acid (HF) under certain applied current values. However, they did not pay much attention to the possible porous structure until Watanabe and his colleagues first reported its porous nature in 1971.[56, 57] Later in the 1990s, Canham discovered that Si wafers subjected to electrochemically and chemically combined dissolution could emit visible photoluminescence at room temperature.[58] From then on, PSi has been widely studied mainly for its optical properties. In his additional studies, Canham reported the behavior of PSi in simulated body fluid (SBF) in 1995, which showed that PSi possessed resorbability and biocompatibility, in contrast to bulk Si.[59] Since then, extensive research by the scientific community has explored the potential biotechnological applications of PSi. PSi has been extensively studied, with a

particular kind of nanostructured silicon (BioSilicon^{TM}), patented by the company pSiVida, mainly for drug delivery applications,.[60]

1.3.1 Fabrication of Porous Silicon

1.3.1.1 Anodization — Electrochemical Etching

The initial discovery of PSi by electrochemical etching of crystalline silicon in aqueous HF solution laid the foundation for later refinements.

In a typical experimental setup (Figure 5),[60] dilute aqueous HF is placed in a cell in which the silicon wafer attached on a metal layer acts as anode and a HF-resistant electrode acts as cathode. The cell body is constructed with a highly acid resistant material, such as Teflon. Ethanol is often used as the electrolyte to reduce formation of hydrogen bubbles, and also to help HF penetrate into the pores, since the freshly-etched PSi has hydrogen-termination and therefore is hydrophobic.[61] This most commonly used type of cell is able to yield the formation of PSi layers with good uniformity. Currently, this technique has been controlled up to a very high reproducible level of parameters, such as porosity, pore size, and thickness of porous silicon layer.[62]

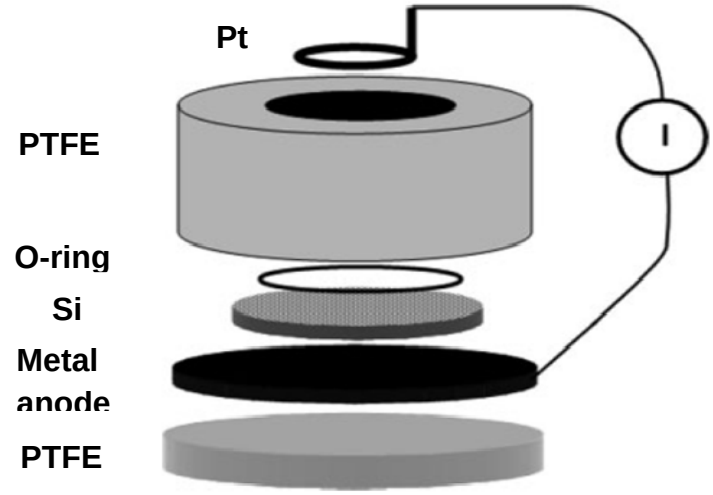

Figure 5. Scheme of an anodization cell for one side etching, in which the metal anode is used to ensure a constant current density through the Si sample.[60]

1.3.1.2 Stain Etching

An alternative method for fabrication of PSi is called stain etching. In a typical process, the dissolution is carried out in a mixture of hydrofluoric acid and a strong oxidizing agent, such as nitric acid, with no electrical bias.[63, 64] This method is even simpler than anodization, however, it is limited on the control of porosity, pore size and layer thickness.[65]

1.3.1.3 Mechanism of Pore Formation

The exact mechanism for pore formation is still in question. Several mechanisms have been proposed in the past several years.[66] Among those proposals, the theory presented by Lehmann and Gosele is more complete and thus has received more attention than others. This mechanism explains the hydrogen gas evolved during anodization, and the need for a supply of positive charge carriers (known as holes, h^+) in order for the dissolution to occur. Figure 6 illustrates this electrochemical dissolution mechanism.[66]

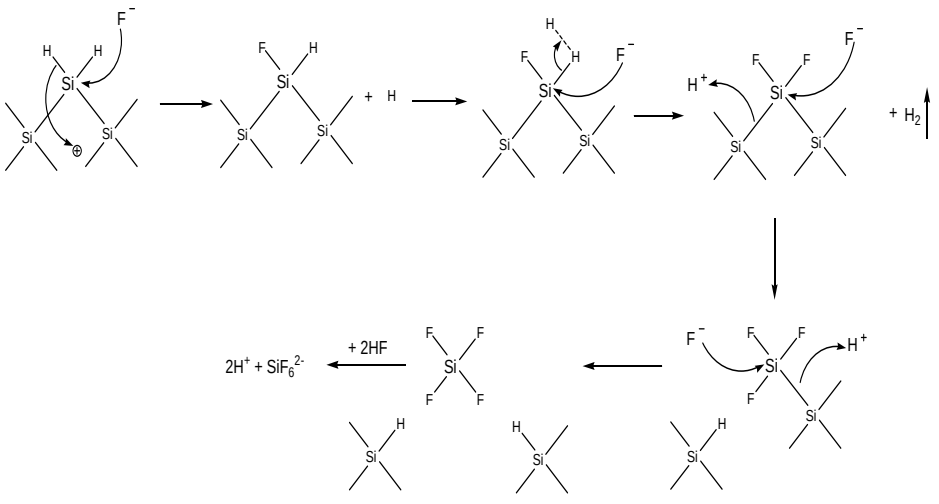

Figure 6. Proposed dissolution mechanism of silicon electrodes in HF associated with porous silicon formation.[66]

Firstly, the present consensus is that porous silicon surfaces are terminated with silicon–hydrogen bonds. This hydrogen is virtually free from attack by fluoride ions in the HF based electrolyte in the absence of positive charge. Because the electron affinity of hydrogen is about same as of that of silicon, the polarization between the hydrogen and silicon atoms is low. If there is positive charge (a hole) close to the surface, nucleophillic attack on a Si-H bond by a fluoride ion can occur and a Si-F bond is formed, as shown in the first step in Figure 6. Since a Si-F bond causes a polarization effect, a second fluorine ion is allowed to attack and replace the remaining Si-H bonds. In a redox process, H_2 is eliminated, injecting an electron into the substrate, as shown in the third step. Two Si-F bonds cause an even stronger polarization effect, which makes Si-Si backbonds susceptible to be attacked by HF (shown in steps four and five), resulting in the formation of silicon tetrafluoride and then the surface returns to its "neutral" state, terminated with hydrogen again. Silicon tetrafluoride reacts with HF to form the stable H_2SiF_6 (shown in step 6). These reactions repeat until another positive charge carrier is supplied to the surface.

As with the anodic oxidation of Si under bias, the key component of stain etch routes to PSi formation is the positive charge (hole) generation. In the stain etching method described above, nitric acid is often used as a strong oxidizing agent in the procedure, which serves as a hole injector by reacting with HF.[63]

Cathode: $HNO_3 + 3\ H^+ \longrightarrow NO + 2H_2O + 3h^+$

Anode: $n\ h^+ + Si + 2\ H_2O \longrightarrow SiO_2 + 4\ H^+ + (4-n)\ e^-$

$SiO_2 + 6\ HF \longrightarrow H_2SiF_6 + H_2O$

Overall: $3\ Si + 4\ HNO_3 + 18\ HF \longrightarrow 3\ H_2SiF_6 + 4NO + 8\ H_2O + 3(4-n)\ h^+ + 3(4-n)\ e^-$

1.3.1.4 Fabrication of Porous Silicon Particles

After the fabrication of the porous silicon layer, free standing micro- or nano-particles are needed in order to meet the requirements of the applications of PSi in biomedical applications. Sonication or ball milling is the standard technique to obtain PSi particles. They are employed usually after the formation of the free standing PSi layer through an abruptly-increased current.[67] However, the disadvantage of these techniques is the polydisperse fragmentation with random sizes and shapes. As a result, the particular size distribution can only be roughly controlled by sieving.[68] In studies of the applications of PSi *in vivo*, it has been shown that in the interaction of the drug delivery system with target cells, the rates and mechanisms of cellular internalization are strongly influenced by the size and shape of particles.[69] In Ferrari's work, tailored hemispherical mesoporous silicon microparticles with a monodisperse size range were fabricated reproducibly by the electrochemical etching of patterned silicon trenches.[69] As shown in Figure 7, a heavily doped p^{++} silicon wafer (doped with boron) was first patterned by photolithography, and then etched through a silicon nitride sacrificial layer. After the formation of the mesopores by electrochemical etching, the silicon nitride layer was removed in HF and the PSi particles were released from the substrate. Such PSi particles, as shown in Figure 8, are more uniform on size and shape, which are presumably more easily controlled with regard to its distribution in the human body. However, the preparation of such identically sized PSi particles is expensive and very slow.

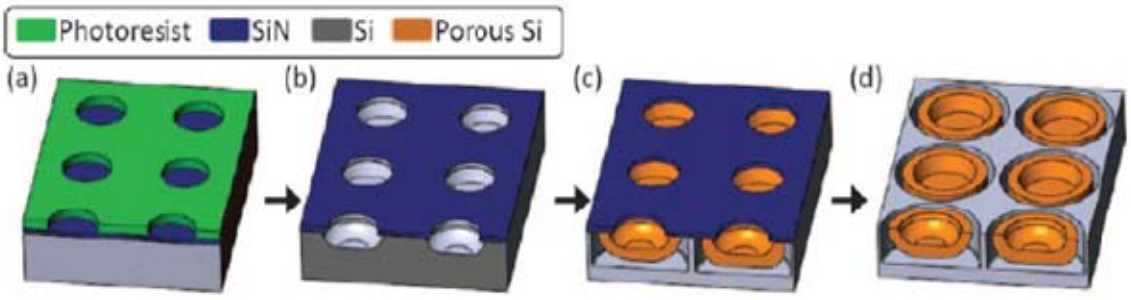

Figure 7. Schematic depiction of the fabrication process. a) Pattern transfer to the photoresist layer on top of the sacrificial SiN layer. b) Trench formation in the Si substrate through a combination of dry and wet etching. c) Formation of the particles and release layer following anodic etching. d) Particles are ready to be released by ultrasonication.[69]

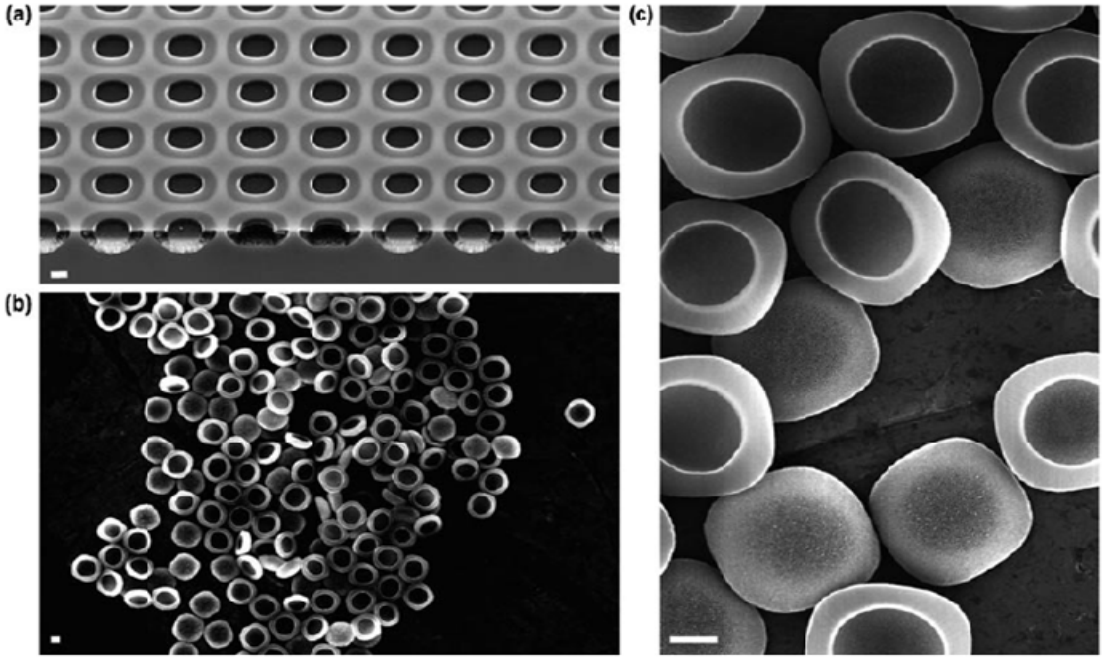

Figure 8. SEM images of large clusters of PSi particles. a) PSi particles still attached to the silicon substrate. b) Overview of a large cluster of PSi particles. c) Close-up of a small cluster of PSi particles. All scale bars: 1μm.[69]

1.3.2 Parameters and Morphology of PSi

Porosity is defined as the fraction of void volume in the porous silicon layer, which is a combined function of HF concentration in the etching solution and of current density. Porosity increases with increasing current density for a given HF concentration, and decreases with increasing HF concentration for a fixed current density. The thickness of porous silicon layer increases linearly with increasing anodization time, once other formation parameters are fixed.[70]

The specific surface area of porous silicon is defined as the accessible area of solid surface per unit volume of material. PSi has very high specific surface area, ranging from ~ 100 m^2/cm^3 for macroporous silicon to ~ 900 m^2/cm^3 for nanoporous silicon. This significant characteristic of PSi leads to its wide applications in biomedicine. Surface area depends on porosity. Generally speaking, the bigger the porosity, the larger the surface area (as measured by a N_2 adsorption method (BET)). However, once the porosity is beyond 50%, the specific surface area decreases with increasing porosity, as shown in Figure 9.[71]

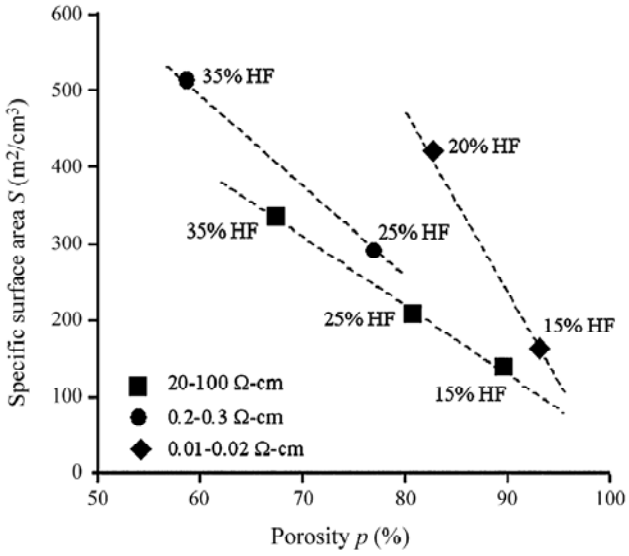

Figure 9. Porous silicon specific area vs. porosity.[71]

Pore size is also a combined function of various parameters of the formation process. Bomchil and his colleagues pointed out that the similar pore size range is obtained for the same porosity. For example, the pore size distributions obtained for heavily doped P-silicon (0.01 Ωcm) prepared at 10 mA/cm^2 in 10% HF and 240 mA/cm^2 in 25% HF, which both present a porosity of about 69%, are very similar, as shown in Figure 10.[72]

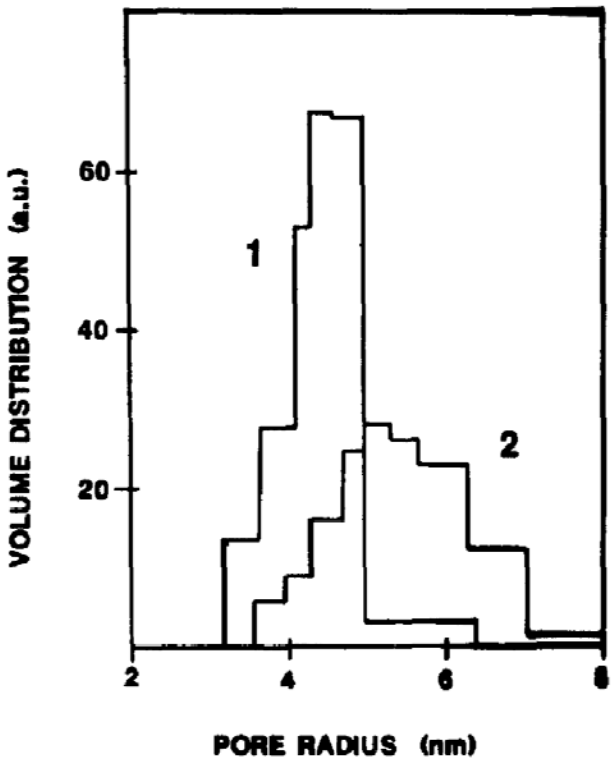

Figure 10. Comporison of pore size distributions of porous layers of same porosity (69%) prepared on heavily doped P-silicon (0.01 Ωcm) under different conditions, 1). 240 mA/cm^2, 25% HF; 2). 10 mA/cm^2, 10% HF.[72]

However, the distribution of pore sizes is generally much more complicated than the above case. Morphology, including pore size, shape, branching, orientation, interconnection, and distribution is very difficult to systematically characterize, and each

of them is extremely rich in detail and co-influenced by various factors. Figure 11 schematically summarizes the diverse morphological features observed in PSi.[73]

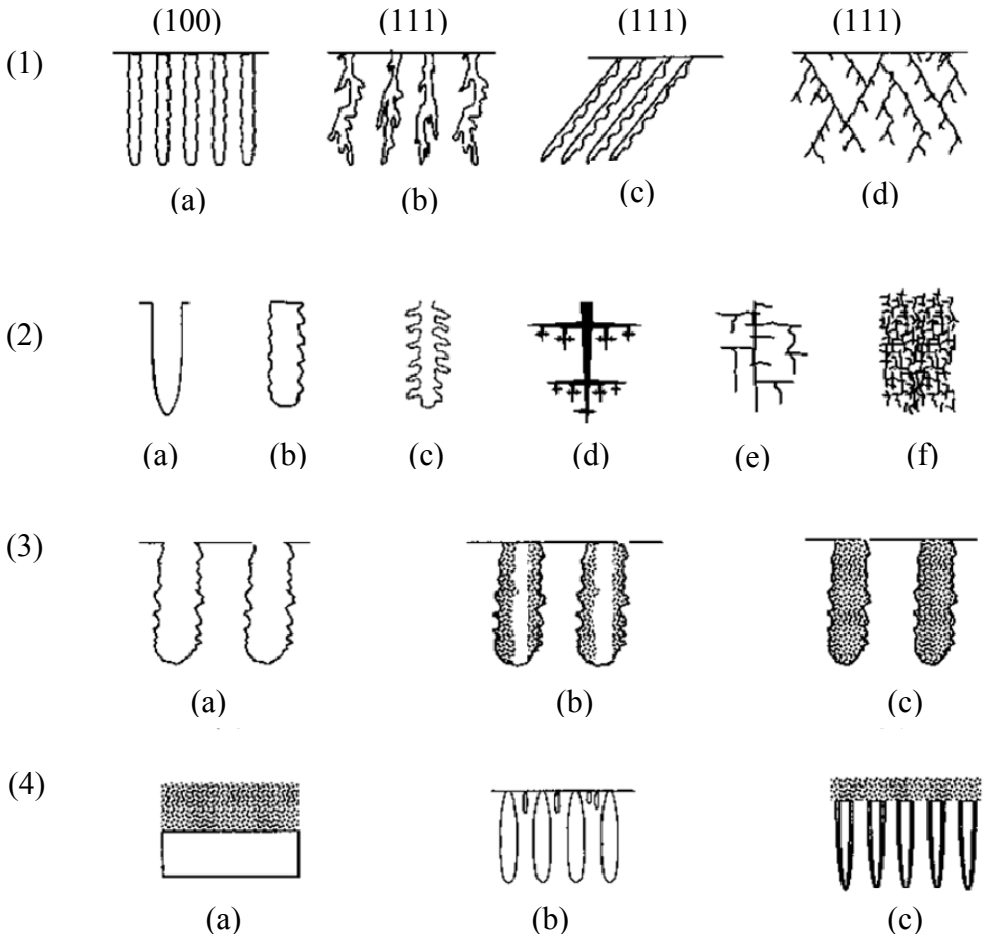

(1) Orientation
- (a) aligned to <100> and source of holes
- (b) roughly aligned to source of holes
- (c) partially aligned to <100> and source of holes
- (d) aligned only to <100>

(2) Branching
- (a) smooth pore wall
- (b) branches shorter than diameter
- (c) second level branches only
- (d) dendritic branches
- (e) main pore with second and third level branches
- (f) dense, random and short branches

(3) Mixture of pore types
- (a) Pure macropores
- (b) partially filled mix of macropores with some micropores
- (c) macropores fully filled with micropores

(4) Depth variation of PS layer
- (a) single layer of micro PS
- (b) single layer of macro PS with smaller pores near the surface
- (c) a layer of micro PS on top of macro PS (Pores may be filled by micro PS)

Figure 11. Schematic summary of the diverse morphological features of PSi.[73]

Pore size, orientation and degree of branching are more affected by the types of dopant and its concentration in PSi than by the other etching conditions (concentration of electrolyte, current density etc). In particular, the pore size typically increases with the increasing dopant concentration for p-Si and decreases with increasing dopant concentration for n-Si.[73] Depending on the pore diameter, PSi can be classified as either microporous, mesoporous, or macroporous with pore sizes varying from 1 nm to 2 nm, between 2 nm to 50 nm, and larger than 50 nm, respectively. Figure 12 shows TEM images of typical morphologies of microporous silicon, mesoporous silicon and macroporous silicon.[74]

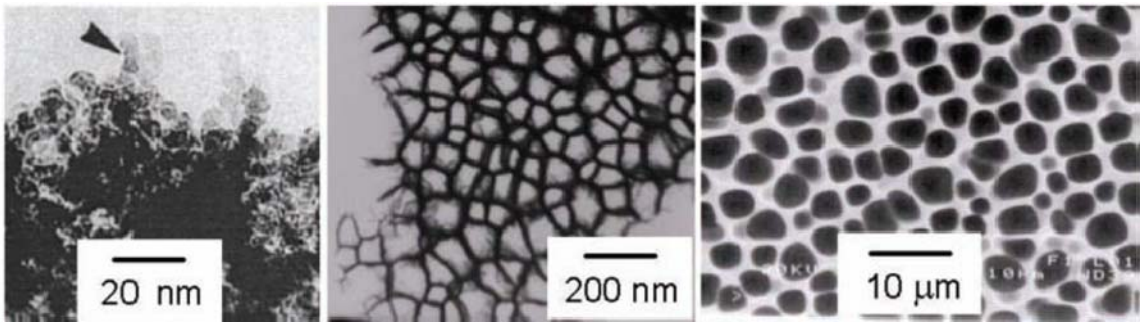

Figure 12. TEM images of microporous (left), mesoporous (middle), and macroporous (right) porous silicon.[74]

1.3.3 Surface Chemistry and Modification of PSi

As mentioned in the previous section, porous silicon possesses huge surface areas of up to 900 m^2/cm^3. Due to this high surface-to-volume ratio and the metastable Si-H termination, the surface chemistry of porous silicon has been considered to be a critical property. The functionalization of porous silicon surfaces with species such as halogens or oxides, strongly influences the photoluminescence of porous silicon and affects its light emission.[75, 76] Also, the surface bonding or conjugating with organic substituents

can be modulated for a variety of purposes, such as stabilization of PSi, providing biologically relevant molecules for sensing, targeting, and diagnosing in the drug delivery process, or promoting cell adhesion and other applications in biology. Selected surface chemical properties of PSi, including freshly etched, oxidized, and modified forms (such as nitridation, halogenations and hydrosilylation), will be specified in the following section.

1.3.3.1 Freshly Etched PSi

The surface of freshly etched PSi is almost completely covered by hydride species, mainly in Si-H and $Si-H_2$ forms, sometimes in $Si-H_3$, as evidenced by infrared vibrational spectroscopy. Freshly etched PSi shows the absorption bands associated with vibrations of the $Si-H_x$ (2114 cm^{-1} for ν(Si-H), 2090 cm^{-1} for ν($Si-H_2$), 906 cm^{-1} for δ($Si-H_2$), and 630-670 cm^{-1} for δ(Si-H); some samples have an absorption band at 2140 cm^{-1} for ν($Si-H_3$)) (Figure 13).[77] Hydrogen-terminated PSi exhibits a highly hydrophobic character, but limited long-term stability. Upon storage in air at room temperature, the surface gets naturally oxidized in a slow fashion.[78]

Besides Si-H formed during the fabrication, other impurities are also present on the surface, including fluorine, and oxygen. The presence of small quantities of fluorine, a few percent, was first demonstrated by Earwaker[79] and confirmed by other authors using nuclear microananlysis[80] or secondary ion mass spectroscopy (SIMS).[81] Stutzmann *et al.* have observed an isotropic hyperfine structure by spin-dependent photoconductivity resonance (SDPR). They assigned this structure to SiF_3 radicals.[82] The presence of SiF and SiF_2 has also been observed from FTIR absorption experiments.[83] In Konishi's work, it is proposed that SiF bonds on the surface of PSi are progressively replaced by Si-OH

bonds through hydrolysis reactions with water vapor in the air.[84] This explains the decrease of fluorine content in PSi with time.

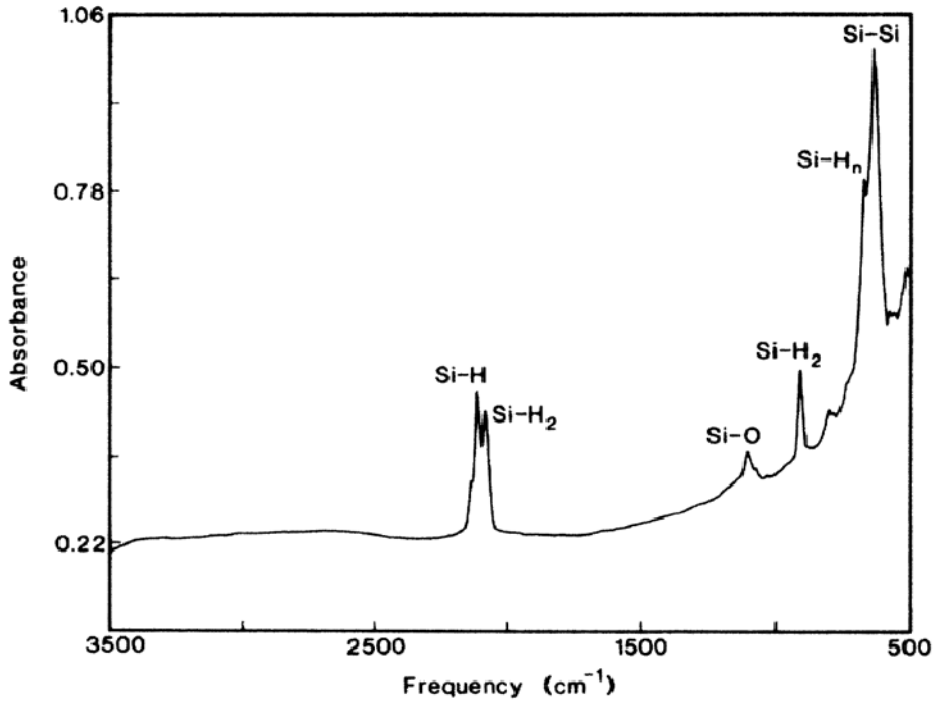

Figure 13. Infrared spectrum of a freshly prepared porous silicon sample.[77]

It has been observed that a few percent of oxygen atoms can be incorporated on the surface of PSi very rapidly after drying (within a few tens of minutes in ambient air).[85] Anderson and coworkers found Si-O-Si modes (1100 cm^{-1}), but O_x-Si-H groups (2260 cm^{-1}) were not observed by IR absorption a few hours after PSi formation, different from the results of PSi exposed in saturated water vapor at 23 °C for 5 and 20 hours as shown in Figure 14.[86] It is interesting that the formation of such groups does not modify hydrogen passivation. Further studies on oxidized PSi will be described in the following section.

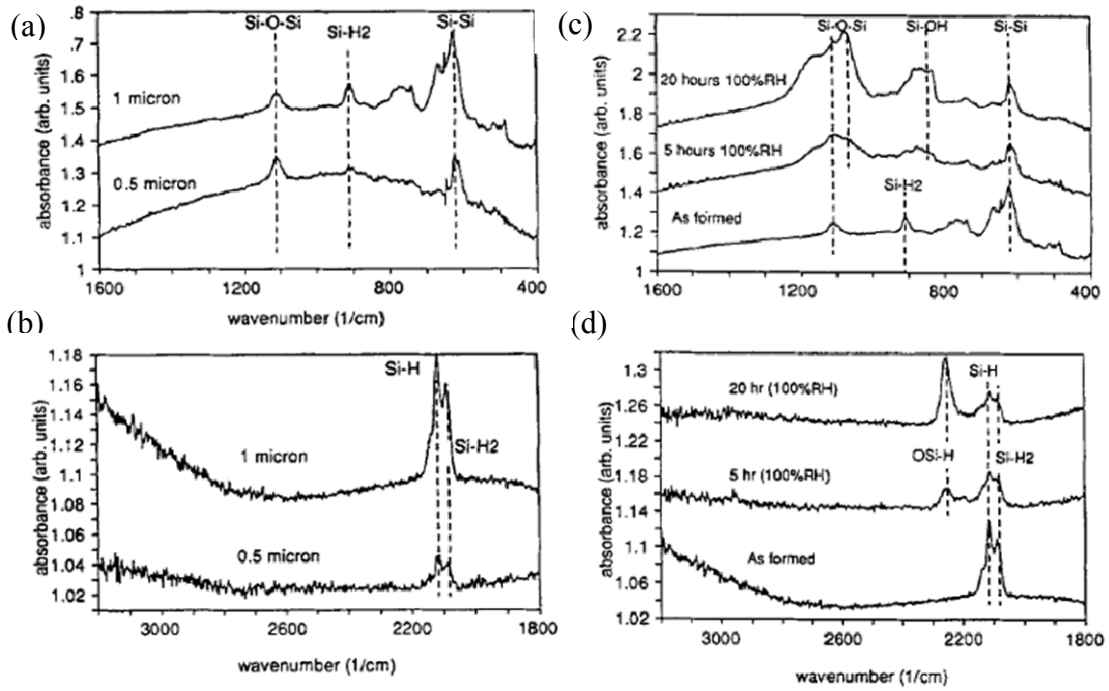

Figure 14. Transmission FTIR of unmodified porous silicon samples (0.5 μm and 1 μm thick) taken within 30 min of formation (a, b); and porous silicon (1 μm thick) under room temperature oxidation after 5 h and 20 h (c, d with different ranges of wavenumbers).[86]

1.3.3.2 Degradation of PSi

Porous silicon is widely studied in biologically relevant applications because of its biocompatibility and its non-toxicity.[87] The important feature that contributes to its biocompatibility is that PSi is degradable and absorbable in the human body. PSi degrades mainly into monomeric silicic acid, $Si(OH)_4$, the most natural form of Si in the environment and the only form in which it can be easily absorbed.[60] PSi biodegradation can be controlled by the overall porosity, pore size, shape and surface composition.[88] Figure 15 shows the different dissolution behavior of porous silicon films with three different porosities at pH 7.[89] Usually, depending on the degree of porosity, silicon particles may be bioactive, bioinert, or biodegradable.

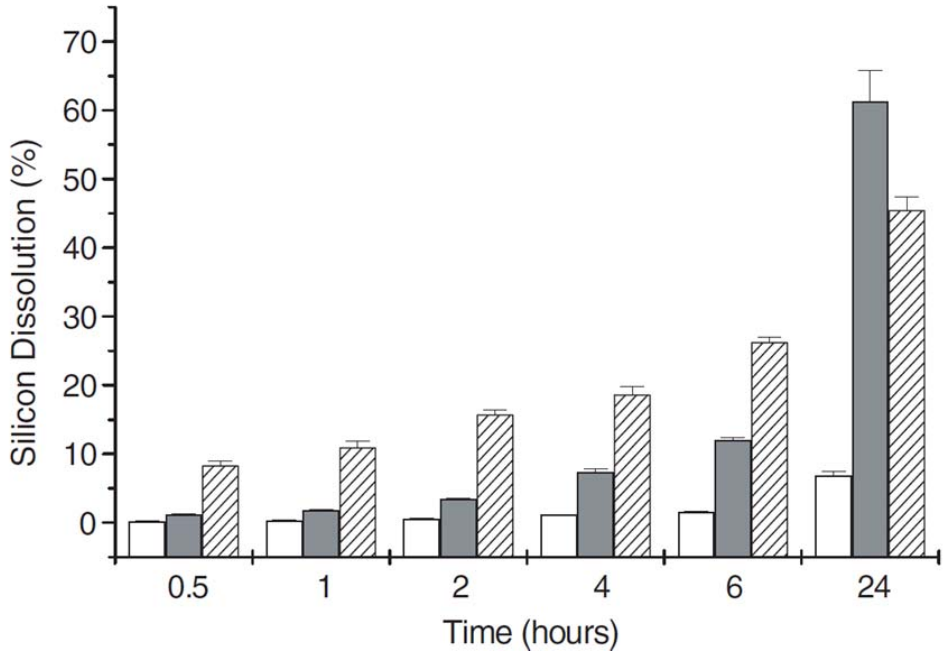

Figure 15. Dissolution kinetics of PSi. Medium (62%) porosity silicon film (white), high (83%) porosity (grey) and very high (88%) porosity film (hatched).[89]

Silicic acid produced during PSi degradation can be determined by means of an ammonium molybdate colorimetric assay.[90] When ammonium molybdate reacts with silicic acid, a yellow color of silicomolybdic acid appears. This method is simple but the yellow color of product is often faint and is not easy to match visually, nor is its intensity strictly proportional to the concentration of silicic acid. Therefore, a more sensitive method was developed, in which silicomolybdic acid is formed and then reduced to molybdenum blue. After 20 - 60 minutes of the reaction, the intensity of color can be quantitatively measured at 700 - 810 nm by UV/visible spectrophotometry. Currently this modified method is widely used for determining trace amounts of silicon in other materials.[90]

1.3.3.3 Oxidized PSi

Freshly etched PSi reacts slowly with ambient air upon storage in air and is gradually oxidized. This procedure is called aging. There are a number of options to minimize the extent of such storage effects. The simplest way is to optimize storage conditions (such as short-term storage in a dark environment), avoid moisture, and protect the sample under an ultra-dry inert gas. However, the effects of these conditions greatly depend upon the timescale. In some research, it is preferred to avoid storage-related problems by an intentionally-controlled oxidation of PSi. Additionally, many oxidation treatments have been used recently as a means to study the photoluminescence of PSi. Therefore, some alternative processes of PSi oxidation have been employed, including thermal oxidation, anodic oxidation, photo-oxidation and chemical oxidation. In this section, some of these approaches will be briefly introduced.

1.3.3.3.1 Thermal oxidation

Thermal oxidation is the simplest and most commonly used technique for the stabilization of PSi. Salonen studied the thermal oxidation of free-standing PSi films from room temperature to 730 °C. Three different stages were observed for thermal oxidation of PSi.[91] As shown in Figure 16, only backbonded oxidized Si-H_x (2150 - 2300 cm^{-1} for ν(-OSiH)) is observed in the first stage when PSi is heated at 350 °C, without traces of Si-H_x observed. After the oxidation at 750 °C, peaks of backbonded oxidized Si-H_x disappear and the absorption of peaks associated with thermal oxide (900 - 1300 cm^{-1} for ν(Si-O-Si)) increases. The broad peak at 3400 cm^{-1} indicates ν(Si-OH), and the sharp peaks at 1720 cm^{-1} and 3745 cm^{-1} arise from interstitial oxygen atoms and isolated Si-OH,

respectively. Salonen proposed a possible mechanism according to their observations (Figure 17).[91] The first stage of PSi oxidization involves the backbond oxidation of Si-H_x, in which oxygen is inserted into Si-Si bonds. The second and third stages are associated with the replacement of hydrogen with oxygen in O_y-Si-H_x species and with the formation of Si-O_y-H_x. These assumptions are supported by the disappearance of peaks of backbond oxidation at 2150 - 2300 cm^{-1}, and by the increased absorption at 3400 cm^{-1} for ν(Si-OH), as shown in Figure 16. This assumption also agrees with Takahagi group's study, in which oxygen is observed to preferentially attack the Si-Si backbonds rather than the Si-H bonds on the surface of an HF treated bulk Si in the initial stage.[92]

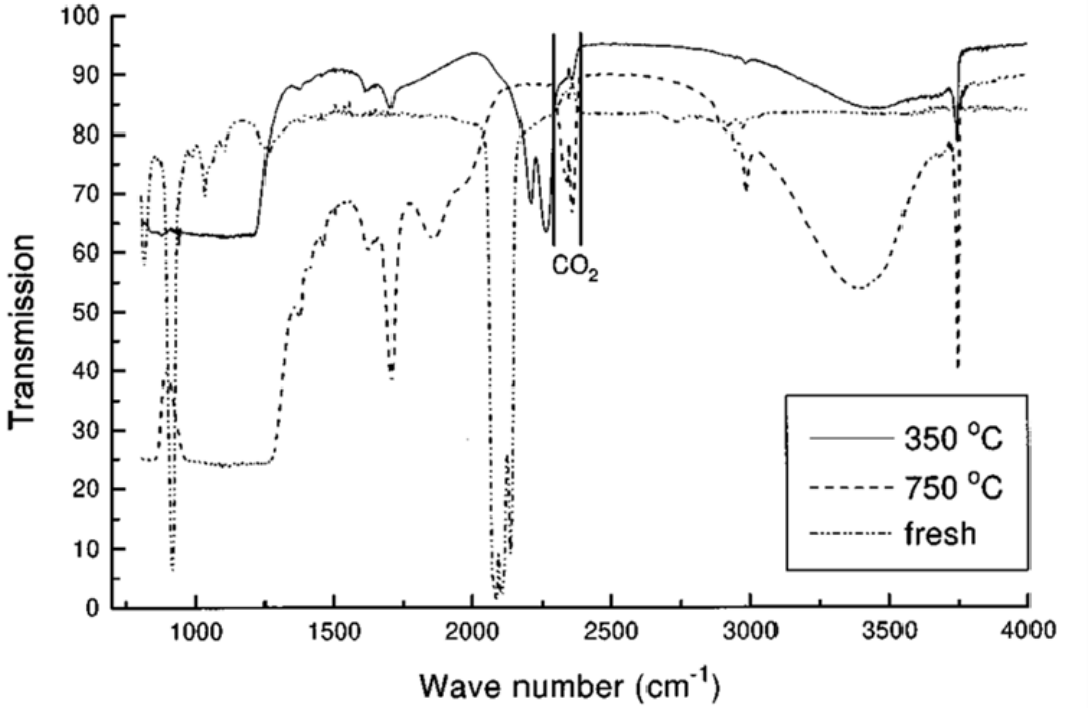

Figure 16. FTIR spectra of thermally oxidized samples and a freshly anodized sample.[91]

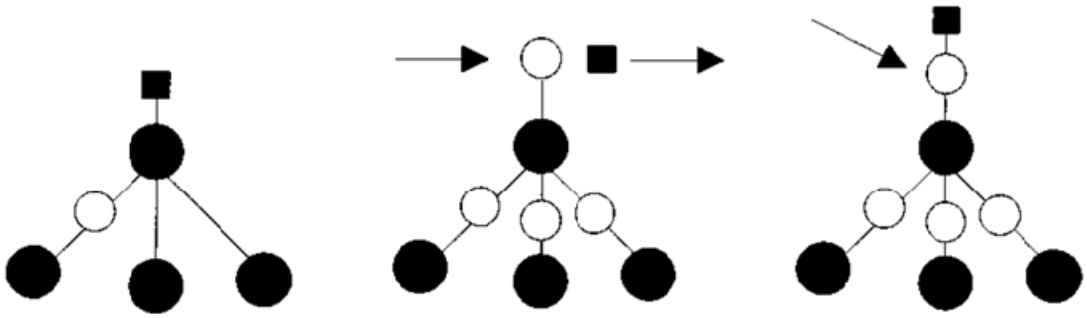

Figure 17. Proposed mechanism of oxidation of PSi. (a) Backbond oxidation of Si-H; (b) the oxygen replacing the hydrogen in O_3-Si-H, and (c) the oxygen goes between Si-H bond. Si: solid circles; H: solid box; O: open circle.[91]

1.3.3.3.2 Anodic oxidation

Anodic oxidation is performed in an electrochemical cell immediately after the porous silicon layer (PSL) is formed. A non-fluoride electrolyte such as KNO_3 solution is often used instead of HF solution. A typical anodic oxidation is carried out under a constant current density of 1-10 mA/cm^2, with the duration of 10-10^3 s.[93-95] In some reports, it is pointed out that the electrochemical process occurs preferentially near the bottom of the pores, but increasing the current density can diminish this geometrical effect.[93] This process may not affect the homogeneity of oxidation for layers with the thickness of a few micrometers. However, complete oxidation is not achieved by anodic oxidation, because electrical isolation of the Si skeleton parts occurs, preventing further current flow. For example, for mesoporous samples of 65% porosity on P$^-$ type doped substrates, about 40% of the Si remains unoxidized at the end of the process, corresponding to about a monolayer of oxide coating. [93, 94, 96]

1.3.3.3.3 Chemical oxidation

A wide range of chemical oxidation routes of PSi have been developed. A variety of chemicals and processes are involved in this technique. In Hou's study, a large blue shift of the PSi's photoluminescence spectrum is observed when PSi is simply treated with boiling water. Meanwhile, this treatment also strengthens the skeleton of PSi by filling up many pores with oxygen from water.[97] Oxidation of PSi can also be achieved by the treatment of either 49 wt% aqueous H_2O_2 solution or 20 wt% aqueous HNO_3 solution for 30 minutes at room temperature.[98] Ozone oxidation, performed at room temperature for 15-18 minutes, can give the same effect.[99] Some organic solvents are also employed, such as dimethyl sulfoxide (DMSO),[100] benzoquinone,[101] or pyridine,[102] as milder chemical oxidants. These mild oxidants are sometimes preferred because they can improve the mechanical stability of highly porous Si films, which are typically quite fragile.[103]

1.3.3.4 Surface Modification of PSi

1.3.3.4.1 Nitridation

In addition to oxidization, nitridation also effectively stabilizes and passivates PSi. Rapid thermal treatments (30 s at 1100 °C) in N_2 or NH_3 promote the formation of a thin N rich layer on the PSi surface, as evidenced by the buildup of a Si-N-Si vibrational peak at 915 cm^{-1} in FTIR spectra.[94] The reaction appears more efficient in ammonia than in nitrogen.[93, 94]

1.3.3.4.2 Halogenation

Halogenation, in general, is often utilized as an intermediate step for further surface chemistry, such as Si-C bond formation.[94] Bansal and his group exposed H-terminated Si to PCl_5 in chlorobenzene for 20 – 60 minutes at 80-100 °C, using benzoyl peroxide as the radical initiator. The chlorinated Si formed was then further exposed to alkyllithium to achieve the desired alkylation of Si surface.[104] The equations below show the reactants and conditions often used in the formation of Si-Cl and Si-Br terminated PSi.[76]

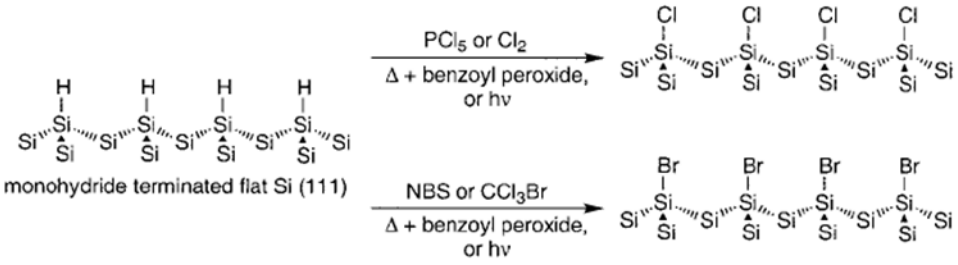

Figure 18. Summary of routes to produce halide-terminated silicon.[76]
NBS: N-bromosuccinimide

1.3.3.4.3 Hydrosilylation

Hydrosilylation involves the insertion of an unsaturated C-C bond into a silicon-hydride group. Alkyne and alkene hydrosilylations on Si-H terminated surfaces yield alkenyl and alkyl terminations, respectively, as shown in Figure 19.[76]

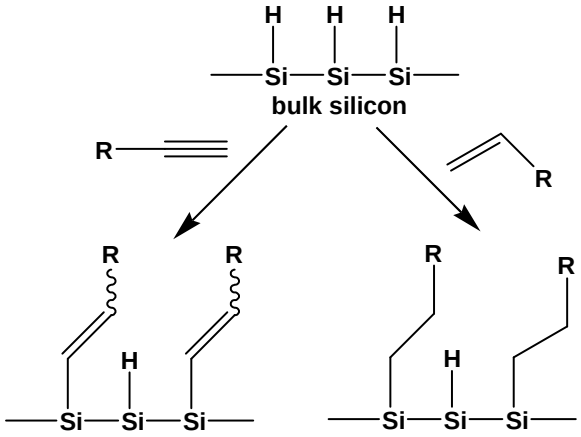

Figure 19. Schematic of hydrosilylation chemistry.[76]

In Stewart and Buriak's work,[105] photoluminescent nanocrystalline silicon undergoes the hydrosilylation with alkenes and alkynes, promoted by a novel white light reaction. The proposed mechanism involves attack of a surface-localized positive charge carrier (hole) in a nucleophilic fashion by an alkene or alkyne, which results in Si-C bond formation, as shown in Figure 20.[105] Excitation produced by light absorption leads to a surface-localized positive charge. This surface charge can then interact with an alkene to form a silylated β-carbocation upon Si-C bond formation. The neutral organic termination is then formed after this carbocation abstracting a hydride from an adjacent Si-H bond.

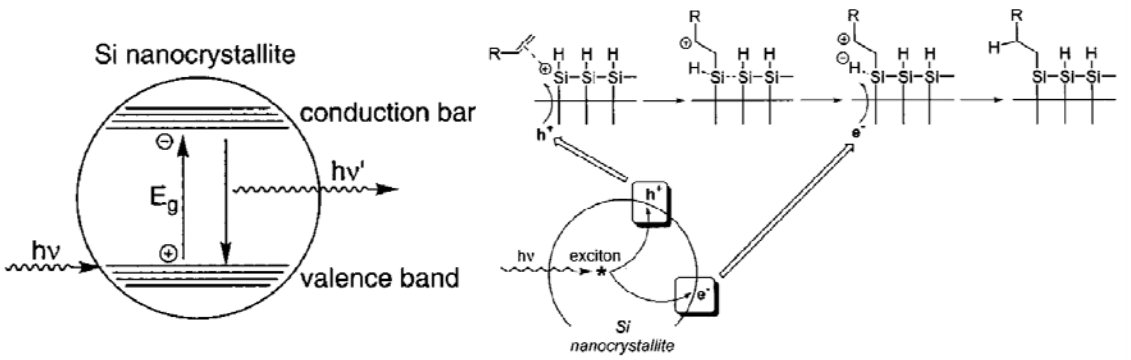

Figure 20. Proposed mechanism for the exciton-mediated hydrosilylation event.[105]

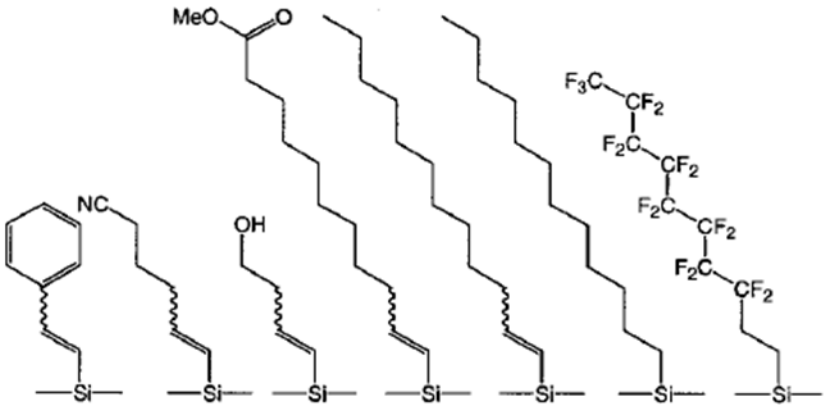

Figure 21. Representative porous silicon surface functionalities prepared through hydrosilylation of alkenes or alkynes.[108]

An analogous reaction has been done by Schmeltzer, in which a triphenyl carbenium cation is used to remove H^- from the surface, producing a surface silicon-based positive charge. Nucleophilic attack of this positive charge by an alkene results in Si-C bond formation.[106] So far, a number of methods have been developed for the formation of covalently bound organic monolayers on the surface of PSi.[107] Figure 21 shows some other examples of different terminal groups prepared through hydrosilylation.[108]

1.3.4 Applications of Porous Silicon

Porous silicon has been extensively investigated and utilized for various applications, due to its many remarkable properties. The discovery that PSi has light emitting properties in the visible region initiated a number of investigations relevant to silicon-based optoelectronic devices. In addition to these luminescent properties, other interesting properties including a tunable refractive index, conductivity, low visible light absorption, and variable surface chemistry allow its use in a wide range of fields, such as optics, chemical sensors, and solar cells.[56] This section reviews another important

application of PSi in the biomedical area, taking advantage of its unique large surface area, biodegradability and biocompatibility properties in the fields of drug delivery, tissue engineering, and biosensors. Figure 22 provides a scheme showing the range of PSi applications, dependent upon its porosity.[109]

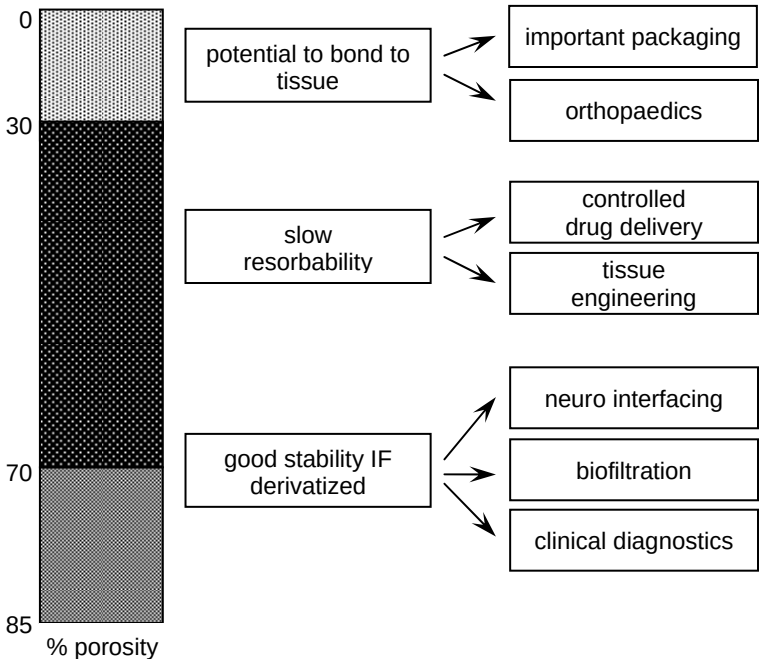

Figure 22. Potential clinical application areas for PSi with various porosity.[109]

1.3.4.1 Porous Silicon for Drug Delivery

Research on mesoporous silicon for drug delivery applications started in the late 1990s.[110] In looking at the published studies in this area, PSi as a drug delivery carrier or vehicle can be viewed from the following aspects.

Firstly, drug delivery based on PSi is not only used for delivery of therapeutic drugs,[111] but also versatile for nutrients, such as vitamins, lycopene, fish oils, coenzyme Q10,[112] nucleotides, vaccines,[113] etc. Among the applications of drug delivery, the

transport of anticancer agents has been studied most extensively.[114] In 1998, our group first demonstrated that hydroxyapatite layers grown electrochemically on a porous Si/Si substrate can be used as a delivery vehicle. Model studies involved encapsulation of the transition metal complexes *cis*-$Pt(NH_3)_2Cl_2$, $Ru(bpy)_3^{2+}$, and $Ru(phen)_3^{2+}$. The controlled release of these complexes from the hydroxyapatite layer was achieved.[110]

In further investigations, another group of anticancer agents, *cis*-platin (*cis*-diamminedichloroplatinum(II)), carboplatin (*cis*-diammine(cyclobutane-1,1-dicarboxylato) platinum(II)), and $Pt(en)Cl_2$ (ethylenediamminedichloro platinum(II)) were successfully incorporated with layers of calcium phosphate on PSi/Si substrates. The impact of initial platinum concentration, the influence of thermal annealing of the matrix, and the effect of the ligand coordination sphere variation of the Pt complexes on the delivery were also investigated.[111]

Secondly, various approaches to introduce a molecular payload into a PSi host can be categorized into simple immersion, impregnation, covalent attachment, and physical trapping.[60,103] Simple immersion is the most commonly used method in which the desired drug is dissolved in a suitable solvent and given higher volume than the volume of PSi pores. Impregnation involves adding the solution of the controlled amount of drug into the particles, by infusing through capillary action into pores.[115] Covalent attachment is a more stable route than others, because it links a biomolecule typically via Si-C bonds, which can be achieved by hydrosilylation, silanization, Grignard and alkyl/aryllithium reagents,[103] crosslinkers,[116] etc.

Thirdly, PSi delivery system is also able to provide a controlled, sustainable and targeted release of drugs. As mentioned above, hydroxyapatite layers loaded with *cis*-

$Pt(NH_3)_2Cl_2$, $Ru(bpy)_3^{2+,}$ and $Ru(phen)_3^{2+}$on a PSi/Si substrate is a good example of this controlled release. The given complex can be released into the surroundings through thermal heating has also been proposed.[110]

In another study from E. C. Wu *et al.*, daunorubicin was covalently attached on the surface of porous silicon and slowly released affected by the gradual degradation of PSi.[117] As shown in Figure 23, 1-undecylenic acid was first attached with Si-H termination on the surface of the particles, then daunorubicin was bound by the reaction between the amine group from the drug and acidic group from the linker. A sustained release of daunorubicin was achieved for 30 days by the degradation of the porous Si matrix.

As a targeted drug delivery system, Gu demonstrated a magnetic manipulation, fluorescent tracking and localized delivery of a drug by using nanostructured porous silicon microparticles containing both fluorescent and magnetic functions.[118] Superparamagnetic iron oxide nanoparticles were first loaded into a luminescent porous silicon matrix. A large quantity of anti-cancer drug doxorubicin (9.8% by mass) was then loaded into the composite microparticles. Under the guidance of a magnetic field, a high concentration of doxorubicin was released in the proximity of the magnetic field. The death of human cervical cancer (HeLa) cells in that region of the Petri dish confirmed that localized delivery of the doxorubicin can be achieved, which provides a strategy to decrease the systemic toxicity of molecular drugs.[118]

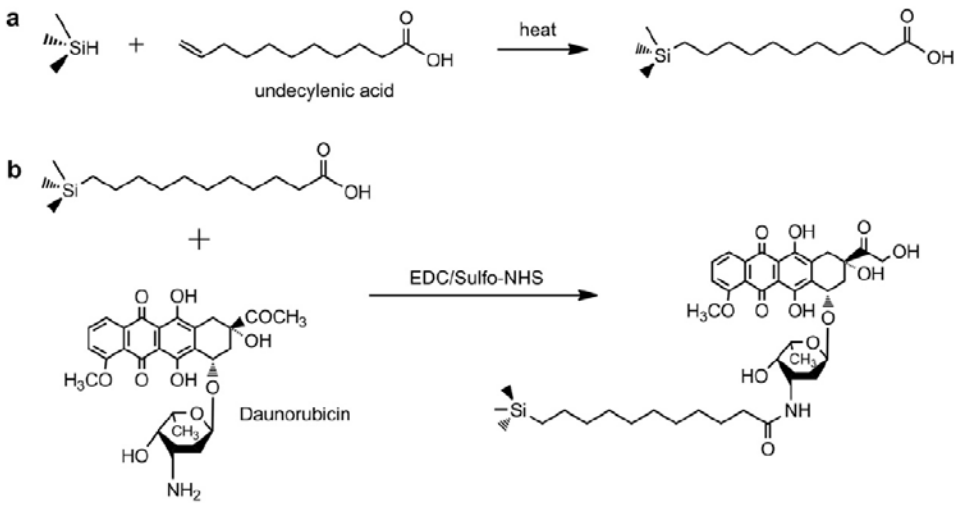

Figure 23. Loading of daunorubicin into porous Si microparticles. The process involves functionalization of the hydrogen-terminated porous Si surface by hydrosilylation of undecylenic acid (a), followed by EDC-mediated coupling of daunorubicin via the pendant amino group (b)[117].

1.3.4.2 Porous Silicon for Tissue Engineering

Nanostructured composite materials composed of PSi and common polymers such as poly (ε-caprolactone) (PCL) have been prepared by Melanie Whitehead in our group, by using salt-leaching and micromulsion / freeze-drying methods.[119] Her results demonstrated that such materials can stimulate the deposition of calcium phosphate in simulated body fluid (SBF). *In vitro* proliferation studies showed that the scaffolds appear nontoxic to human embryonic kidney fibroblast cells (HEK 293). Later, Fan *et al.* did further investigations on materials of the same composition that were prepared in microfibrous form by an electrospinning method.[120] She investigated the effects of these composite materials on mesenchymal stem cell differentiation. Studies of alkaline phosphatase expression as a specific biomarker for mensenchymal to bone cell differentiation show that the scaffolds have the ability to mediate such processes.[120]

Overall, PSi has been widely investigated as a scaffold for orthopaedic implants, and appropriately-derivatized PSi will support the attachment and growth of a variety of mammalian cells.[121] Stabilization of the PSi surface in contact with physiological fluids is important in order to preserve the structural integrity of the material and to control the degradation kinetics during implantation.

1.3.4.3 Porous Silicon for Biosensing

The first biosensor having PSi as the substrate for molecule immobilization appeared in 1997.[122] From then on, an increasing attention has been directed to this material for this purpose. PSi has been used as an optical interferometric transducer for detecting small organic molecules, DNA, and proteins at pico- and femto-molar analyte concentrations.[123] PSi based biosensors, which are incorporated with Fabry-Perot signal transduction, offer several advantages. The most notable one is the label-free analyte sensing.[124] In a study by Dancil *et al.*, a sensor system consisting of a thin layer (5 μm) of PSi modified with Protein A was probed with various fragments of an aqueous human IgG analyte.[125] Molecular binding was detected as a shift in the wavelength of the Fabry-Perot fringes in the white light reflection spectrum from the PSi layer. It is proposed that the shifts in the Fabry-Perot fringe pattern result from changes in the refractive index of the material.

1.4 Antibacterial Assays

In this research work, antibacterial assays are employed for assessing the bacterial inhibition gradient of antibiotics released from PSi, involving antibiotics – triclosan, ciprofloxacin and its hydrochloride salt, against the bacteria *Staphylococcus Aureus*. The

method used is similar to antimicrobial susceptibility testing (to test the antibiotic sensitivity to bacteria).

1.4.1 Antibiotics Used in This Research

In this research, triclosan, ciprofloxacin (as Cipro) and ciprofloxacin hydrochloride (Cipro HCl) are employed to investigate the role of PSi as a vehicle in drug delivery. The main consideration for this choice is that triclosan and ciprofloxacin both have a critical drawback property of low solubility, which makes their delivery challenging. Hydrophilic ciprofloxacin hydrochloride was chosen as a comparison with hydrophobic ciprofloxacin. Also, other properties of these drugs, like low melting point and boiling point of triclosan, the UV sensitivity of ciprofloxacin and its salt, are all considered. In order to facilitate the experimental part of the antibacterial assay, triclosan and Cipro were chosen due to their common activity of inhibiting the growth of same bacterial species, *Staphylococcus Aureus* (*S. aureus*). Each antibiotic will be briefly described in the following section.

Triclosan: 5-chloro-2-(2,4-dichlorophenoxy)phenol, which is a broad-spectrum antibacterial and antimicrobial agent. The molar weight of triclosan is 289.54 g/mol. Its melting point and boiling point are 55-57 °C and 120 °C, respectively. Triclosan has a very low water-solubility of ~10 μg/mL (at room temperature), but it is soluble in ethanol, methanol and many other organic solvents.[126]

Triclosan is widely used in personal care products, such as toothpastes, deodorant soaps, cosmetic, antimicrobial creams and lotions. It has been shown that triclosan is very effective in reducing and controlling bacterial contamination. A concentration of only 2%

of triclosan can inhibit the growth of methicillin-resistant *Staphylococcus Aureus* (MRSA).[127]

Cipro and Cipro HCl: Ciprofloxacin is a synthetic antibiotic of the fluoroquinolone drug class,[128] and was first patented in 1983 by Bayer, A. G. and approved by the FDA in 1987. The molar weight is 331.4 g/mol for Cipro and 367.8 g/mol for Cipro HCl. The water solubility of Cipro is 67 μg/mL[129] and 30 mg/mL for Cipro HCl.[130] Cipro is decomposed at about 257-268 °C and the melting point of Cipro HCl is about 314-330 °C.[131]

Ciprofloxacin is used to treat a number of infections including bone and joints infections, endocarditis, gastroenteritis, urinary tract infections and others.[132] Ciprofloxacin is available as tablets, intravenous solutions, eye and ear drops. However, because of the low water solubility of Cipro, Cipro HCl is used instead to increase the solubility in water and makes its digestion easier in the body. Cipro, in neutral or salt form may have some side effects, including acute liver failure, serious liver injury, toxic epidermal necrolysis, and others.[133]

1.4.2 *Staphylococcus Aureus* and Its Related Antibiotics

Staphylococcus Aureus (S. aureus) is a bacterial species, which appears as a grape-like cluster. The colonies of *S. aureus* are large, round, golden-yellow, so called as "golden staph". It is a facultative anaerobic Gram-positive coccal bacterium. *S. aureus* is long-term carried by about 20% of the human population, and often exists on the normal skin and nose.[134]

S. aureus can exist without harming its host or causing symptoms; however, if there is a break in the skin from a wound or surgery, or if there is a suppression of the

person's immune system, *S. aureus* can cause an infection, called a *Staph* infection.[135] *Staph* infections include skin infections such as pimples, boils, abscesses, or can lead to a range of life-threatening diseases including pneumonia, meningitis, osteomyelitis, etc.[136]

The main problem existing in the treatment of *S. aureus* infections is drug resistance. Penicillin is commonly chosen for treatment in most countries, but now it is extreme suffering drug resistance, from the uncommon resistance at the period of its discovery in 1943, to 40% of hospital *S. aureus* isolated being penicillin resistant by 1950, and 80% by 1960.[137] With an increased population density and the widespread use of antibiotics, another strain called methicillin resistant *Staphylococcus aureus* (MRSA) was found, after the antibiotic treated the penicillin resistant stains. Infections caused by MRSA are frequently resistant to a wide range of antibiotics and causes higher rates of complications and death.[138]

1.4.3 Specific Antibacterial Assays

The antibacterial assay is adapted from antimicrobial susceptibility testing. Two methods are employed in this research, one of which is called disk diffusion method, and the other one is the broth dilution method.

1.4.3.1 Disk Diffusion Method

Disk diffusion is described as an antibiotic diffused from disks, tablets or strips to a solid growth medium prior seeded with a lawn of bacteria. The diffusion of antibiotic can inhibit the growth of bacteria around disks or tablets and form a clear region, which is an inhibition zone. When the concentration of antibiotic is low and cannot inhibit the bacterial growth, this concentration is the minimum inhibitory concentration (MIC) for

that particular bacterial/antibiotic combination. The inhibition zone is related to the MIC of the test bacterium and the diffusibility of the antibiotic. Generally, the formation of a larger inhibition zone indicates the inhibition of bacterial growth will occur at a lower concentration of antibiotic.

The disk diffusion is easy to perform and repeat, low cost, and does not require expensive equipment, but the manual measurement of zones of inhibition may be time consuming and the disks must be distributed evenly so that the zones of inhibition around disk with antibiotic do not overlap or form a random shape; otherwise, it is difficult to determine the zone of inhibition.[139]

1.4.3.2 Broth Dilution Methods

The original aim of broth dilution methods is also to determine the MIC. The purpose of applying this method into this research is the same as the disk diffusion method, which is to monitor how the antibiotics released from the PSi drug delivery system, affect bacterial growth.

In the antibacterial assays using a broth dilution method, a suspension of bacterium with a predetermined concentration in a minimum volume of 2 mL in tubes is tested against various concentrations of antibiotic. The turbidity of the bacterial medium indicates the extent of the inhibition of bacterium growth by antibiotic. The clearer the medium, the more bacterial growth is inhibited. The MIC does not always represent an absolute value. The 'true' MIC is a value between the lowest test concentration that inhibits the growth of the bacterium and the next lower test concentration. In this research work, the optical density of the medium smaller than 0.5 is defined as positive inhibition, while optical density bigger than 0.5 is considered as negative inhibition.

The broth dilution method appears to be more reproducible and quantitative than the disk diffusion method, but it needs associated equipment. Contamination and the restriction on performance are the two big drawbacks of this method.[140]

II. The Effects of PSi Parameters on Loading and Delivery of Triclosan

2.1 Introduction

As previously discussed in Chapter I, porous silicon, as a type of nanomaterial, possesses several useful properties relevant to its possible use in medical therapies, especially in drug delivery.[61] Both the biodegradability of mesoporous Si and its ability to nanostructure (decrease size to nanoscale) a given encapsulated substance present marked advantages, with initial studies focusing on chemotherapeutic cancer agents.[111, 112] The ability of mesoporous silicon to stimulate calcification *in vitro* upon degradation adds further value to its use as a drug delivery platform for oral medicine.[60(a)]

The controlled delivery of antibacterial agents remains a topic of widespread significance, given the need for sustained release of therapeutically relevant concentrations of the active agent.[141] Not only does sustained drug release reduce administration times and keep steadier levels of the drug in the blood stream, but also it prevents undesired side effects and consequently improves the patients' compliance and comfort significantly.[142]

Porous carrier materials have the ability to achieve sustained release, and improve aqueous solubility of these compounds (with an associated enhanced bioavailability, if relevant) at the same time.[61] Although a number of groups have studied the effects of porous silicon on drug delivery, [61, 69(a), 114, 118, 119, 121] not many works have systematically studied antibacterial compounds using mesoporous silicon carriers and the impact of the parameters of mesoporous silicon, such as porosity and particle size. For example, in Salonen et al's study of five model oral drugs (antipyrine, ibuprofen, griseofulvin, ranitidine and furosemide) loading and release from mesoporous silicon microparticles, only the surface properties (which correspond to the stability of PSi), the chemical nature

of the drugs, and the loading efficiencies were investigated.[69(a)] Some studies have also been done that involved the controlled or sustained release of drugs based on porous silicon, but usually from the combined composite, such as PSi/PCL, instead of individual components.[143]

In this chapter, the incorporation of the antibacterial agent Triclosan (Figure 24) loaded into free standing mesoporous silicon microparticles by a melt method, and an evaluation of its efficacy in killing the known pathogenic bacterium *Staphylococcus aureus* are described. Triclosan has been used as an effective oral antiseptic since the 1960s.[144] While some long-term environmental concerns regarding the use of this compound in large segments of the population have been indentified,[145] it nevertheless serves as a useful initial candidate for an evaluation of loading, release, and associated antibacterial activity when released from porous Si, since it possesses a low melting point, low cost, and is commonly used in a range of consumer products, such as soaps.

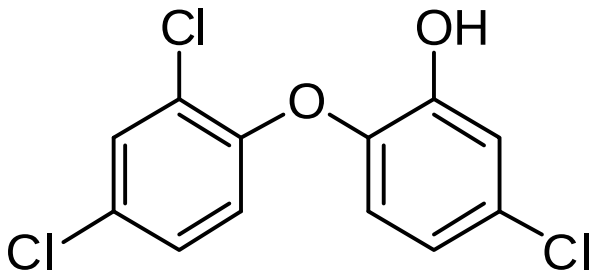

Figure 24. The structure of triclosan.

The motivation for this work is to: i) promote sustained delivery of triclosan which inhibits bacterial growth for sustained periods of time with the observation of an enhanced triclosan concentration released from PSi matrices; ii) investigate the different influence of porous silicon parameters, especially porosity, on the drug delivery, by

utilizing different types of mesoporous Si carriers, compared with macroporous silicon films; and iii) choose and optimize a suitable antibacterial assay for further studies.

A summary of the properties of each PSi sample involved in this study is given in Table 1. Four distinct types of porous silicon structures were utilized: high porosity (81%) mesoporous Si, with particle sizes ranging from 150 μm - 250 μm, referred to as Melt A; midporosity (65-75%) mesoporous Si with two particle size ranges, one smaller than 100 μm (Nonblended) and the other smaller than 50 μm (Blended), and a macroporous Si film with 13% porosity. The loading data for triclosan, as well as the release behavior for each sample, are also summarized in Table 1. Further details will be given in the Results and Discussion section.

Table 1. Triclosan-loaded porous Si samples: loading and release data.

Sample ID / Original porosity	Particle size (μm)	Triclosan loading % (TGA)	Total Triclosan loaded (mg)	Triclosan released in first 15 days (μg)	Average conc. in first 15 days (μg/ml)	% released	Max daily release conc. in first 15 days (μg/ml)
Mesoporous 81% (Melt A)	150-250	72.9	3.645	119.97	8.0	3.29	11.53
Mesoporous 65-75% (Nonblended)	<100	44.08	2.216	176.41	12.6	7.96	17.78
Mesoporous 65-75% (Blended)	<50	47.92	2.270	132.57	10.2	5.84	14.48
Macroporous film 13%	39.59 mm^2	1.1	0.42	33.82	2.25	7.87	3.96

2.2 Experimental

2.2.1 Fabrication of Anodized PSi

Mesoporous silicon particles were supplied by Dr. Armando Loni from Intrinsiq^{TM} Materials Ltd, where these particles were prepared by a three-stage process consisting of silicon wafer anodization, mesoporous membrane detachment, and mesoporous microparticle classification. Heavily boron doped (0.01 Ω cm) 150 mm diameter wafers were anodized in methanoic HF electrolyte in custom-built equipment to create 150 μm thick membranes of either 81% or 65%-75% porosity. These were then mechanically milled and classified into porous microparticles of specific size distributions. For the macroporous Si films, high resistivity n- wafers (phosphorus doped) are used in the etch process, producing films of approximately 48 μm thickness that remain attached to the Si wafer substrate.

2.2.2 Loading Process for Each Sample Type

For drugs with an intrinsically low solubility, simple melt loading processes are suitable options for loading if the drug possesses good thermal stability to its melting point. This is certainly true for triclosan, with a relatively low melting point of 55-57 °C. For each PSi sample described above, slightly different loading processes were employed.

For the sample melt A, a preweighed quantity of PSi powder was immersed in a known weight of molten triclosan at 90 °C for 35 min, with masses selected based on a target loading capacity of 72% by weight. For the midporosity PSi powders, the impact of drug/carrier premixing was evaluated as follows. So-called nonblended samples were loaded by the same process as described above at temperatures under 100 °C. As an

alternative, blended samples were fabricated whereby the PSi powder and triclosan (with masses selected based on a theoretical loading capacity of 70%) were homogeneously mixed first, and then heated together at 100 °C. For triclosan loading into macroporous silicon, a given film (still attached to the underlying Si substrate) was cut into small pieces (0.5×0.7 cm^2), which were subsequently characterized by SEM. Then depending on the size and porosity, the volume of pores and the theoretical loading were calculated. Films were initially soaked in a 1:1 water/ethanol mixture overnight to remove any surface impurities. A small glass slide with molten triclosan was placed face down onto a given macroporous silicon film heated at 80 °C for 10 min to complete the loading process. After completion, any surface liquid was removed when the sample was sandwiched between filter paper and rubbed with light manual pressure. When dry, the extra triclosan on the surface of the macroporous Si was removed by swabbing with ethanol under microscope observation.

2.2.3 Characterization of Loaded PSi samples

After triclosan loading, macroporous silicon films were dried by exposure in air for several hours and mesoporous silicon powder was dried in a low vacuum oven for at least one day.

All triclosan loaded PSi samples were characterized by scanning electron microscopy (SEM) (JEOL JSM-6100) to observe the particle morphology and energy dispersive X-ray (EDX) analysis to confirm the presence of chlorine (from triclosan) and detect the distribution of triclosan in the entire PSi sample. For PSi particles, a tiny amount of the loaded sample was placed and evenly spread (try to get single layer of particles) on the surface of a conductive carbon tape adhered to an aluminum thimble for

SEM and EDX measurements. For macroporous Si films, after plan view (top view) imaging (by attaching films flat on the surface of the carbon tape), a cross-sectional film view can be observed by tilting the film ~90° and attaching it to the carbon tape. All samples were imaged at 20 kV without sputter coating.

For mesoporous silicon powder, because the individual pores are too small to be detected by the JEOL JSM-6100 SEM, transmission electron microscopy (TEM) is needed. The characteristic pore widths on the order of several nm were observed on a high resolution TEM instrument (JEOL JEM-2100, operation at 200 kV). The distribution of triclosan in pores was not detected by TEM due to the instability of triclosan under high temperatures caused by electron beam emission.

For evidence regarding triclosan crystallinity in porous Si, samples of pure triclosan, unloaded PSi powder, and triclosan-loaded samples (melt A, nonblended and blended samples) were examined using a Philips XRG-3100 X-ray diffractometer (XRD). While scans of broad ranges (25–60°) contain several prominent Si peaks and some smaller peaks for triclosan, further investigations revealed that the 20–30° region is a better selection in which several strong triclosan peaks appear, with only one strong Si feature in this range (at 28.4°). The existence of amorphous or nanostructured triclosan can be found through intensity loss or broadening of signature X-ray reflections.

For a more representative evaluation of the macroscopic drug loading in the entire sample, thermogravimetric analysis (TGA) was conducted on a Seiko SSC 5200 TGA instrument. A given loaded sample was placed in a platinum pan and nitrogen gas was introduced into the sample chamber to prevent PSi oxidation during the increased temperature from room temperature to 600 °C during the analysis.

For measurements of release, loaded samples were soaked into sterile water and UV/visible spectroscopy was used to monitor the amount of triclosan released in water at 280 nm in wavelength. The analysis was carried out on an Agilent 8453 UV/visible spectrophotometer.

2.2.4 Triclosan Release Performance of Loaded PSi Samples

As previously mentioned in Chapter I, two methods, including a disk diffusion method and a broth dilution method, are involved in the antibacterial assays. In this research, two modified methods based upon disk diffusion method were employed. One is a disk diffusion method with solid loaded sample placed in the presence of the bacteria, and the other one is a disk diffusion method with triclosan-diffused supernatant. The details for each method are depicted below.

2.2.4.1 Disk Diffusion Method with Solid Loaded Sample

This method involves placing solid triclosan loaded PSi powder directly on top of a filter paper disk on an inoculated Petri dish, where triclosan in PSi is allowed to diffuse into the surroundings.

The first step in this method was to create different dilutions of triclosan loaded PSi with a series of concentrations. The dilutions were carried out by mixing 2 mg of triclosan loaded PSi (melt A, nonblended, blended PSi) with 18 mg unloaded PSi with 81% porosity in a 1.5 mL microfuge tube. The tubes were shaken for a few seconds by Vortex shaker in order to thoroughly mix the contents of this 1:10 dilution. 2 mg of this mixture were then combined again with 18 mg 81% unloaded PSi in a new microfuge tube to create a 1:100 dilution. This process was repeated to create 1:1000 and 1:10,000 dilutions.

Then 2 mg of the diluted melt A, nonblended, or blended PSi samples were placed on top of a 7 mm diameter filter paper disk, and then spread out as evenly as possible over the surface. The disk with PSi face-up was then carefully transferred to an LB-agar (also known as Lysogeny broth, Luria broth, Lennox broth, and Luria-Bertani broth) plate containing 100 μL of LB medium with an overnight culture of incubated *S. aureus*, prepared using the procedure described in Section 2.2.4.3. One paper disk was placed in the dish on the first day; based on the size of its inhibition zone, a certain number of additional disks were placed in subsequent Petri dishes to yield triplicate (or greater) measurements. The Petri dishes were then incubated at 37 °C for either 12 or 24 hours. After the allotted time had passed, a new LB plate was inoculated with *S. aureus* and the disks were transferred again with sterilized forceps to the new plate, which was incubated at 37 °C, again for 12 or 24 hours. The diameters of the halos formed from bacterial inhibition on the old Petri dish were measured with a ruler, by leaving the plate face-up. Incubation, measurements, and transfers were repeated at regular intervals until the disks no longer produced bacterial inhibition zones.

2.2.4.2 Disk Diffusion Method with Triclosan Diffused Supernatant

In the antibacterial assay of triclosan loaded PSi by disk diffusion method, the concentration of triclosan released from PSi is monitored every day. Before the triclosan loaded PSi release assessment using its diffused supernatant, it is necessary to prepare a standard curve that is used for the subsequent calculations of the released triclosan concentration. Figure 25 shows a linear relationship between UV/visible absorbance at 280 nm and the concentration of triclosan, satisfying the functional equation of y =

0.0128x, where x refers to the concentration of triclosan and y is the UV/visible absorbance value.

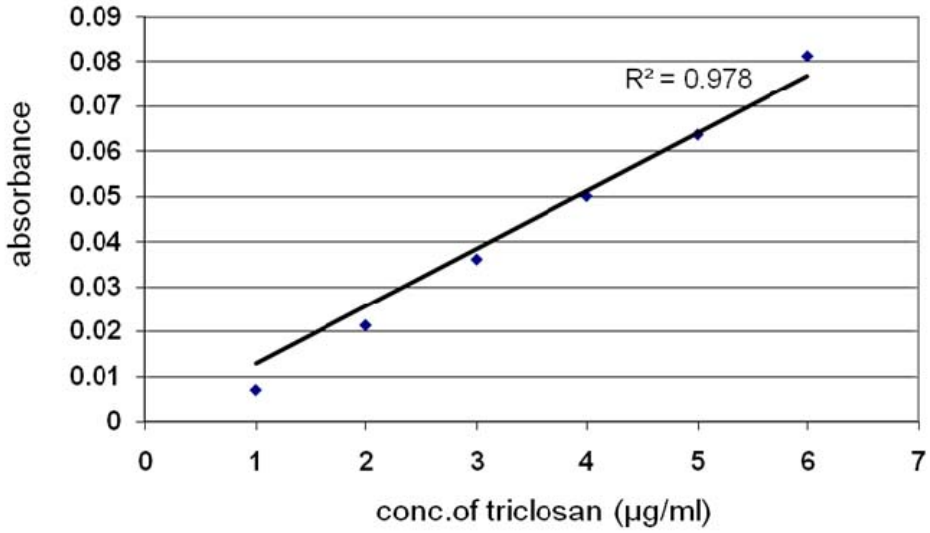

Figure 25. Linear relationship between UV/visible absorbance and triclosan concentration.

For loaded samples, 5 mg of triclosan loaded PSi powder or 1 piece of macroporous silicon film (~ 0.5 ×0.7 cm^2) was soaked in 1.0 mL of sterile water in a 1.5 mL microcentrifuge tube for each type of material (melt A, nonblended and blended). The tubes were continuously rotated using a LabQuake agitating apparatus at 37 °C. After a time interval of 24 hours, the tube was centrifuged and as much supernatant as possible (~ 950 μL) was carefully drawn out of the tube to a new microcentrifuge tube. Another fresh 1.0 mL aliquot of sterile DI water was added into the microcentrifuge tube containing the PSi. These tubes were again rotated in the LabQuake for another 24 hours at 37 ^{o}C. A 20 μL fraction of supernatant was dropped onto a paper disk already placed on the top of a LB-agar plate containing 100 μL of LB medium with incubated *S. aureus* for 24 hr (overnight culture). The Petri dish with paper disks were incubated for 24 hours at 37 °C. The remaining supernatant containing diffused triclosan was quantitatively

evaluated by UV/visible spectrophotometry to determine the concentration of triclosan using absorbance values at 280 nm; such values were converted to triclosan concentrations via use of a standard curve generated independently from solutions of known concentration (see next paragraph). The above procedures (starting from a new soaking by adding another fresh 1.0 mL water) were repeated every 24 hours until no inhibition activity was detected from the supernatant exposed to the porous Si powder. Therefore, this activity was specifically evaluated not only by measuring the inhibition zone of bacterial growth of *S. aureus*, but also by calculating the concentration of triclosan versus the overall duration of inhibition activity for triclosan released from PSi carriers. It should be noted that the triclosan released behavior of macroporous silicon film was only analyzed by this method.

As a control, pure triclosan powder was treated as the same way as triclosan loaded PSi samples. Pure triclosan particles with the amount equivalent to the average level of triclosan loaded in PSi matrices, about 3 mg, were soaked in 1 mL of sterile DI water in a microcentrifuge tube and rotated on a LabQuake. The dissolving equilibrated triclosan solution was subjected to the above evaluation and quantitative UV/visible analysis at hour intervals at 37 °C up to 24 hours. The standard curve of triclosan used for concentration calculation was plotted as a function of the absorbances of triclosan solution versus the given concentrations of 1 μg/mL, 2 μg/mL,3 μg/mL, 4 μg/mL, 5 μg/mL, and 6 μg/mL. The equation correlating the absorbance with concentration of triclosan was obtained by a linear least squares fit.

2.2.4.3 Bacterial Culture

LB-agar plates were prepared in a 2 L Erlenmeyer flask using 25 g of LB medium and 15 g of agar for each liter of DI water. This mixture was autoclaved, and allowed to cool in a water bath at 50 °C for approximately 15–20 minutes. The warm medium was poured into 100 mm Petri dishes, with an average of 30 mL medium per each dish. The plates were left at room temperature for at least 24 hours so as to reduce condensation, and then stored at 4 °C until use.

An autoclaved solution of LB medium (5 g) in 200 mL of DI water was used as the medium for overnight *S. aureus* culture. Approximately 1.5 mL of this medium was poured into a plastic test tube, and inoculated with a few colonies (1-2 colonies) of *S. aureus* by a flame-sterilized loop. The *S. aureus* culture was ready for the antibacterial assay the next day.

On the second day, LB plates were inoculated with 100 μL of overnight liquid LB bacteria culture (containing approximately 10^7 bacteria per dish) using a flame-sterilized glass pipette with a bent tip. Bacteria were thoroughly spread over the entire surface of the medium to establish a confluent lawn of growth. Following the different antibacterial assay methods, autoclaved filter paper discs were transferred into a given Petri dish.

2.3 Results and Discussion

2.3.1 Characterization of Triclosan-Loaded PSi Samples

The triclosan-loaded PSi samples were first characterized by SEM. Figure 26 presents the morphologies of melt A, nonblended and blended PSi particles. In the SEM images shown, the larger particle size of melt A is readily apparent (Figure 26a), and the

particle size of blended PSi seems more uniform (Figure 26c); some individual PSi particle agglomeration is also possible for the melt A sample due to the presence of excess triclosan during the cooling process. For mesoporous silicon powder, the individual pores are too small to be detected by SEM, but for macroporous silicon film, from the plan view, individual macropores are shown clearly on the surface (Figure 26d, e) and the etched pore channels on the order of ~ 10^2 nm are also observed in the cross section images at this level of magnification (Figure 26e, f).

In terms of composition, detection of triclosan loaded into these porous Si structures is possible by energy-dispersive X-ray (EDX) spectroscopy (Figure 27). Because of the limited sampling volume, it can only provide a selected distribution of drug loading in different microscopic areas instead of an entire sample, but nevertheless confirms the presence of the drug in these materials. In this study, chlorine (Cl) is the characteristic element for triclosan, for which it contains 25.9% by weight in melt A in one microscopic area measurement. The elemental analysis is based on their K_α transition peaks. For mesoporous silicon samples, the distribution of triclosan is relatively uniform (measured in ten different areas on each sample under the same magnification). The Cl concentrations of melt A are between 24–33 wt%; for nonblended and blended PSi samples, the Cl concentrations are in the ranges of 6-12 wt% and 6-10 wt%, respectively. For the macroporous silicon film, there is an uneven distribution of Cl levels within a given pore.

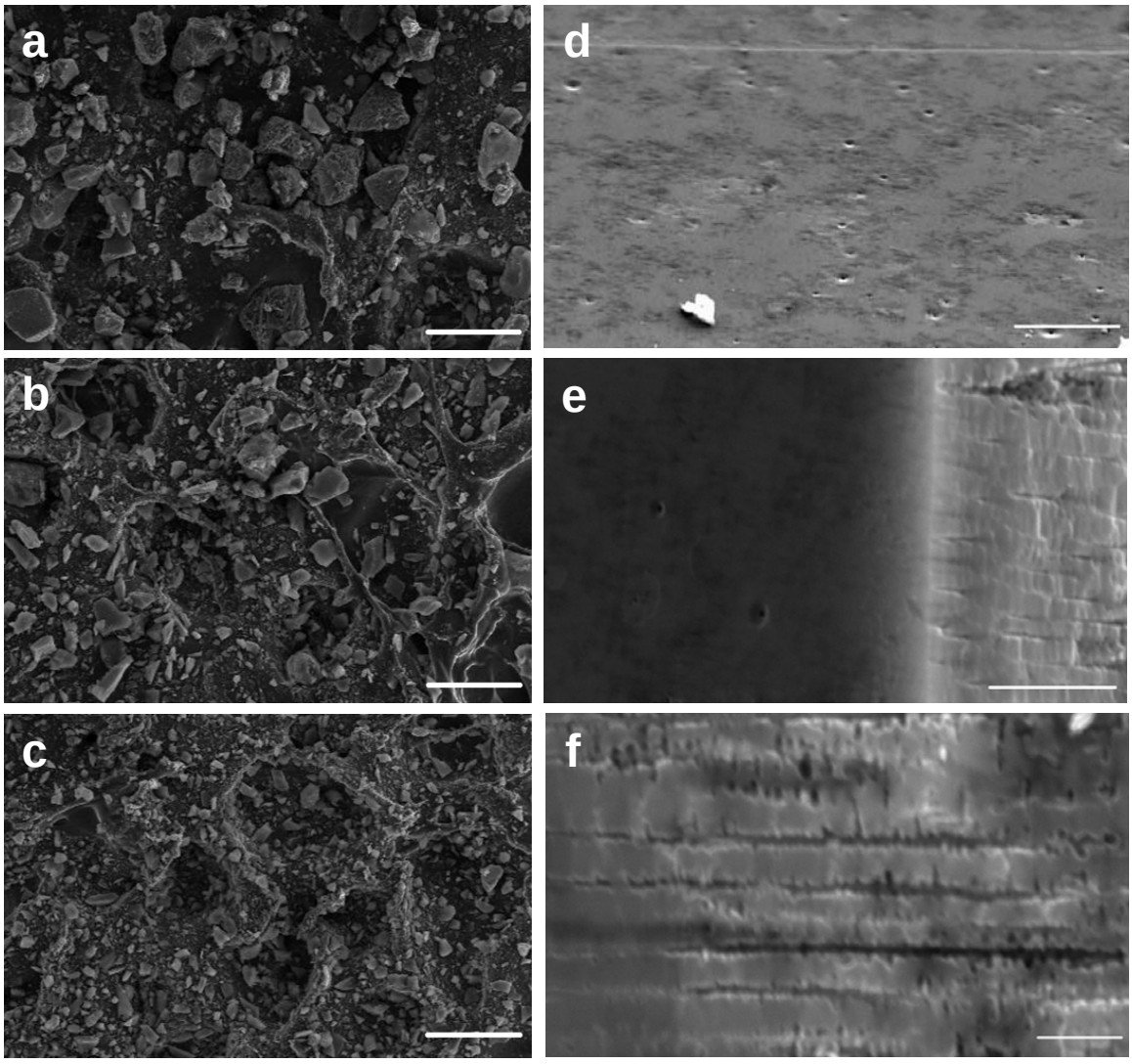

Figure 26. The morphologies of porous silicon samples loaded with triclosan. (a-c) plan view images (SEM) for melt A, nonblended, and blended samples, respectively. (d-f) SEM images for macroporous Si film from (d) plan view; (e) cross sectional view of macroporous Si/solid Si wafer interface; (f) higher magnification cross sectional image of macroporous Si. Scale bars: 200 μm for a-c, 10 μm, 5 μm, 2 μm for d, e, f, respectively.

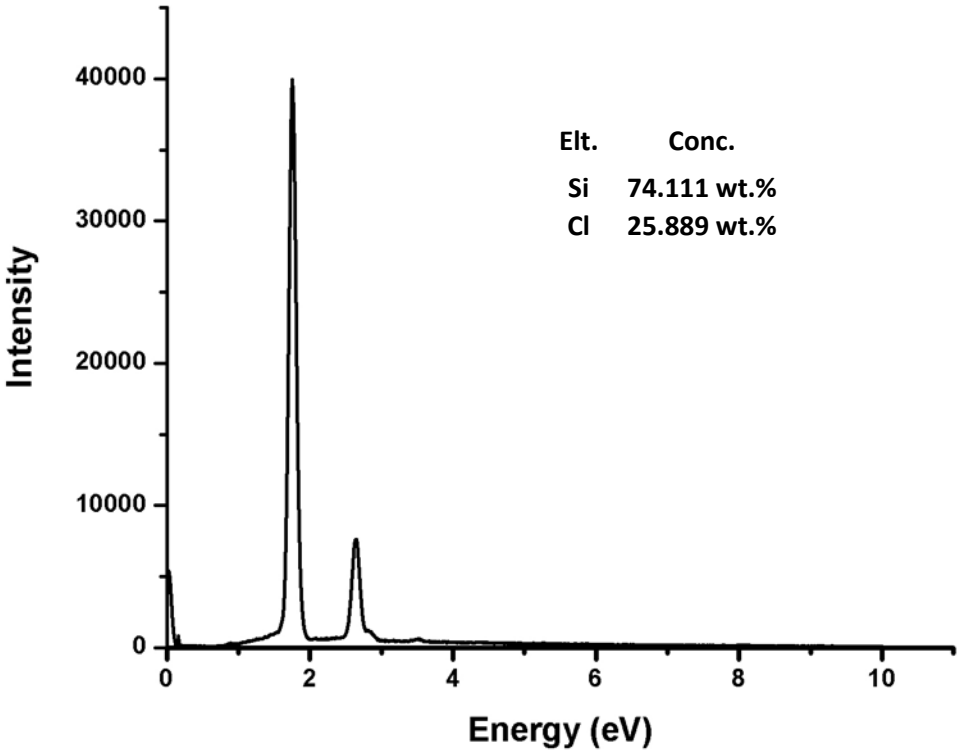

Figure 27. Typical EDX spectrum for melt A sample.

High resolution TEM was used to further observe the internal structure of mesopores in the PSi particles. Figure 28 shows the mesopores morphology of melt A, nonblended, and blended PSi samples. Because of the similar anodization method in their preparation, the pores of these triclosan-loaded mesoporous samples have effectively the same morphology under high resolution TEM. The images taken from melt A, nonblended PSi, and blended sample at lower magnification show the ordered and linear pore channels along the direction of elongation (as shown in Figure 28a, b). Images taken under high magnification from a blended PSi sample (as shown in Figure 28c) provide a close view of the channels, presenting a connected network of nanoscale silicon pores. In some areas, the Si lattice structure can be seen (Figure 28d).

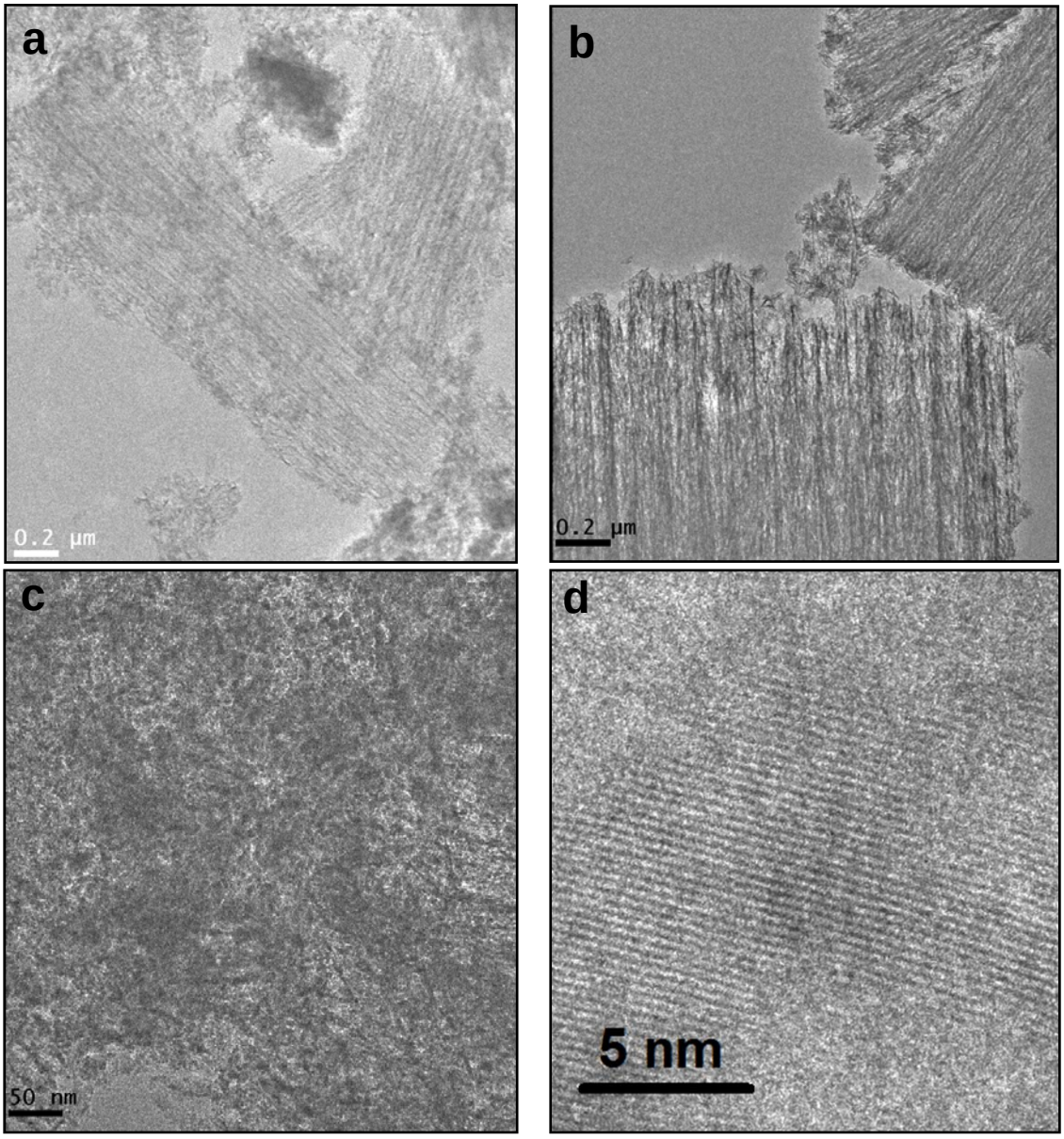

Figure 28. The morphologies of mesopores in PSi particles. TEM images for melt A (a) and nonblended PSi (b) at lower magnification; blended PSi (c, d) at higher magnification.

As mentioned before, TGA provides an evaluation of the drug loading in the entire sample. TGA results for triclosan loading in melt A (Figure 29a), nonblended PSi (Figure 29b), blended PSi (Figure 29c) and macroporous silicon (Figure 29d) are 72.9%, 44.1%, 47.9%, and 1.1%, respectively. For the mesoporous silicon samples analyzed here,

significant mass loss begins at around 125 °C, slightly above the boiling point of triclosan (120 °C). If a large excess of triclosan is present on the surface of a given sample, then there should be two stages of weight loss observed. The first stage is for the surface component, followed by the second stage for loss of triclosan in the pores. In the case of mesoporous Si, the triclosan is eliminated from the carrier in a single extended period ranging from 125 to 225 °C, indicating the diffusion from the porous matrix. For the macroporous silicon film, the lower triclosan loading in large parallel pores is reflected in the small mass loss that is complete by 150 °C required for thermal desorption of the loaded active species.

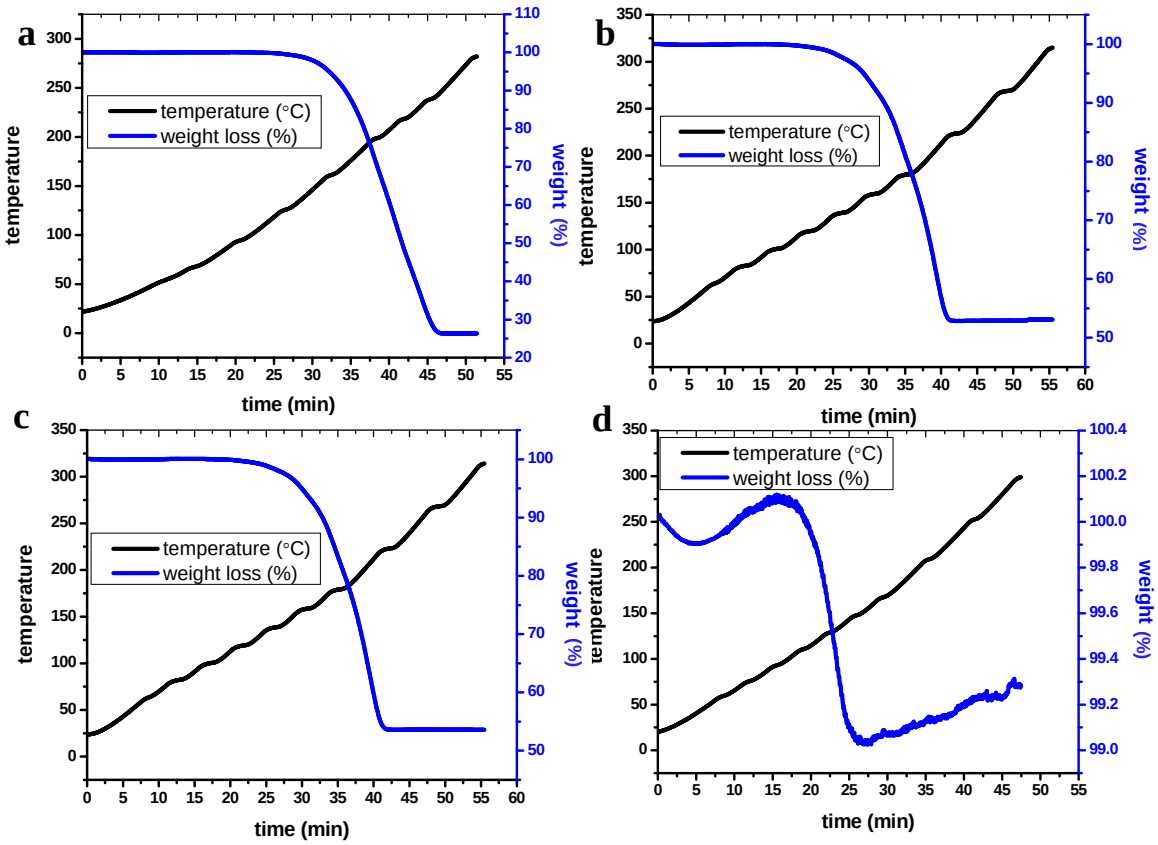

Figure 29. TGA measurements for (a) melt A sample, (b) nonblended sample, (c) blended sample, and (d) macroporous Si film.

X-ray diffraction (XRD) spectra were taken on the triclosan-loaded porous silicon samples, as well as pure triclosan and unloaded PSi as reference. As noted earlier, diffraction angles between 20° and 30° were selected as the best region where significant characteristic peaks of PSi and triclosan are present (Figures 30a and b). For the high porosity triclosan-loaded (melt A) sample, some triclosan features are observed, most notably for the peaks near 24° and 25°; the most significant differences between the sample and pure triclosan include substantial line broadening in the 25° peak (6 times broader for melt A), and unlike pure triclosan, the feature at 25° is more intense than the peak at 24°. This observation suggests that in addition to material confined in the pores, there is some amount of triclosan present with some degree of crystallinity on the surface of PSi. However the relative intensity reversal of the two peaks near 24° and 25° indicates that the crystalline structure of triclosan has been changed, and the broadened peaks are consistent with a reduction in triclosan crystal size. For the nonblended and blended samples, no significant characteristic peaks for crystalline triclosan were discerned. These are presumably the results of a nanostructuring or amorphization effect by induced nanoscale pores of the silicon.

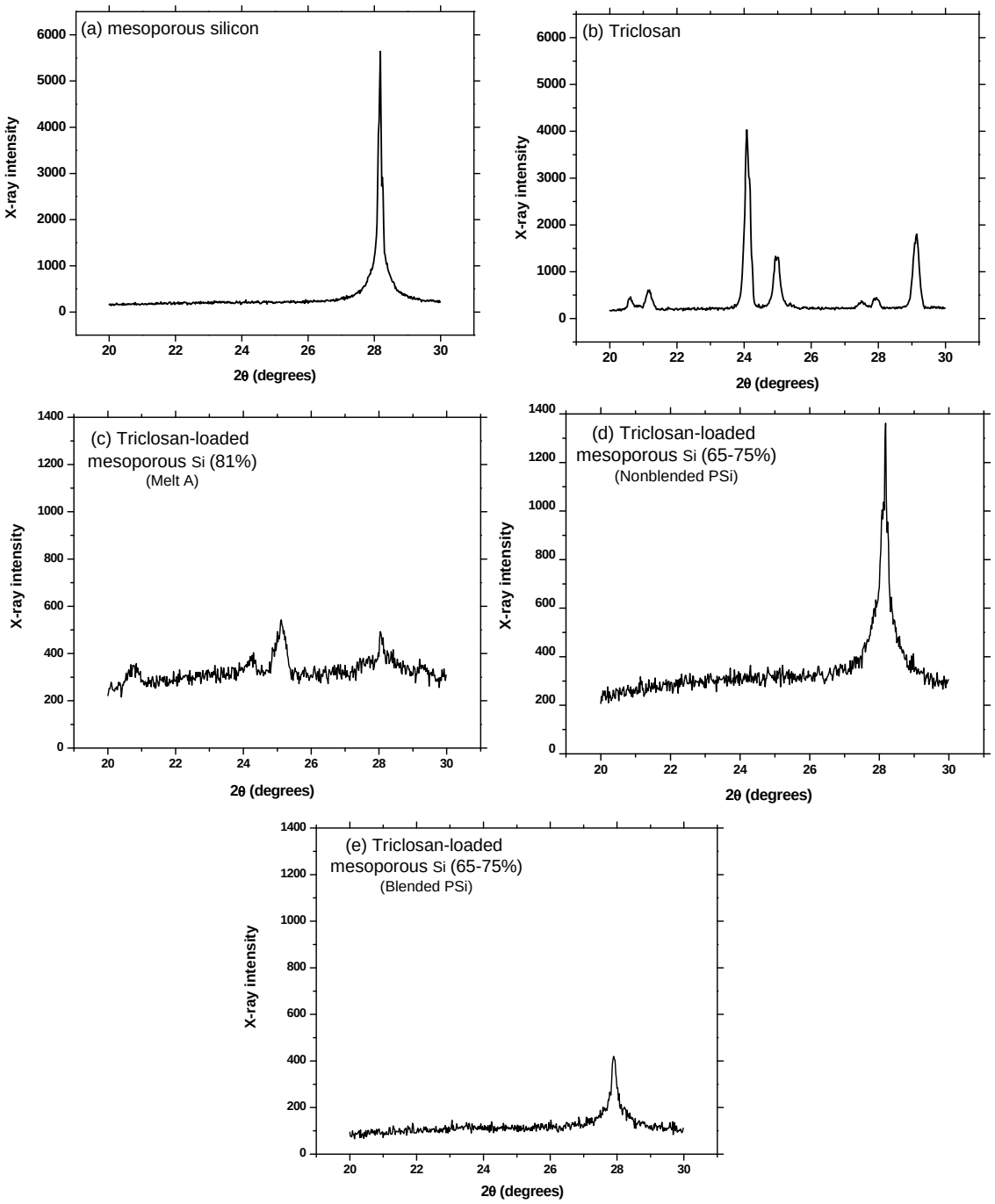

Figure 30. X-ray diffraction spectra for (a) nonleaded mesoporous Si (65-75% porosity), (b) crystalline triclosan, (c) triclosan-loaded mesoporous Si (melt A), (d) triclosan-loaded mesoporous Si, nonblended sample and (e) triclosan-loaded mesoporous Si, blended sample.

2.3.2 Assessment of Antibacterial Activity

2.3.2.1 Disk Diffusion Method with Solid Loaded Sample

As noted in the experimental section, one method to evaluate antibacterial activity of these samples is to release triclosan directly from the solid loaded samples against *S. Aureus*. Figure 31 shows the inhibition of the growth of bacteria *S. aureus* by released triclosan. The halos surrounding the disk containing the porous Si are the inhibition zones.

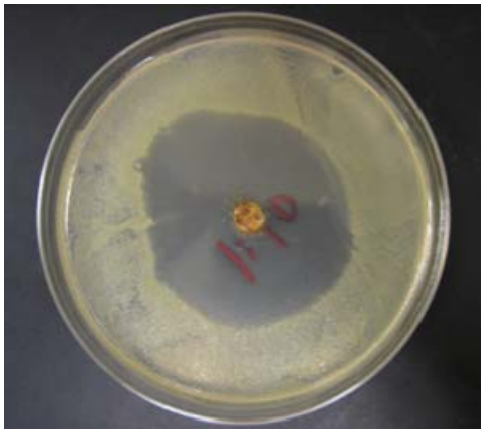

Figure 31.Inhibition zone of bacteria formed by the triclosan released from PSi particles on paper disc (~50 mm).

Figure 32 shows the inhibition zone of bacterial growth formed by the 1:1,000 and 1:10,000 dilutions of melt A, nonblended and blended PSi samples and measured every 12 h. The dimension of a given paper disk is measured as 7 mm; therefore, halo diameters reaching 7 mm means a loss of measurable antibacterial activity. The activity durations of the three dilutions are between 60–84 h, remaining up to 84 h for a 1:1,000 dilution of melt A and nonblended PSi samples, and 72 h for 1:1,000 dilution of blended PSi samples. A 1:10,000 dilution of each sample type has a 12–24 h shorter duration time than that of its 1:1,000 dilution. As melt A with highest porosity (81%) and

corresponding highest loading (72.9%), 1:1,000 dilution of melt A gave the largest inhibition zone, up to 32 mm, contrasting to a 23 mm inhibition zone generated by 1:1,000 dilutions of nonblended PSi and blended PSi with a lower porosity (65%–75%) and lower loading in the original undiluted sample.

The clear disadvantage of the analysis by this method is that there is no way to assess the amount of triclosan released against *S. aureus*. Furthermore, the standard deviation of some specific data points is apparently large, due to random shapes of inhibitions halos generated by the uneven paving of loaded PSi on paper disks, (in Figure 31). Given such considerations, another method was investigated.

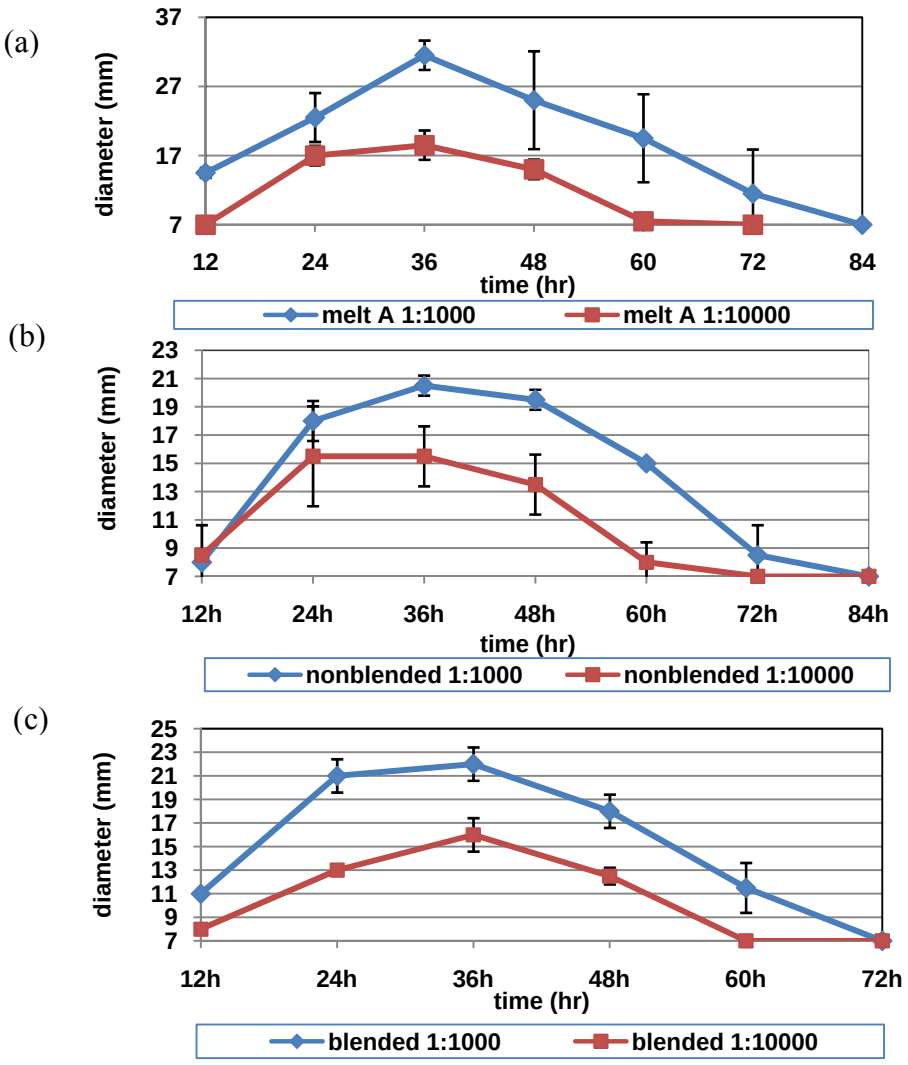

Figure 32. Inhibition zone of bacterial growth for melt A (a), nonblended (b) and blended PSi (c) due to triclosan release as a function of time.

2.3.2.2 Disk Diffusion Method with Triclosan Diffused Supernatant

Figure 33 illustrates the typical antibacterial activity as a function of time for a 5 mg mesoporous Si sample loaded with triclosan (melt A, nonblended and blended PSi), as well as a typical size (39.59 mm^2, shown in Table 1) macroporous Si film. Also shown in this plot are the corresponding concentrations of active drug released (measured spectrophotometrically) per 24 h period.

For the mesoporous materials, the extended release of triclosan over the period measured is quite remarkable; by the 15^{th} day, the highest release percentage of triclosan in total payload to the surroundings was only 7.96% from nonblended PSi sample (and 16.96% in 70 days), and the release and associated activity continues beyond a period of 100 days. Similar behavior is observed in the other mesoporous samples; the sample melt A with the high porosity (81%) loaded with 72.9% triclosan released 3.29% in 15 days (7.87% in 70 days) and the sample of 65–75% porosity loaded by the blended technique released 5.84% of a total 47.92% payload of triclosan in the same time frame (and 12.39% in 70 days). The macroporous sample serves as a useful benchmark for diminished loading and activity, at 13% porosity and a lower triclosan loading percentage (1%), it can only release a maximum of 420 μg, in contrast to the 2–3 mg maximum release capacity of the mesoporous samples as shown in Table 1. Its antibacterial activity is complete within 18 days of release.

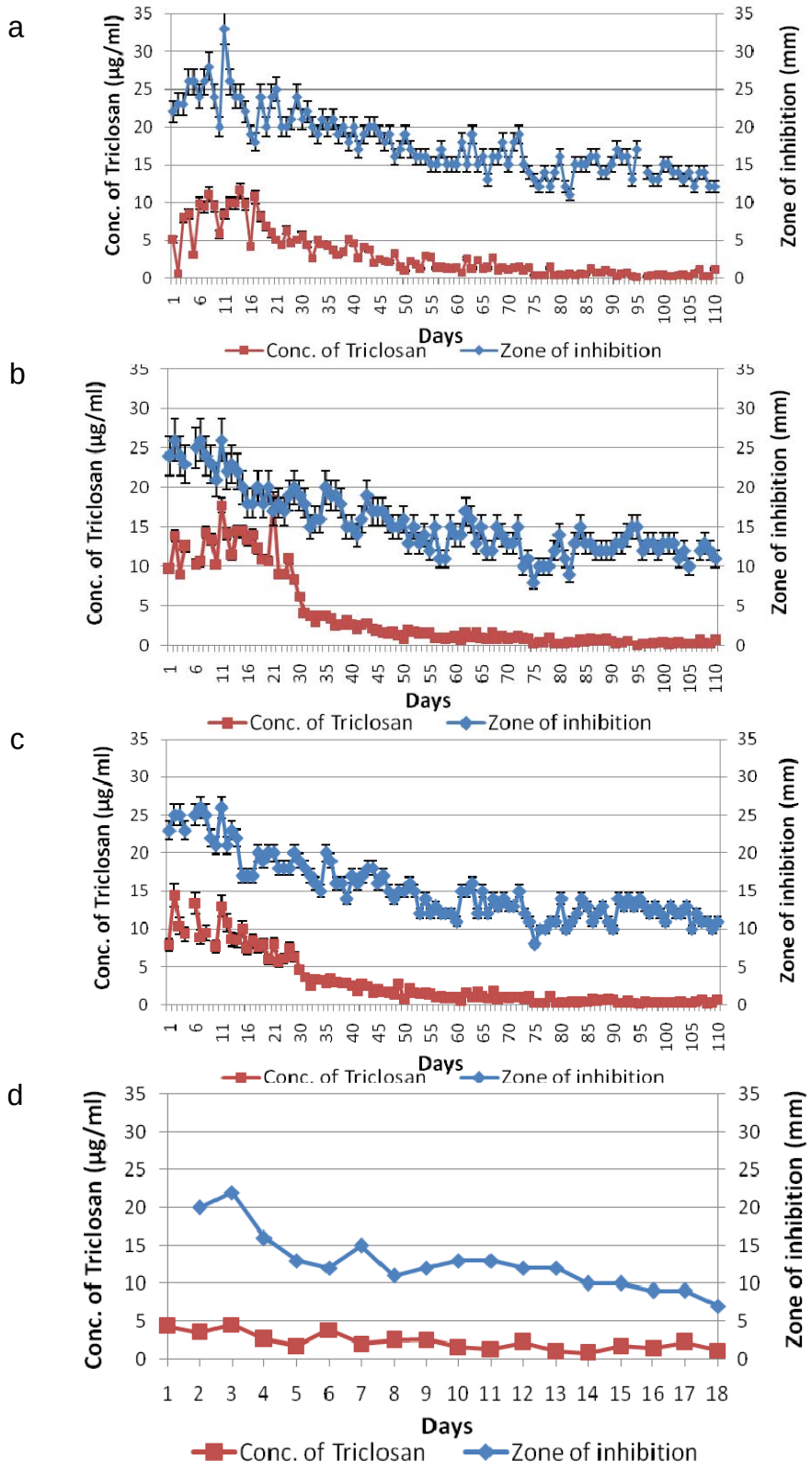

Figure 33. Combined zone inhibition assay/triclosan concentration release assays for (a) melt A, (b) nonblended, (c) blended sample, and (d) macroporous silicon film.

The average concentration of triclosan released from the nonblended PSi samples in the first 15 days is 12 μg/mL (Table 1), which is 3-fold higher than the maximum concentration of the macroporous sample (4 μg/mL). The initial concentration of released active of 4 μg/mL subsequently drops to 2 μg/mL within a week for macroporous silicon sample is significantly different from the release behaviors of mesoporous silicon samples. These differences in drug release concentration do correlate overall with antibacterial activity. For the three mesoporous sample types, the average inhibition zone diameter for the *S. aureus* growth lies above 23 mm (Figure 33) for the first 15 days of activity. In contrast, the triclosan-loaded macroporous sample produces an inhibition zone diameter of 19 mm in the first 24 h, but experiences a precipitous drop after this initial release and reaches a value of ~10 mm in 15 days.

A relevant associated issue that affects the porous Si drug delivery lies in the differences between the concentration of drug released from PSi to the surroundings in a given 24 hours period and triclosan dissolution in water during the same time. To probe this difference, exposure of comparable amounts of triclosan (3 mg) and triclosan (2.3 mg) loaded into mesoporous Si (5 mg total) to water were individually evaluated at hour intervals at 37 °C up to a total of 24 h (Figure 34). At a given time interval the concentration of triclosan released from the mesoporous silicon is effectively 3-4 times greater than the value extracted for the aqueous solution exposed to solid triclosan. For example, at 7 h exposure, the nonblended sample has released triclosan at a concentration of approximately 15 μg/mL, while the amount of triclosan extracted into water from the solid antibacterial compound is 5 μg/mL. The possibility that this specific loading process generates some types of amorphization or nanostructuring by the porous Si matrix for the

triclosan is supported by an examination of release behavior among porous Si samples, which is consistent with the earlier analysis of the results derived from X-ray diffraction.

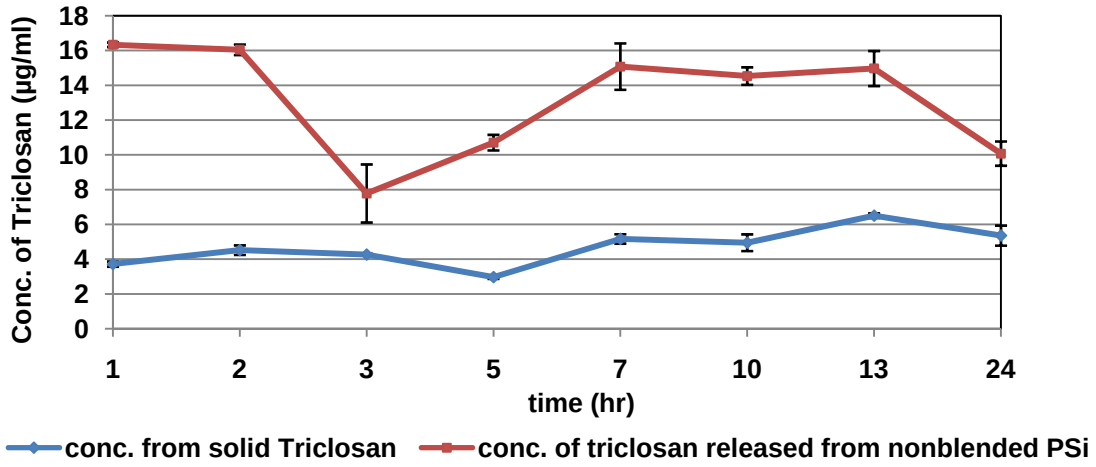

Figure 34. Comparison of triclosan dissolution into water as a function of time for solid triclosan (blue diamonds, bottom line) versus triclosan-loaded mesoporous Si (nonblended sample; red squares, top line) at 37°C.

2.3.3 Factors Affecting Triclosan Delivery from Porous Silicon

The porous silicon samples involved in this research bear different properties, including various porosities, pore sizes and particle sizes. In general, the higher porosity PSi has, the more adequate space can be provided for payload. Particle size is directly related to the surface area. With the pore volume and sample mass fixed, smaller particles have a bigger surface area, in which more molecules for delivery can be attached. In addition, for the smallest mesopores, pore width is expected to play a role in release behavior of loaded species due to nanostructuring effects.

Therefore, in a comparison between the mesoporous silicon samples and the macroporous silicon films, the main factors causing the differences in release and corresponding antibacterial activity are porosity and pore size. A macroporous silicon

film with only 13% porosity cannot provide the same capacity as mesoporous silicon samples with 81% porosity to load comparable amounts of triclosan. Meanwhile, the pores with smaller size have more potential to reduce drug size to the nanoparticles, thereby greatly increasing the surface area and leading to enhanced dissolution. This phenomenon is referred to as a nanostructuring effect. Macropores are in the order of 200 nm and mesopores are between 5-50 nm. Depending on the pore size, mesoporous silicon samples have the ability to reduce triclosan crystalline domains to 5-50 nm, while macropores can only reduce triclosan particles to around 200 nm. Thus, the samller the triclosan particles, the higher their solubility. Hence, mesoporous silicon samples released higher concentration and amount of triclosan than macroporous silicon films.

In a comparison among three different mesoporous silicon samples, because of the coexistence of multiple variables, including porosity, particle size, and loading method or conditions, it is difficult to distinguish the specific impact of one single factor from others on drug delivery. These three samples are all mesoporous silicon, with similar pore size, in the order of a few nanometers up to 50 nm. The most significant difference between these three samples is porosity, as melt A with an 81% porosity has a 72.9% loading of triclosan, higher than the PSi with porosity value in the nonblended and blended PSi with 65-75% porosity, and ~40% loading. It is clear that PSi with higher porosity gives the higher loading.

However, slight differences in the other factors may affect drug delivery. For example, there are slight differences in particle size (150-250 μm *vs.* 100 μm *vs.* 50 μm), loading temperatures (90 °C *vs.* 100 °C), and the mixing method of triclosan and PSi particles.

The most interesting observation is that the melt A has highest loading of triclosan. However, for the overall time period evaluated, the concentration and amount of triclosan released from melt A are lower than that of nonblended and blended PSi samples. This is possibly due to an overfill of triclosan in melt A samples, which is reflected in the XRD data. As mentioned earlier, XRD spectra suggest that there is a trace amount of triclosan with some degree of crystallinity in the melt A sample, but for nonblended and blended PSi, triclosan exists in amorphous form or the triclosan particle size is of a very small nanocrystalline dimension. The nanocrystalline/amorphous triclosan not only possesses a relatively higher surface area, but also a higher equilibrium solubility.

In terms of antibacterial assays, it is clear that the second method is preferred, and that the first method suffers from many problems: (1) uniform placement of PSi particles on different disks for different experiments, causing an asymmetric release of drug around the disk; (2) facile contamination when transferring PSi-containing disks from one petri dish to the next; (3) the amount of triclosan released into the bacterial surroundings cannot be determined quantitatively. The second method overcomes all of these limitations and was used in the further studies.

2.4 Summary

This comparison of the mesoporous silicon and macroporous silicon on loading and release behavior of an antibacterial agent triclosan provides insight as to how the key factors of porous silicon structure influence drug delivery. Porosity is considered to be a critical element for high capacity loading. Pore types including macropores and mesopores also represent differences in their influence on incorporated drug structure.

The remarkable achievement in this study is mesoporous silicon ideally acts as an effective carrier for the sustained delivery (up to 100 days) of the antibacterial agent with an enhanced solubility by the nanostruturing effect with mesopores. In conclusion, the first attempt using different PSi matrices mainly investigates the role of porosity on the drug delivery, and also gives the direction of future exploration, such as investigations on surface chemistry and particle size of PSi. Finally, an appropriate method for the antibacterial assay is selected for the further studies.

III. Investigations of Triclosan Release Affected by PSi Surface Chemistry and Solution and Melt Loading Methods

3.1 Introduction

In the previous chapter, the utility of porous silicon in drug delivery was investigated by a comparison between macroporous silicon and mesoporous silicon samples. Porosity and pore size were considered as the main factors affecting the drug delivery behaviors.

In this chapter, additional properties are studied in detail. First, the role of surface chemistry is analyzed using PSi samples with hydrophobic and hydrophilic surfaces. For each type of surface, a solution method for loading triclosan is introduced to compare with the melt method developed in Chapter I. Two different particle sizes are also employed to evaluate if the particle size is a significant factor affecting drug delivery.

Overall, five groups of anodized mesoporous PSi samples loaded with triclosan are involved in this study. Group I is as-prepared PSi loaded by a solution method; group II is oxidized PSi loaded with a solution method; group III is as-prepared PSi loaded by a melt method; group IV is oxidized PSi loaded by a melt method; and group V is octyl-functionalized PSi loaded by both solution and melt methods. In groups I – IV, PSi with two particle size ranges of 38 – 75 μm and 150 – 250 μm are used, while only the smaller particle size range 38 – 75 μm is used for octyl-functionalization group V. All of the PSi materials are fabricated by the anodized electrochemical etching method described earlier, with the same porosity of 81% and similar pore size range. As-prepared PSi is freshly etched, with hydrogen termination on the surface, while oxidized PSi is obtained by thermal oxidation, with PSi surface converted from Si–H bonds to Si–OH bonds, and oxygen atoms inserted between some Si–Si bonds. Octyl-functionalization is achieved via a hydrosilylation route using 1-octene, thereby introducing long alkane chains on the

surface of PSi. Different from the melt method, the solution method involves the dissolution of triclosan in a suitable solvent, followed by its exposure to a mesoporous Si sample.

In terms of surface chemistry, oxidized PSi and as-prepared PSi have hydrophilic and hydrophobic surfaces, respectively. Octyl-functionalized PSi provides a hydrophobic surface, that resists degradation *in vitro* and *in vivo*. Thus, these different surfaces provide multiple points of comparison for analysis of the hydrophobic triclosan and either hydrophobic or hydrophilic PSi surfaces.

As described in last chapter, the melt method is the most suitable loading method for drugs with good thermal stability and low water solubility like triclosan. However, one challenge of the melt method is the uniformity of PSi powder blending with a given drug. The particle size, density, flowability, and the amount are important factors affecting PSi-drug blending.[146] In contrast, a solution based system is able to offer a homogenous environment for facile blending with the PSi particles. Hence, we also employ a solution method in this case in order to evaluate the differences between these two methods on both the loading triclosan into PSi matrices and their subsequent release behavior.

Finally, with the exception of octyl-functionalized PSi, two particle sizes (38 – 75 μm and 150 – 250 μm) are chosen for each group of PSi. Under the same conditions of fabrication, porosity, pore size, and loading method, particle size as the only variable is investigated to evaluate if it affects the drug delivery.

3.2 Experimental

3.2.1 Functionalization of PSi

PSi particles with both size ranges (38 – 75 μm and 150 – 250 μm) were surface oxidized by a 60 minute anneal in air at 600 °C, in order to convert the PSi surface from hydrophobic to hydrophilic character.

In order to introduce octyl groups and keep the surface hydrophobic, as-prepared PSi particles with 38 – 75 μm in size were functionalized by the following procedure:[76] 1) prepare a 1M 1-octene solution (in toluene); 2) add 10 mg of PSi to approximately 4 mL of 1M octene solution; 3) heat the mixture at reflux (113 °C) under argon for 20 hours; 4) cool the sample down to room temperature under argon protection, followed by centrifugation and drying the sample in vacuum overnight. The dry sample obtained was ready for subsequent characterization and triclosan loading.

The oxidized and octyl-functionalized PSi materials were characterized by Fourier Transform Infrared Spectroscopy (FTIR). Typically, a mixture of 1 mg: 100 mg of functionalized PSi to dry KBr was used in pellet form for FTIR measurements.

3.2.2 PSi Dissolution

As previously introduced in Chapter I, porous silicon is degradable in aqueous media in the form of silicic acid [$Si(OH)_4$].[61] Drug release is achieved by the cooperation of both drug diffusion from pores as well as PSi degradation over time. Therefore, the PSi degradation rate needs to be explicitly evaluated.

The measurement of PSi dissolution rate was achieved by monitoring silicic acid concentration spectrophotometrically. Samples were obtained by the same procedure

used in drug release/antibacterial assays from PSi, starting by soaking 5 mg of each type of unloaded PSi (as-prepared PSi, oxidized PSi and octyl-functionalized PSi) in 1 mL of sterile DI water in a microcentrifuge tube. After the microcentrifuge tubes were shaken at 37 °C for 24 hours, as much as possible of the dissolved solution was removed. A fresh 1 mL aliquot of sterile water was added to the original microcentrifuge tube to let the PSi dissolution continue. These steps were repeated in 24 hour intervals up to 15 days. The concentration of silicic acid in dissolved solution was determined by the Molybdenum Blue Method described below.

Reagents involved in the molybdenum blue method include: reagent a: 0.25 M hydrochloric acid prepared by mixing 22 mL of conc. HCl with water up to 1 liter; reagent b: 5% ammonium molybdate prepared by dissolving 5.2 g of $(NH_4)_6Mo_7O_{24}\cdot 4H_2O$ in water to a total volume of 100 mL; reagent c: 1% ethylenediaminetetraacetic acid disodium salt dihydrate (disodium EDTA) prepared by dissolving 1 g of disodium EDTA in water to 100 mL; reagent d: 17% sodium sulphite prepared by 42.5 g of sodium sulphite in water to total volume of 250 mL.[90]

A stock solution for silicic acid standard measurements was prepared by using sodium silicate pentahydrate as the Si source. A series of silica standards with concentration of 2.5 mg/L, 5 mg/L, 10 mg/L, 15 mg/L, 20 mg/L, and 40 mg/L were prepared.

All standard solutions (10.00 mL volume of different concentrations) as well as dissolved PSi solutions (0.50 mL of original dissolved solution diluted to 10.00 mL with water) and 10.00 mL of deionized water as blank were prepared in 50 mL Erlenmeyer flasks. 5.00 mL of hydrochloric acid solution (reagent a), 5.00 mL of ammonium

molybdate solution (reagent b), 5.00 mL of disodium EDTA solution (reagent c) and 5.00 mL of sodium sulphite solution (reagent d) were added into the above solutions in order. Sodium sulphite solution (reagent d) was added 5 minutes after the addition of molybdate (reagent b) to make sure the reaction was complete. After the addition of all reagents, the solutions were allowed to stand for approximately 30 minutes to reach the highest absorbance value possible (at 700 nm) using UV/visible spectrophotometry. The absorbances of standard solutions with known concentration against a deionized water blank were plotted as the reference, from which silica concentration (relative concentration of silicic acid) could then be determined.

3.2.3 Solution versus Melt Loading Method

The procedure for triclosan loading by melt method was similar to that of blended samples in Chapter II, in which 10 mg of PSi was pre-mixed with 25.7 mg of triclosan (loading target: 72%) in a glass vial by vortex spinning. In the case of small particle oxidized PSi by melt loading, a loading target of 42% was used. The resulting mixture was heated in an oven at 95 °C for 35 minutes. The loaded PSi sample was then cooled to room temperature and dried in vacuum overnight.

For solution loading, since triclosan has a high solubility in ethanol, and water can slow down the evaporation of ethanol and keep the volume of solvent in a certain range under heating, 2 mL of an ethanol/water solution (1:1) were used to dissolve 1.25 g of triclosan. Then 10 mg of PSi particles were soaked in the above triclosan solution. The mixture was heated by a water bath at 70 °C for one hour, and then centrifuged and dried in vacuum. All loaded samples were characterized by SEM, TEM, X-ray diffraction, and

TGA, followed by the antibacterial assays using the disk diffusion method with triclosan diffused supernatant (similar to the process described in Chapter II).

3.3 Results and Discussion

3.3.1 Characterization of PSi and Triclosan Loaded PSi

3.3.1.1 FTIR Measurement of Functionalized PSi

Figure 35 shows the surface characteristics of as-prepared PSi, oxidized PSi, and octyl-functionalized PSi in terms of their FTIR spectra. Figures 35a and 35b show the characteristics of PSi samples before and after octyl-functionalization, which are used for melt loading; while Figures 35c and 35d refer to the samples loaded by solution method.

Freshly HF etched PSi (Figures 35a and c) shows the main absorption bands associated with vibrations of ν(Si-H) at 2114 cm^{-1}, ν(Si-H_2) at 2090 cm^{-1}, ν(Si-O-Si) at 1095 cm^{-1}, δ(Si-H) at 630-670 cm^{-1}, and ν(Si-Si) at 628 cm^{-1}. Compared with the freshly HF etched PSi, it is noted that there is a vibration around 2800-3000 cm^{-1} for ν(C-H) in the spectra of the octyl-functionalized PSi samples (Figures 35b and d). This is consistent with the presence of an alkyl chain (Figure 35f), and confirms that the octyl group is successfully attached on the PSi surface. In the spectrum of oxidized PSi (Figure 35e), the absorption of Si-O at 1100 cm^{-1} (Si-O-Si) and 805 cm^{-1} (Si-OH), and O-H peaks (SiO-H) at 1600 cm^{-1} and 3500 cm^{-1} indicates the surface of the PSi has been oxidized.

Figure 36 presents the visual changes on the hydrophilicity of PSi before and after the surface modifications. A drop of water is added onto the surface of a given PSi sample. The one in the center is the as-prepared PSi with particle repulsion to the edges, showing its hydrophobicity; the octyl-functionalized PSi on the left behaves in a similar

manner. In contrast, the oxidized PSi on the right is clearly hydrophilic, as the PSi is dispersed in a relatively uniform way across the droplet. It is confirmed that PSi with the expected surface chemistry can be achieved successfully by the above transformations.

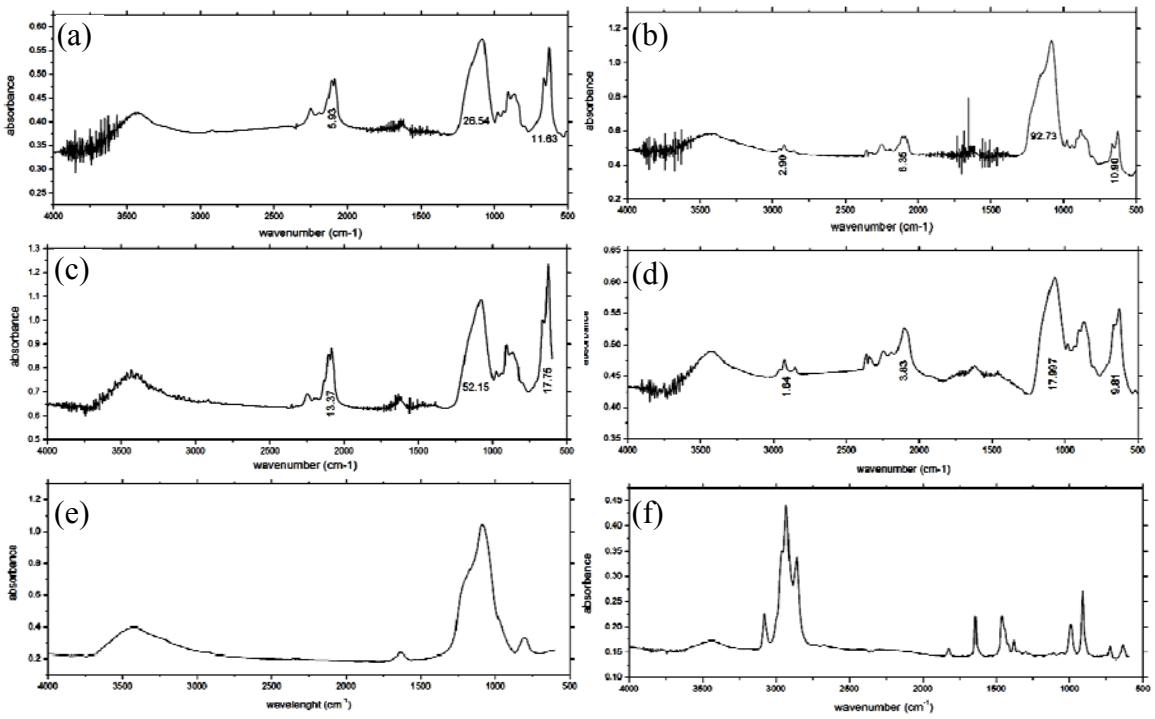

Figure 35. FTIR spectra of (a) freshly HF etched PSi samples (38 – 75 μm) used for melt loading, (b) octyl-functionalized PSi for melt loading; (c) as-prepared PSi used for solution loading, (d) octyl-functionalized PSi for solution loading; (e) oxidized PSi (38 – 75 μm); and (f) 1-octene.

Figure 36. Optical images of the PSi samples with different surface chemistry. Left: octyl-functionalized PSi; Center: as-prepared PSi; Right: oxidized PSi.

3.3.1.2 Anodized PSi Morphology Characterization by TEM and Combined Analysis

Figure 37 shows the TEM images of as-prepared PSi and octyl-functionalized PSi. In order to see pore structures of PSi by TEM, very small and thin particles were selected for characterization. Figure 37a shows the deep and ordered porous channels with a columnar nature, which is the result of anodized etching. A close magnification (Figure 37b) presents the porous structure, where dark areas are the remaining solid Si. For octyl-functionalized PSi, TEM images give substantially different surface morphological features (Figures 37c and 37d).

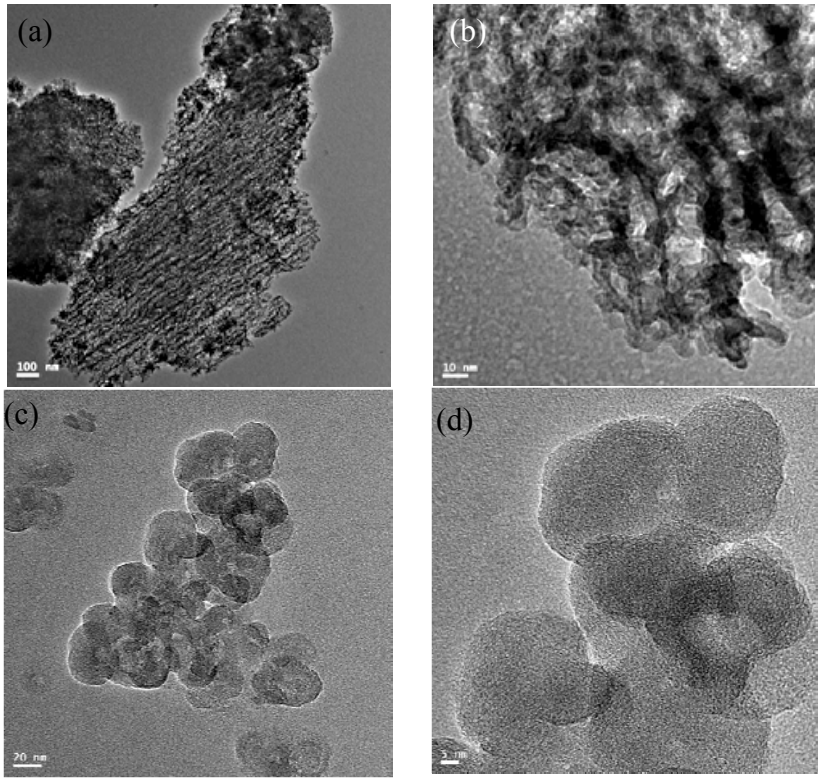

Figure 37. The morphology of (a) anodized as-prepared PSi particles and (b) a close magnification; (c) octyl-functionalized PSi and (d) under high magnification**.**

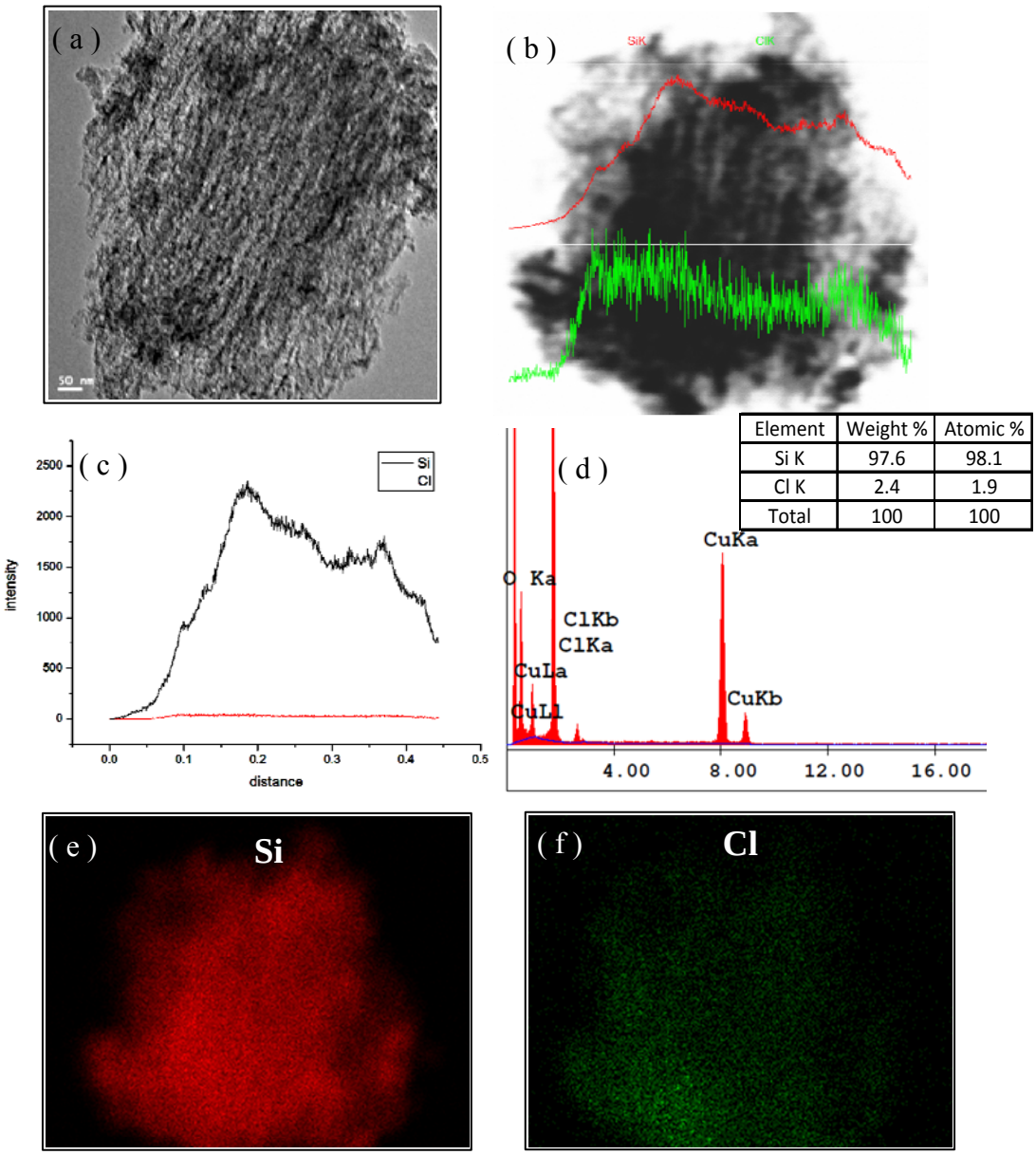

Figure 38. A single triclosan loaded PSi particle (as-prepared) characterized by TEM and analysis. (a) TEM image, (b, c) line scan, (d) EDX spectrum and element analysis, (e,f) EDX mapping.

Figure 38 shows the TEM image of a single PSi particle loaded with triclosan (Figure 38a) and the associated line scan (Figures 38b-c), EDX elemental analysis (Figure 38d), and EDX mapping (Figures 38e and f) of the same particle. The line scan crossing the particle shows significant intensity for silicon (Figures 38b and c). Although

the chlorine intensity is relatively weak, the elemental analysis and EDX mapping both confirm the presence of triclosan. The average weight percent of chlorine in this image is 1.9%.

3.3.1.3 TGA Measurements of Loaded PSi

Figure 39 shows typical TGA measurements of loaded PSi samples, which includes as-prepared PSi with small particle sizes loaded with triclosan by the a solution method (Figure 39a), oxidized PSi with big sizes loaded by a melt method (Figure 39b), and octyl-functionalized PSi with small sizes loaded by melt method (Figure 39c). The TGA measurements for these three representative types of loaded PSi, as well as melt A and other types described in Chapter II, reveal that all triclosan loaded PSi samples have similar loading, regardless of the particle size, surface chemistry and loading methods. The weight loss starts from around 120 °C, consistent with the boiling point of triclosan; and the entire process takes about 20 minutes to evaporate all the payload, finally keeping the weight at a stable level (the flat part at the end of the plots). Actual percentage values for each PSi sample will be given later in the discussion.

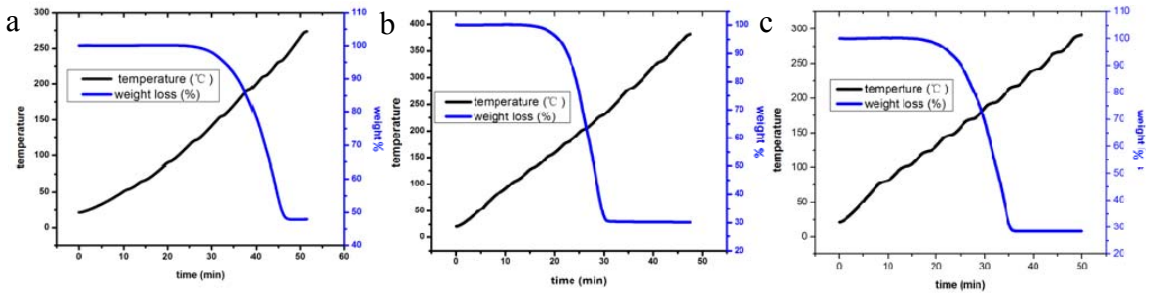

Figure 39. TGA measurements of (a) as-prepared PSi with 38-75 μm in size loaded by solution method, (b) oxidized PSi with 150-250 μm in size loaded by melt method, (c) octyl-functionalized PSi with 38-75 μm in size loaded by melt method.

3.3.1.4 X-ray Diffraction Examination

All loaded PSi were characterized by X-ray diffraction (XRD) in order to search for crystalline triclosan existence on the PSi surface. The spectra of two samples (PSi with small and big particles) in each group are shown within one figure (Figure 40). Compared with the spectra for as-prepared PSi and triclosan, oxidized PSi samples with a

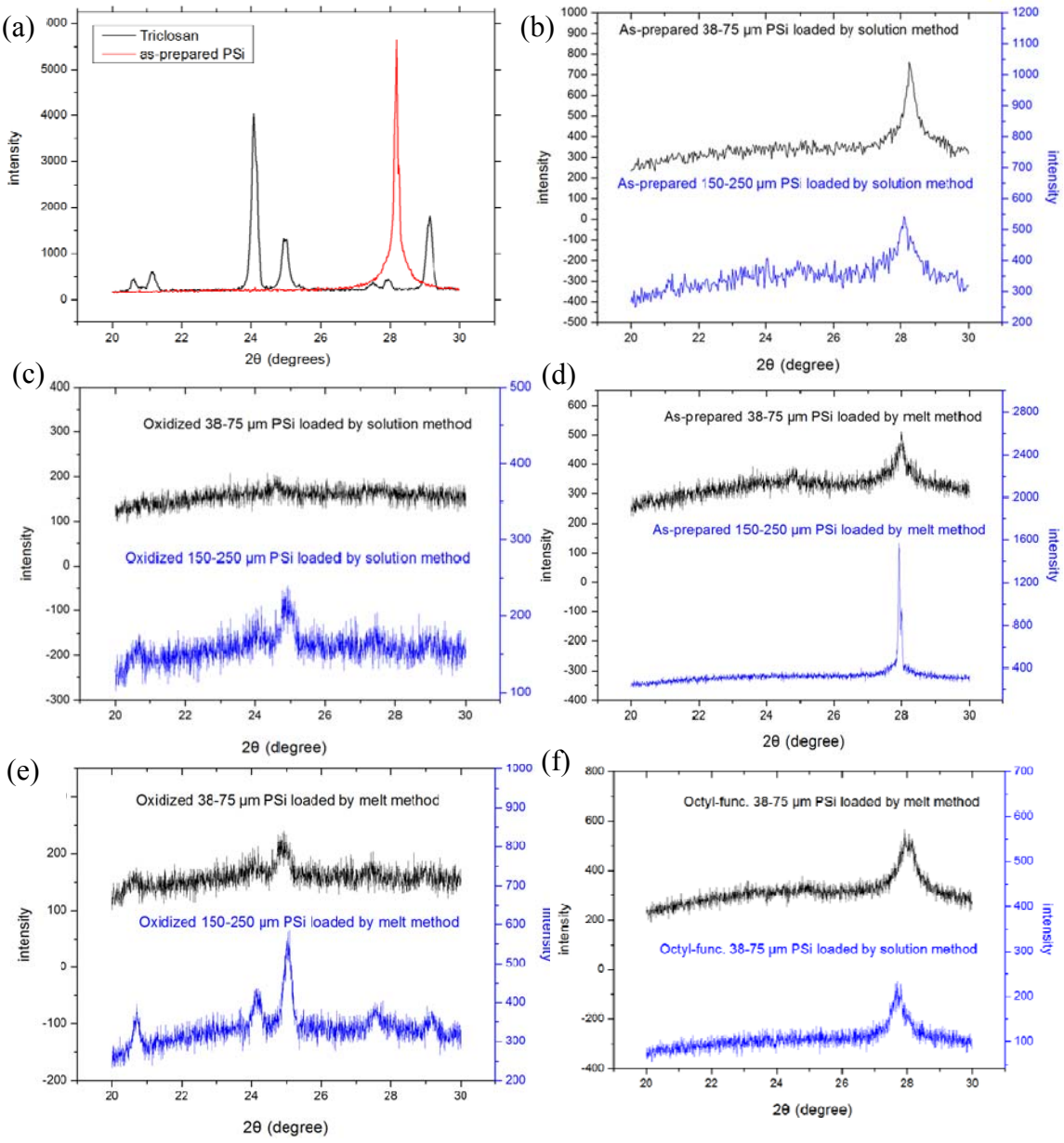

Figure 40. X-ray diffraction spectra of pure triclosan and unloaded as-prepared PSi (a), and all loaded PSi samples in five groups (b-f).

large particle size loaded by both solution and melt methods (Figures 40c and e) have significant crystalline triclosan presence, presumably on the surface. These results will be discussed in the following sections.

3.3.1.5 Antibacterial Assays

Figure 41 illustrates the antibacterial activity (inhibition zone) as a function of time for 5 mg samples of each type of loaded PSi, along with the concentrations of active drug released per 24 h period. All release activity was sustained up to 90 days, and the bacterial growth inhibition zones were kept in the range of 10 – 15 mm. Details regarding the maximum and average concentration, total amount of triclosan released from each sample, as well as the inhibition zone sizes are compiled in Tables 2−7.

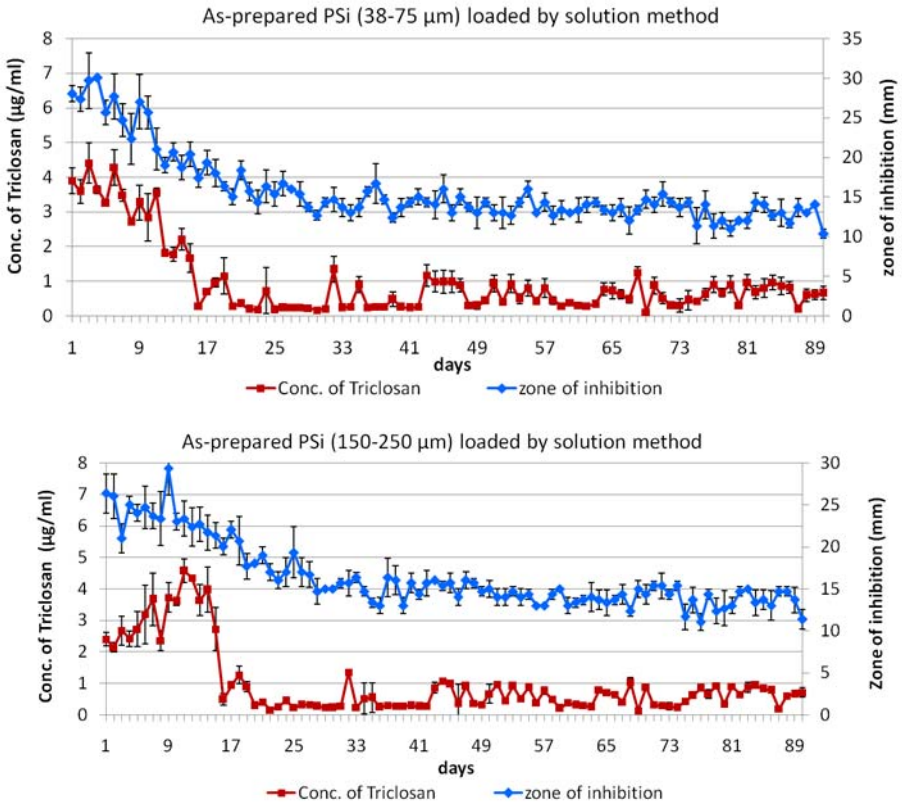

Figure 41. Combined zone inhibition assay/triclosan concentration release assays for all loaded PSi samples.

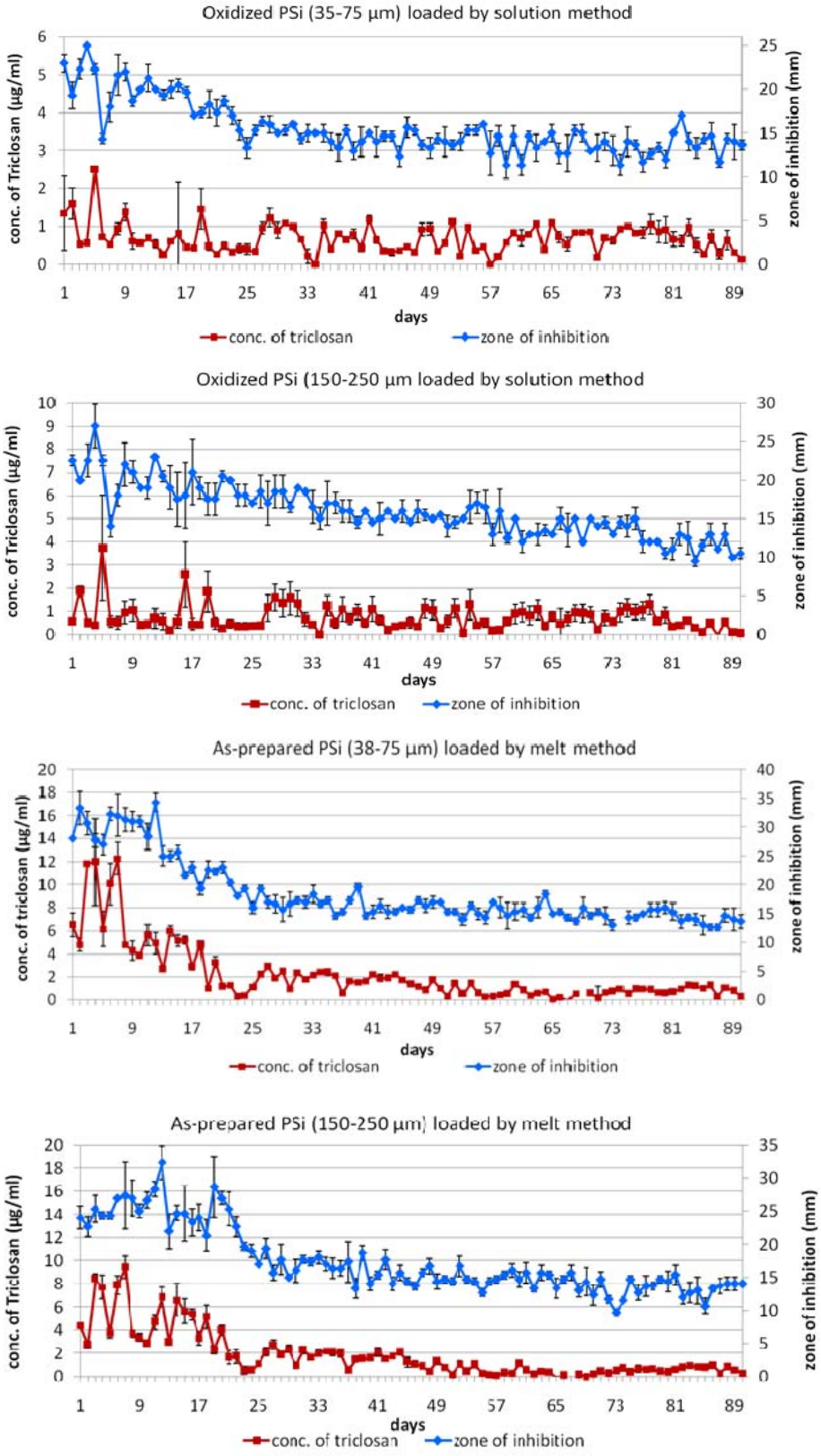

Figure 41(cont'd). Combined zone inhibition assay/triclosan concentration release assays for all loaded PSi samples.

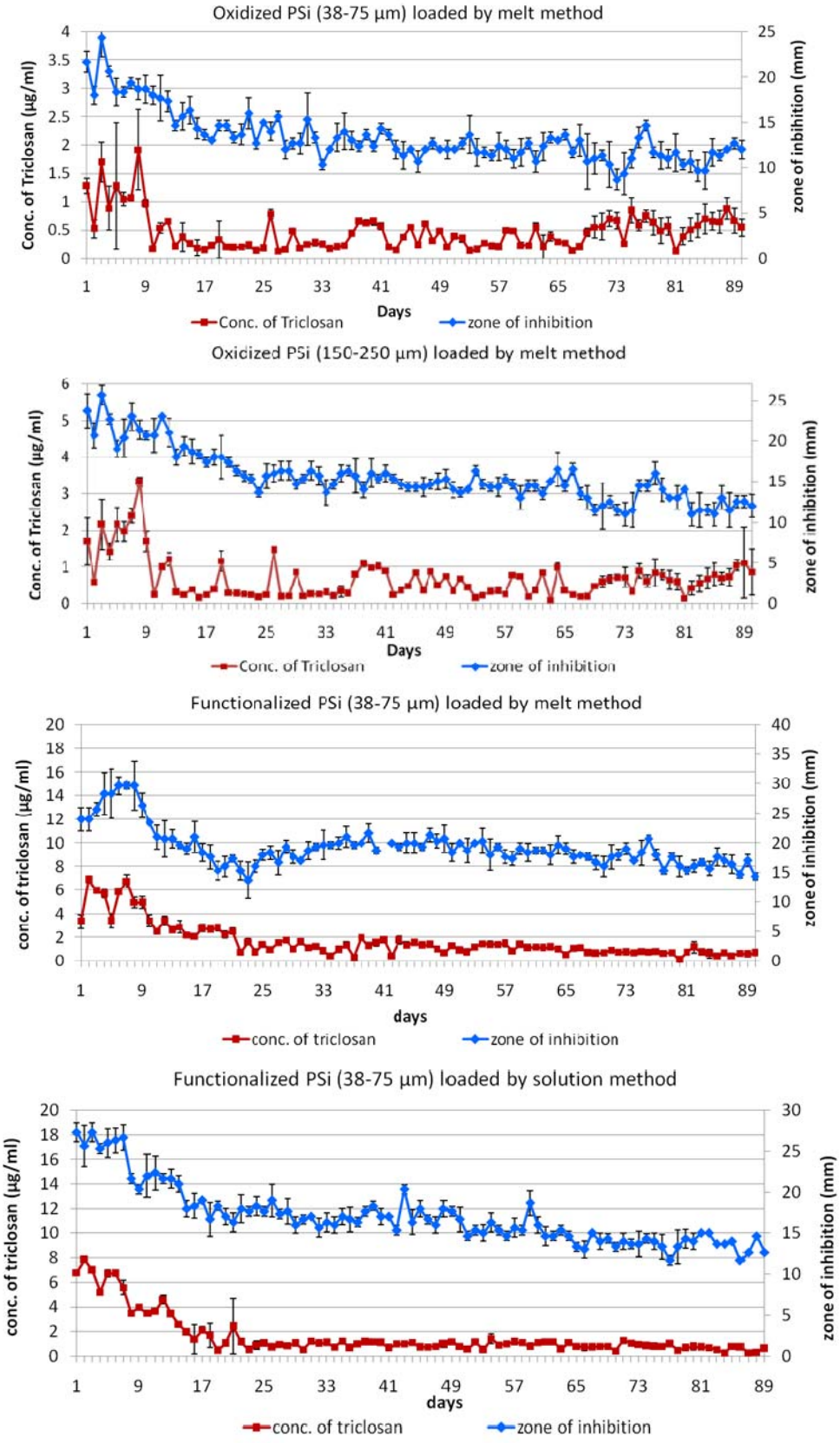

Figure 41(cont'd). Combined zone inhibition assay/triclosan concentration release assays for all loaded PSi samples.

3.3.1.6 Dissolution of As-prepared PSi (Anodized), Oxidized PSi (Anodized) and Octyl-functionalized PSi.

Figure 42 shows the dissolution behavior of as-prepared PSi, oxidized PSi, and octyl-functionalized PSi. It is clear that as-prepared PSi has the highest concentration of silicic acid during the time period evaluated, with an average concentration of 266 μg/mL. The extent of dissolution of octyl-functionalized and oxidized PSi are similar, but octyl-functionalized PSi is slightly higher than oxidized PSi (average level: 98 μg for octyl-functionalized PSi versus 62 μg for oxidized PSi), likely because of the incomplete surface functionalization in the octyl case (Figures 35b, d and e). These observations are consistent with our initial expectations, which are that oxidation and octyl-functionalization indeed decrease the rate of PSi dissolution, and the drug release from the PSi carrier will be strongly influenced consequently by the low dissolution rate.

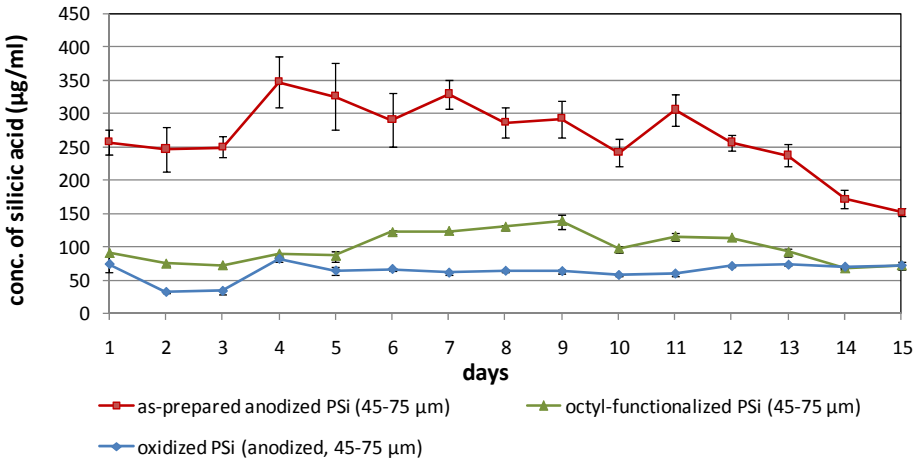

Figure 42. The degradation of as-prepared PSi, oxidized PSi and octyl-functionalized PSi in water, described by the concentration of silicic acid dissolved after each interval.

3.3.2 Comparison of Triclosan Loading and Release between As-prepared and Oxidized PSi.

In this section, the properties of the loaded PSi samples are compared in a pairwise fashion in order to focus on individual specific factors that affect drug delivery. Loaded PSi samples in group I and II are selected for comparisons between as-prepared and oxidized PSi, which are all loaded by the solution method. Within each group, PSi samples with two different particle sizes are selected and the same sized samples are compared in parallel. Except for the different surface chemistries, all other properties are the same. According to the previous characterization data, Table 2 summarizes the main characterization data and highlights some key points in the release behaviors of solution-loaded PSi samples.

Table 2. Comprison of triclosan loading and release between as-prepared and oxidized PSi loaded by the solution method.

Samples			Triclosan loading% (TGA)	Signal of crystalline triclosan on surface (XRD)	Theoretical loading of triclosan in 5 mg loaded PSi (mg)
group I	As-prep.	Small, Soln.	51.78	None	2.589
group II	Oxi.		59.32	None	2.966
group I	As-prep.	Big, Soln.	62.29	None	3.115
group II	Oxi.		60.14	weak	3.007

Samples			Triclosan released in first 15 days			Triclosan release in 90 days	
			Max conc. of triclosan (μg/mL)	Average conc. (μg/mL)	Max inhibition zone (mm)	Total released amount (μg)	Triclosan released% in theoretical loading
group I	As-prep.	Small, Soln.	4.40	3.089	31	87.13	3.365
group II	Oxi.		2.49	0.89	25	61.09	2.060
group I	As-prep.	Big, Soln.	4.57	3.23	29	88.09	2.828
group II	Oxi.		3.74	0.86	27	64.45	2.143

(In Tables 2-7: As-prep .= as-prepared PSi freshly etched; Oxi. = oxidized PSi; Small = particle size of 38-75 μm; Big = particle size of 150-250 μm; Soln. = solution loading method; Melt = melt loading method; Funct. = octyl-functionalized PSi)

As shown in Table 2, from TGA measurements, no significant loading differences appear between as-prepared and oxidized PSi loaded by the solution method (51.78% *vs.* 59.32% for small particles, 62.29% *vs.* 60.14% for big particles). From the X-ray spectra, all samples have no significant triclosan features except for the oxidized PSi with a relatively large particle size. This sample exhibits relatively weak triclosan signals suggesting a minor degree of crystallinity for the loaded drug.

The most significant differences between as-prepared PSi samples and oxidized PSi samples are the triclosan release behaviors. The maximum and average concentrations of released triclosan in as-prepared PSi samples are much higher than that in oxidized PSi samples. For example, the maximum concentration of triclosan released from as-prepared PSi with small particle size is 4.40 ± 0.57μg/mL, while 2.49 ± 0.04 μg/mL for oxidized PSi with small particle size; and the average concentration of triclosan released from as-prepared PSi with small particle size is 3.09 μg/mL, while 0.89 μg/mL for oxidized PSi with small particle size. The main reason behind the above observations is presumably due to the different dissolution rates of the PSi materials. As shown in Figure 42, the dissolution rate of as-prepared PSi is around 4-fold higher than that of oxidized PSi. Such a dissolution difference ultimately leads to the triclosan release from carrier with different kinetics.

Similar observations are shown in Table 3, in which the loading and release data for as-prepared PSi and oxidized PSi samples loaded by the melt method are compared. Some crystalline triclosan is detected in all oxidized PSi samples. The common feature observed in this class of samples is that the released triclosan concentrations are still much lower in oxidized PSi compared with as-prepared PSi.

Table 3. Comparison of triclosan loading and release from as-prepared and oxidized PSi loaded by the melt method.

Samples			Triclosan loading% (TGA)	signal of crystalline triclosan on surface (XRD)	Theoretical loading of triclosan in 5 mg loaded PSi (mg)
group III	As-prep.	Small, Melt	70.66	None	3.533
group IV	Oxi.		37.52	Weak	1.876
group III	As-prep.	Big, Melt	67.22	None	3.361
group IV	Oxi.		69.64	Weak	3.482

Samples			Triclosan released in first 15 days			Triclosan release in 90 days	
			Max conc. of triclosan (μg/mL)	Average conc. (μg/mL)	Max inhibition zone (mm)	Total released amount (μg)	Triclosan released% in theretical loading
group III	As-prep.	Small, Melt	12.28	6.73	34	194.10	5.494
group IV	Oxi.		1.92	0.86	24	41.73	2.225
group III	As-prep.	Big, Melt	9.45	5.39	32	164.81	4.903
group IV	Oxi.		3.32	1.38	25	60.26	1.731

3.3.3 Comparison of the Triclosan Loading and Release from As-prepared PSi and Octyl-functionalized PSi

The triclosan loading and release of functionalized PSi and as-prepared PSi are compared in Table 4, which includes as-prepared PSi samples in group III versus functionalized PSi samples in group V loaded by melt method, and as-prepared PSi samples in group I versus functionalized PSi samples in group V loaded by solution method. In this comparison, only small particle samples (38 – 75 μm) are involved.

Table 4. Comparison of triclosan loading and release from as-prepared PSi and octyl-fucntionalized PSi loaded by the melt method and the solution method.

Samples			Triclosan loading% (TGA)	signal of crystalline triclosan on surface (XRD)	Theoretical loading of triclosan in 5 mg loaded PSi (mg)
group III	As-prep.	Small, Melt	70.66	None	3.533
group V	Funct.		70.60	None	3.530
group I	As-prep.	Small, Soln.	51.78	None	2.589
group V	Funct.		72.97	None	3.649

Samples			Triclosan released in first 15 days			Triclosan release in 90 days	
			Max conc. of triclosan (μg/mL)	Average conc. (μg/mL)	Max inhibition zone (mm)	Total released amount (μg)	Triclosan released% in theretical loading
group III	As-prep.	Small, Melt	12.28	6.73	34	194.10	5.494
group V	Funct.		6.90	4.32	30	150.68	4.269
group I	As-prep.	Small, Soln.	4.40	3.09	31	87.13	3.365
group V	Funct.		7.83	4.87	27	139.61	3.826

In the comparison between octyl-functionalized PSi samples and as-prepared PSi samples loaded by the melt method, similar loading amounts are obtained (70.66% for as-prepared PSi versus 70.6% for octyl-functionalized PSi). The ocyl-functionalized PSi sample releases triclosan at lower maximum concentrations, average concentrations, and the total released amount than of the as-prepared PSi. However, these differences between octyl-functionalized PSi and as-prepared PSi are much smaller than the differences between oxidized PSi and as-prepared PSi. For example, octyl-functionalized PSi has 43.8% less {(12.28-6.9)/12.28} in terms of maximum triclosan released concentration compared to that of as-prepared PSi. However, for oxidized PSi versus as-prepared PSi with relatively small particle size loaded by melt method, oxidized PSi has 84.4% less {(12.28-1.92)/12.28} in terms of maximum triclosan concentration than that of as-prepared PSi (see Table 3). Also, in terms of average concentration, octyl-functionalized PSi has 35.8% less than as-prepared PSi, while oxidized PSi has 87.2% less than as-prepared PSi (see Table 3).

Furthermore, in the comparison between octyl-functionalized PSi samples and as-prepared PSi samples loaded by the solution method, octyl-functionalized PSi samples have higher loadings, release concentration, and loaded amount than as-prepared PSi. As shown in Table 4, functionalized PSi has 72.97% of triclosan loading compared with 51.78% in as-prepared PSi; 7.82 μg/mL is the maximum concentration of triclosan released from functionalized PSi versus 4.4 μg/mL for as-prepared PSi; and 4.87 μg/mL of average concentration for octyl-functionalized PSi versus 3.09 μg/mL for as-prepared PSi.

Both octyl-functionalized PSi and oxidized PSi have lower dissolution rates than as-prepared PSi, as shown in Figure 42. The average dissolution rate of octyl-functionalized PSi is 98 μg/mL (per 24 h period), 2.7-fold lower than that of as-prepared PSi (266 μg/mL). However, the triclosan release from octyl-functionalized PSi is not decreased significantly relative to as-prepared PSi samples, quite unlike the difference between oxidized PSi and as-prepared PSi (data described earlier). This indicates that the main factor affecting the triclosan release from octyl-functionalized PSi is not the dissolution rate. Rather, the most likely factor is the type of interaction between PSi surface and triclosan: hydrophobic triclosan- hydrophobic PSi surface (as-prepared PSi and octyl-functionalized PSi) versus hydrophobic triclosan- hydrophilic PSi surface (oxidized PSi). During the triclosan release, the water diffusing into the pores is repelled by the hydrophobic surfaces of as-prepared PSi and octyl-functionalized PSi, but rather wets the hydrophilic surface of oxidized PSi. Accordingly, the interaction between PSi surface and triclosan plays a leading role in the case of loaded octyl-functionalized PSi samples. As mentioned earlier, drug release is achieved by the cooperation of drug

diffusion from pores and PSi degradation over time. However, use of octyl-functionalized PSi surfaces provides a useful probe of decoupling Si dissolution effects from hydrophobic/hydrophilic surface contributions, as the alkyl species inhibit rapid PSi degradation while providing a nanostructured hydrophobic interface for the triclosan. Both hydrophobic surfaces inhibit drug crystallization during triclosan solidification. These smaller domains and corresponding higher surface area of the encapsulated drug allow it to readily dissolve in water.

3.3.4 Comparison of the Triclosan Loading and Release from PSi Loaded by the Solution Method and the Melt Method.

In this section, loaded PSi samples in group I versus group III and group II versus group IV are selected for comparison of different loading methods on drug delivery. PSi in groups I and III are the as-prepared particles, while PSi in groups II and IV are surface oxidized. Additionally, PSi samples with the same particle sizes are used for each comparison to keep the properties of type identical, except for the loading methods. The triclosan loading and release behaviors of as-prepared PSi loaded by different methods are shown in Table 5.

For both sets (small particles *vs.* big particles) in Table 5, the melt method always provides both a high loading and a high level of release. Small-particle-sized PSi loaded by melt method with higher loading (70.66%) and no signal of crystalline triclosan on the surface, gives higher maximum released concentration (12.3 μg/mL) and total amount (194.1 μg), compared with the same particles loaded by the solution method, which only has 51.78% loading and corresponding lower maximum released concentration (4.40

μg/mL) and total amount (87.13 μg). A similar phenomenon is observed in the comparison between as-prepared PSi with big particles loaded by the solution method and the melt method. A higher loading is obtained by this melt method, possibly because triclosan molecules are more easily driven into pores during the melting process and without the presence of additional solvent molecules.

Table 5. Comparison of triclosan loading and release from as-prepared PSi loaded by the solution method and the melt method.

Samples			Triclosan loading% (TGA)	signal of crystalline triclosan on surface (XRD)	Theoretical loading of triclosan in 5 mg loaded PSi (mg)
group I	Soln.	As-prep. Small,	51.78	None	2.589
group III	Melt		70.66	None	3.533
group I	Soln.	As-prep. Big	62.29	None	3.115
group III	Melt		67.22	None	3.361

Samples			Triclosan released in first 15 days			Triclosan release in 90 days	
			Max conc. of triclosan (μg/mL)	Average conc. (μg/mL)	Max inhibition zone (mm)	Total released amount (μg)	Triclosan released% in theretical loading
group I	Soln.	As-prep. Small.	4.40	3.09	31	87.13	3.365
group III	Melt		12.28	6.73	34	194.10	5.494
group I	Soln.	As-prep. Big,	4.57	3.20	29	88.09	2.828
group III	Melt		9.41	5.39	32	164.81	4.903

Table 6 shows oxidized PSi samples loaded by the solution and melt methods. The melt method also gives a higher loading for oxidizied PSi with big particle size. For oxidized PSi with small particle size, because the loading target in the melt method is 42% (metioned in section 3.2.3, different from other samples, 72% as loading target), the final loading is only 37.52%, but this result is still similar as other samples, whose loading results are close to their loading targets. From the results in terms of maximum/average concentrations, and total amount, there is no significant difference between the solution and melt methods for oxidized PSi; this situation is quite different compared to the

differences between as-prepared PSi loaded by the solution method and melt methods. For example, the maximum concentration of released triclosan from as-prepared PSi (small particle size) loaded by the solution method is 4.40 μg/mL and 12.28 μg/mL for the melt method (see Table 5), a difference of ~64.2%. However, for oxidized PSi, the maximum concentrations of PSi with small particle size loaded by the solution method and the melt method are 2.49 μg/mL and 1.92 μg/mL, respectively; the difference is only 16.7%. Similar results are obtained in comparisons of other measurements, including average concentrations and total amounts for both large and small particle size.

Table 6. Comparison of triclosan loading and release from oxidized PSi loaded by the solution method and the melt method.

Samples			Triclosan loading% (TGA)	signal of crystalline triclosan on surface (XRD)	Theoretical loading of triclosan in 5 mg loaded PSi (mg)
group II	Soln.	Oxi. Small	59.32	None	2.966
group IV	Melt		37.52	Weak	1.876
group II	Soln.	Oxi. Big.	60.14	Weak	3.007
group IV	Melt		69.64	Weak	3.482

Samples			Triclosan released in first 15 days			Triclosan release in 90 days	
			Max conc. of triclosan (μg/mL)	Average conc. (μg/mL)	Max inhibition zone (mm)	Total released amount (μg)	Triclosan released% in theretical loading
group II	Soln.	Oxi. Small	2.49	0.89	25	61.09	2.060
group IV	Melt		1.92	0.86	24	41.73	2.225
group II	Soln.	Oxi. Big.	3.74	0.86	27	64.45	2.143
group IV	Melt		3.32	1.38	25	60.26	1.731

It is clear from the above the results that (1) a significant difference between melt and solution loading methods exists in the case of as-prepared anodized porous Si, and (2) this difference is minimized upon oxidation of the surface. The former point may be understood possibly in light of the local structure of the triclosan during the infiltration process into the pores. For the case of molten triclosan, no solvent species are present;

this is unlike the case of solution loading, whereby the triclosan is surrounded by ethanol/water. The presence of slight amounts of hydrophilic H_2O in the solution may affect local trisclosan structure during solidification of the active drug. The melt loaded method is apparently superior in producing a higher surface area triclosan form capable of larger release concentrations. In the case of oxidized surfaces, a lack of difference in release behavior between loading methods is presumably a consequence of the interactions between hydrophobic triclosan and the hydrophilic oxidized porous Si surface. Irrespective of local triclosan structure, the triclosan cannot effectively wet the surface of the oxidized porous Si, and minimizes contact surface area between the two. Thus, for both melt and solution-loading methods on oxidized porous Si, similar results are obtained.

3.3.5 Comparison of the Particle Sizes of PSi and Their Effects on Drug Delivery

Table 7 compares all as-prepared PSi and oxidized PSi samples with small (38 – 75 μm) and large (150 – 250 μm) particle sizes.

In the triclosan release, each set of PSi samples with different sizes releases triclosan at an extremely similar level, especially in the average concentration and total released amount. The maximum concentrations of triclosan have slight differences, which are related to the extent of crystallization of triclosan on the surface, as characterized by XRD. For example, in Group II, the large PSi particle size, oxidized PSi loaded by a solution method possesses some slight crystalline features for triclosan in its associated X-ray pattern; at the same time, its maximum tricosan concentration and the total amount

released are higher. In those cases where differences in triclosan X-ray behavior exist, the release data are comparable.

Table 7. Comparison of triclosan loading and release from PSi with small (38 – 75 μm) and big (150 – 250 μm) particle size.

Samples			Triclosan loading% (TGA)	signal of crystalline triclosan on surface (XRD)	Theoretical loading of triclosan in 5 mg loaded PSi (mg)
group I	Small	As-prep. Soln.	51.78	None	2.589
	Big		62.29	None	3.115
group II	Small	Oxi. Soln.	59.32	None	2.966
	Big.		60.14	Weak	3.007
group III	Small	As-prep. Melt	70.66	None	3.533
	Big		67.22	None	3.361
group IV	Small	Oxi. Melt	37.52	Weak	1.876
	Big		69.64	Weak	3.482

Samples			Triclosan released in first 15 days			Triclosan release in 90 days	
			Max conc. of triclosan (μg/mL)	Average conc. (μg/mL)	Max inhibition zone (mm)	Total released amount (μg)	Triclosan released% in theretical loading
group I	Small	As-prep. Soln.	4.40	3.09	31	87.13	3.365
	Big		4.57	3.20	29	88.09	2.828
group II	Small	Oxi. Soln.	2.49	0.89	25	61.09	2.060
	Big.		3.74	0.86	27	64.45	2.143
group III	Small	As-prep. Melt	12.28	6.73	34	194.10	5.494
	Big		9.41	5.39	32	164.81	4.903
group IV	Small	Oxi. Melt	1.918	0.86	24	41.73	2.225
	Big		3.319	1.38	25	60.26	1.731

Theoretically, when the morphology, porosity and amount of sample are fixed, small particles have larger surface area than that of big particles, leading to a higher dissolution rate, as shown in Figure 43. The difference of the dissolution rate between the small-particle-sized PSi (average of 266 μg/mL) and the big ones (average of 135 μg/mL) is appreciable, but this does not significantly affect triclosan release from PSi materials with large or small particle size. The release data discussed earlier suggest that surface chemistry and loading method play more important roles in drug delivery.

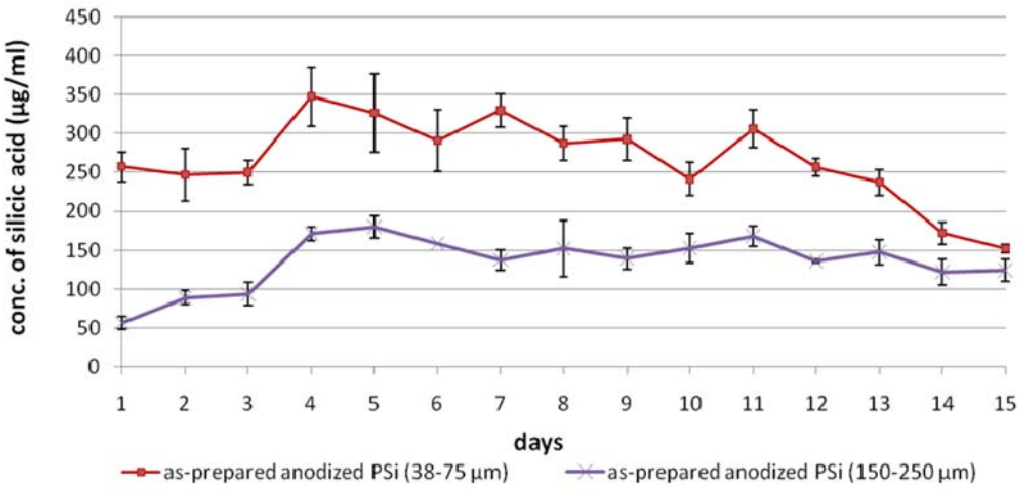

Figure 43. The dissolution rates of as-prepared PSi with the sizes in range of 38-75 μm and 150-250 μm.

3.4 Summary

In this study, five different types of triclosan loaded PSi samples were prepared. Selected comparisons among samples in these five groups were carried out, including as-prepared PSi versus oxidized PSi, as-prepared PSi versus octyl-functionalized PSi, melt loaded PSi versus solution loaded PSi, and small-particle-sized PSi (38 – 75 μm) versus big-particle-sized PSi (150 – 250 μm). These conclusions can be summarized as follows:

(1) In the comparison between as-prepared and oxidized PSi, as-prepared PSi samples always provide a higher release level than oxidized samples, which is believed to be mainly affected by the dissolution rate of PSi materials.

(2) In the comparison between as-prepared PSi and octyl-functionalized PSi, the triclosan loading and release are not so much affected by the low dissolution rate of the octyl-functionalized PSi, unlike oxidized PSi samples. In contrast, because octyl-functionalized PSi has a hydrophobic surface (same as as-prepared PSi), the release behavior is much closer to that of the as-prepared PSi samples. Therefore, the use of

octyl-functionalized PSi surfaces provides a useful probe of decoupling Si dissolution effects from hyrophobic/hydrophilic surface contributions, as the alkyl species inhibit rapid PSi degradation while providing a nanostructured hydrophobic interface for the triclosan.

(3) In the comparison between the melt method and solution method, for as-prepared PSi, the melt method exhibits a higher loading and released amount of triclosan than the solution loading method, because more triclosan molecules are driven into pores during melting. However, this difference is diminished upon surface oxidation.

(4) In the comparison between different sizes of PSi particles, PSi samples with the sizes in the range of 38 – 75 μm and 150 – 250 μm do not exhibit significant differences on loading and release behaviors of triclosan. Thus, particle size is not a key factor on drug delivery.

IV. Comparisons of Triclosan Loading into Stain Etched PSi Versus Anodized PSi to Investigate the Role of Morphology

4.1 Introduction

In the previous chapters, the role of porosity, surface chemistry and particle size on the triclosan loading and release from mesoporous silicon particles has been investigated. Although all of these samples possess different properties, they are all fabricated by the common method of anodization, which gives them a similar pore morphology in terms of size, shape, orientation, interconnectivity, and distribution. With this in mind, a hypothesis that a different network of pores may have a different influence on drug delivery is proposed. Thus, in this chapter, another type of PSi is introduced, which is fabricated by stain etching methods and possesses a totally different morphology than the anodized material.

In Chapter I, the main fabrication methods for porous silicon (anodization and stain etching) were introduced, along with their associated mechanisms of pore formation. In this chapter, the morphology of these two types of PSi will be represented and the loading and release of triclosan based on these two types of PSi will be compared in order to investigate how the morphology affects drug delivery behavior. For a more comprehensive understanding, as-prepared PSi and oxidized PSi for both types are employed.

4.2 Experimental

Table 8 lists the samples involved in this study and their associated properties. Anodized PSi is the same as used in the previous study in Chapter III, the particle size of which is 38-75 μm and the porosity is 81%. Oxidized anodized PSi is also obtained by thermal oxidation at 600 °C for 1 hour. Stain etched PSi samples and their oxidized form

are all supplied by Dr. Armando Loni (from Inrinsiq^{TM} Materials, Malvern, UK). The average particle size is 2.2 μm and porosity is 55%. Compared to pores evenly distributed in an anodized PSi particle, the porous region of stain etched PSi is localized to an area distributed near the surface, with the remainder of the particle possessing a relatively solid core. The corresponding surface area of stain etched PSi with 55% porosity is 402 m^2/g, much larger than that of anodized PSi with 81% porosity, ~200 m^2/g in surface area.

Table 8. Triclosan-loaded anodized and stain etched PSi.

Type of PSi	Surface Chemistry	Particle size (μm)	Porosity (%)	surface area (m^2/g)	loading target
Anodized PSi	as-prepared	38-75	81	200	72%
	oxidized				
Stain etched PSi	as-prepared	D_{50}=2.2 (average)	55	402	50%
	oxidized				

Before loading, the dissolution behavior of stain etched PSi and its oxidized form were measured in order to compare with that of anodized PSi. Triclosan was then loaded by a melt method through premixing PSi and triclosan, and then the mixture was heated at 95 °C for 35 minutes. The loading target for anodized PSi was 72%. For stain etched PSi, because of its lower porosity, 50% was set as the loading target (PSi : triclosan ratio of 1:1 by mass).

After loading, all triclosan loaded samples were characterized by SEM, EDX, TEM, TGA, XRD, and followed by antibacterial/triclosan release assays. Since the characterization data for triclosan loaded anodized PSi (38-75 μm) have been shown in Chapter III, this specific data will not be represented once again, but some critical numbers will be shown for comparison with triclosan loaded stain etched PSi.

4.3 Results and Discussion

4.3.1 Characterization of Triclosan Loaded As-prepared and Oxidized Stain Etched PSi Samples

4.3.1.1 The Morphology of Stain Etched PSi and Anodized PSi Characterized by TEM and Combined Analysis

Figure 44 shows the SEM and TEM images of stain etched PSi and anodized PSi prepared as described in the experimental section. The size of the biggest particle in SEM image of stain etched PSi (Figure 44a) is about 10 μm (particle located at the top edge of image a with arrow), which is much smaller than the particle size of anodized PSi (in the range of 38-75 μm) (Figure 44b). The significant differences in pore morphology between stain etched PSi and anodized PSi shown in the TEM images (Figures 44c, d) include: 1) pore shape: shallow and random pits and pores in stain etched PSi versus deep and ordered columnar channels in anodized PSi; 2) distribution: most of porous structure is located on the surface in stain etched PSi versus the uniform deep pores in anodized PSi. This can be also confirmed by the surface areas and the later measurements of PSi dissolution rate (vide infra).

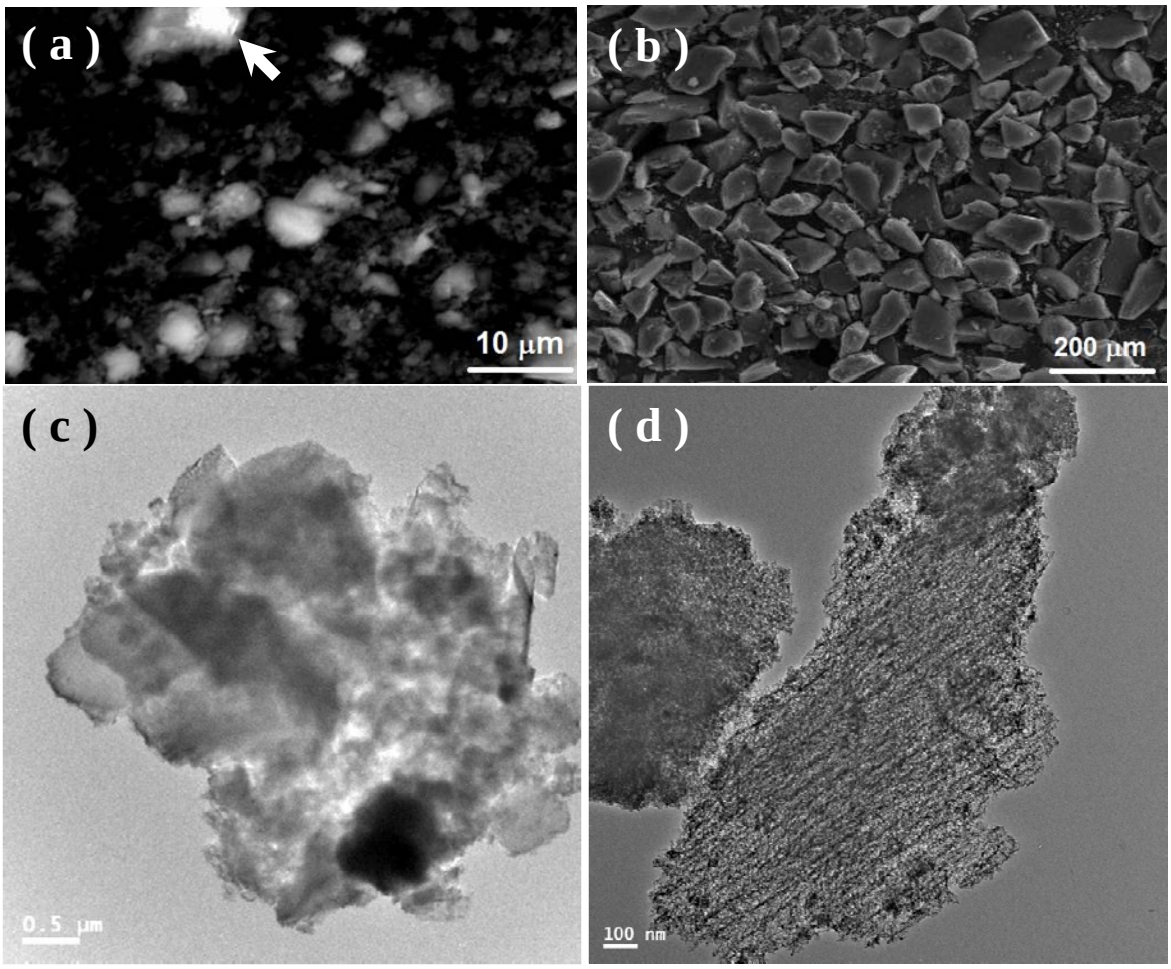

Figure 44. SEM images of stain etched PSi (a) and anodized PSi (b); TEM images of stain etched PSi (c) and anodized PSi (d).

Figure 45 displays the line scan and EDX mapping images of a microscopic area of triclosan loaded stain etched PSi. Image 45a is the corresponding TEM image of the particles being analyzed. The intensity along the line scan crossing the particle reflects the distribution of chlorine and silicon concentrations in this particle. Compared to the silicon signal, chlorine has very weak intensity (Figure 45c). However, the elemental analysis and EDX mapping (Figures 45d and e) both confirm the existence of chlorine in stain etched PSi and its uniform distribution on the surface.

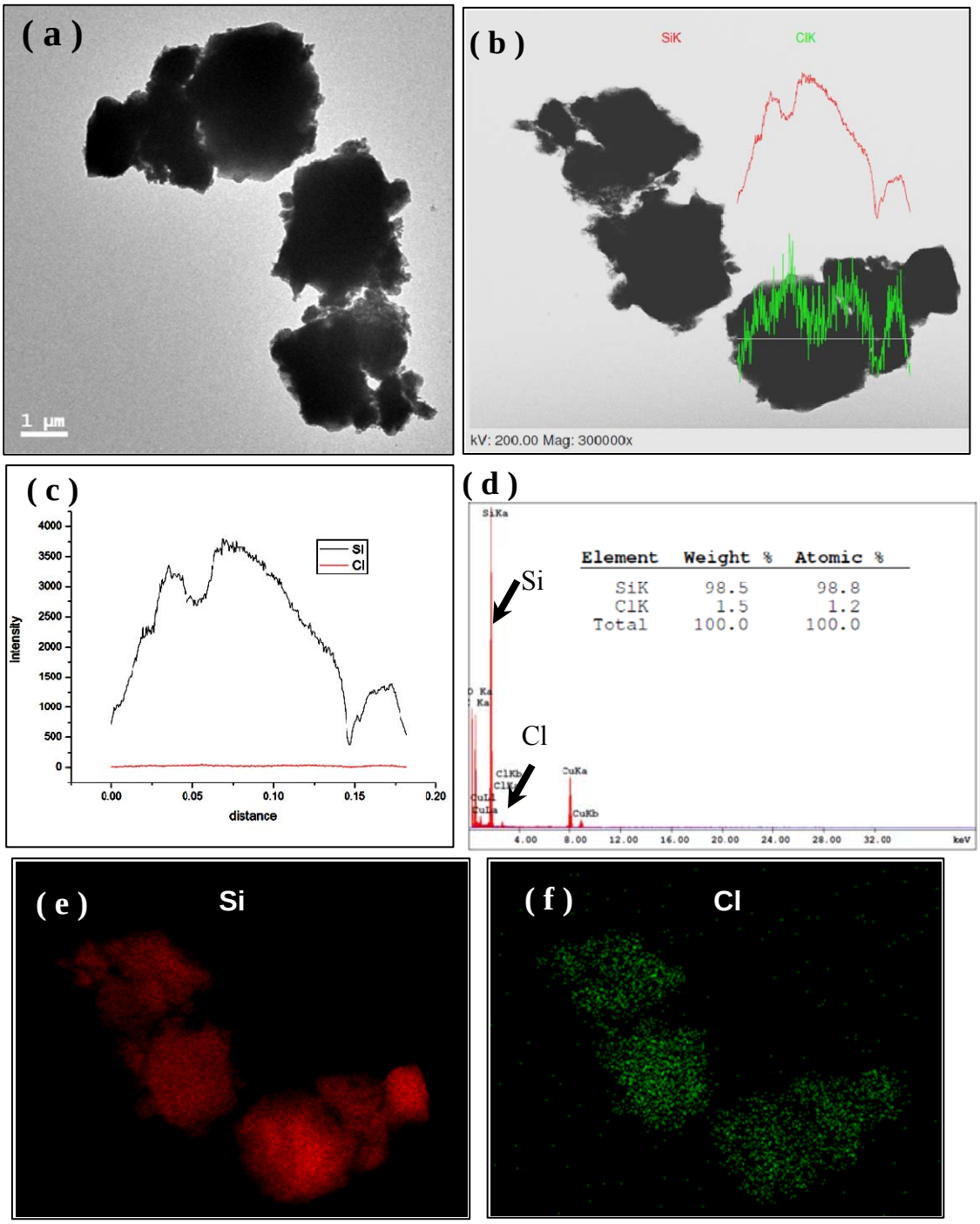

Figure 45. A single triclosan loaded stain etched PSi (as-prepared) characterized by TEM and analysis. (a) TEM image, (b, c) line scan, (d) elemental analysis, and (e) EDX mapping for element Si, (f) EDX mapping for Cl.

4.3.1.2 TGA Measurements and X-ray Diffraction of Triclosan Loaded Stain Etched PSi Samples

Triclosan was loaded into stain etched PSi samples in three separate trials. The average triclosan loading was 44% in as-prepared stain etched PSi and 50% in oxidized stain etched PSi. Similar to triclosan loaded anodized PSi, the onset of triclosan elimination from the particle begins at ~125 °C and requires about 15 minutes to complete.

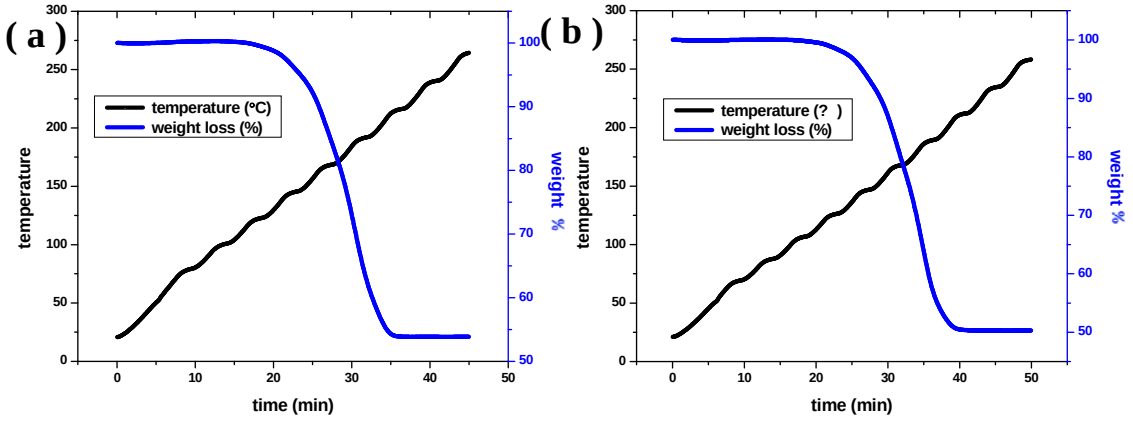

Figure 46. TGA measurements of triclosan loaded as-prepared (a) and oxidized (b) stain etched PSi samples

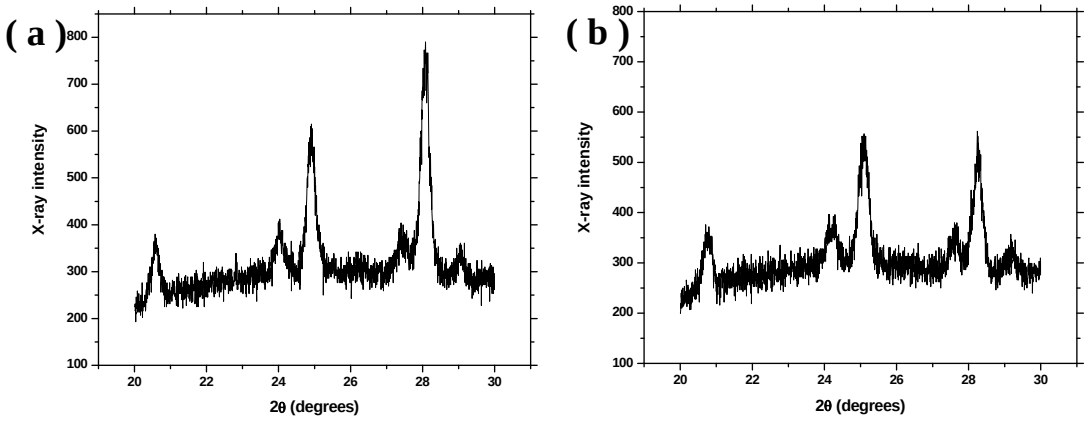

Figure 47. X-ray diffraction of triclosan loaded as-prepared stain etched PSi (a) and oxidized stain etched PSi (b).

X-ray diffraction spectra for both triclosan loaded as-prepared and oxidized stain etched PSi exhibit clear crystalline triclosan features including the main peaks located near 20.5°, 24°, and 25° (see Figure 47). The presence of this crystalline materials is likely due to the morphology of stain etched PSi. Significant amounts of triclosan were located in the shallow pores at the surface. The weaker intensities of these characteristic peaks and relative intensity reversal of the two peaks near 24° and 25° in the solid crystalline triclosan suggest that the crystallite dimensions/surface area are affected by this carrier.

4.3.2 Stain Etched PSi Dissolution and the Antibacterial Assay

4.3.2.1 Comparison of the Dissolution between Stain etched PSi and Anodized PSi

Figure 48 displays a comparison of the dissolution rate between the anodized PSi and stain etched PSi materials utilized in this particular study. Compared to anodized PSi with a 81% porosity and 38-75 μm particle size (266.1 μg/mL per 24 h), the average dissolution rate of stain etched PSi was lower (140.8 μg/mL per 24 h). However, in the first two days, stain etched PSi had much higher rate than anodized PSi (561.8 μg/mL of silicic acid for stain etched PSi versus 257.1 μg/mL for anodized PSi on 1st day). This observation confirms that the surface of stain etched PSi is more exposed than anodized PSi. As the dissolution of the silicon proceeded over the time, the solid core of stain etched Si is reached, and a significant drop in dissolution rate is observed (from 561.8 μg/mL on the 1st day drop to 162.0 μg/mL on the 3rd day) because of the decreased surface area. In the comparison between oxidized stain etched PSi and oxidized anodized PSi, the dissolution rate of oxidized stain etched PSi (silicic acid concentration of

104.1μg/mL on the 1st day) was still higher than that of oxidized anodized PSi (73.1 μg/mL) on the first day, followed by the lower average rate (28.8 μg/mL for oxidized stain etched PSi and 62.0 μg/mL for oxidized anodized PSi in average silicic acid concentration). However, this difference was not very obvious because oxidized surface decreased the dissolution rate for both types of PSi.

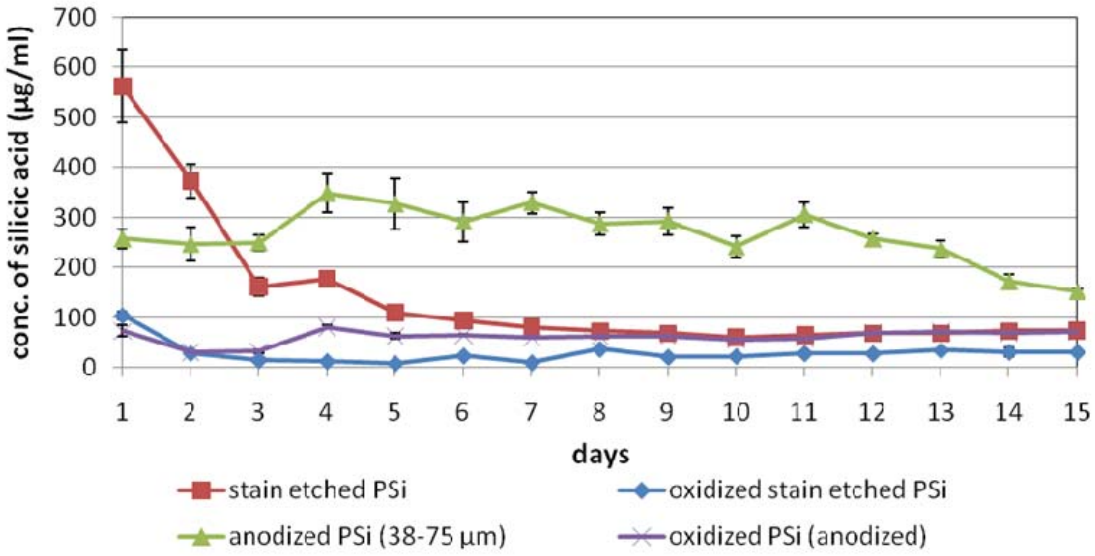

Figure 48. Dissolution of stain etched PSi and anodized PSi in H_2O at 37°C.

4.3.2.2 Antibacterial Assays of Triclosan Loaded As-prepared and Oxidized PSi Samples

Figure 49 presents the results of antibacterial assays for as-prepared and oxidized stain etched PSi showing the inhibition zones (versus *S. Aureus*) and released triclosan concentration over time. For as-prepared stain etched PSi (Figure 49a), the highest concentration of triclosan was up to 13 μg/mL on the first two days, followed by an abrupt decrease in concentration between 6 μg/mL and 4 μg/mL from the 3rd day to 5th

day, subsequently followed by the very low concentrations around or below 1 μg/mL after the 17th day. The inhibition zone also rapidly decreased from 27 mm on the 1st day to 22 mm on the 2nd day, followed by a steady drop in zone diameter on the order of 1 or 2 mm daily. Similar trends for triclosan concentration and inhibition zone were also observed for oxidized stain etched PSi, but the average concentration was much lower than that of as-prepared stain etched PSi, consistent with the observed trend between as-prepared and oxidized PSi prepared by anodic etching.

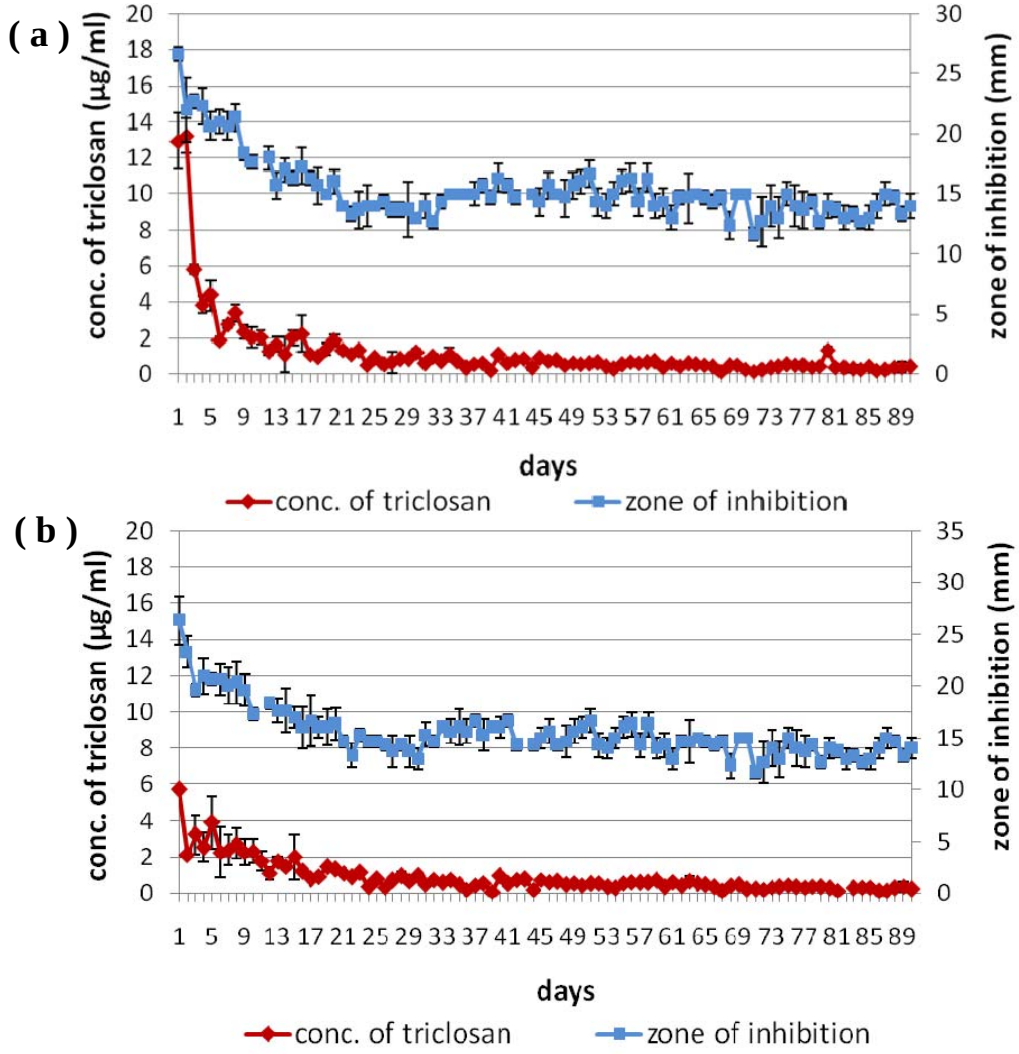

Figure 49. Combined zone inhibition assay/triclosan concentration release assays for as-prepared (a) and oxidized (b) stain etched PSi samples.

4.3.3 Comparison of Triclosan Loading and Release between Stain Etched PSi and Anodized PSi

Table 9. Comparison of triclosan loading and release from anodized PSi and stain etched PSi

Types of PSi	Surface chemistry	Triclosan loading % (TGA)	Signal of cryst. triclosan on surface (XRD)	Theoretical loading of triclosan in 5 mg loaded PSi (mg)
Anodized	As-prepared	70.66	None	3.53
	Oxidized	37.52	Weak	1.88
Stain etched	As-prepared	44.33	Weak	2.22
	Oxidized	50.23	Weak	2.51

Types of PSi	Surface chemistry	in 15 days			in 90 days	
		Max conc. of triclosan (μg/mL)	Average conc. (μg/mL)	Max inhibition zone (mm)	Total released amount (μg)	Triclosan released% in theretical loading
Anodized	As-prep.	12.28	6.73	34	194.104	5.494
	Oxi.	1.92	0.86	24	41.734	2.225
Stain etched	As-prep.	13.23	4.05	27	108.745	4.90
	Oxi.	5.71	2.51	26	77.429	3.08

Table 9 summarizes the key values of triclosan loading and release from stain etched PSi and anodized PSi. For as-prepared PSi, anodized PSi has a significantly higher triclosan loading (70.66% as measured by TGA) than that of stain etched PSi (44.23%), which is due to the higher porosity of anodized PSi (see Table 8). For stain etched PSi, the oxidized surface does not exhibit a significant influence on triclosan loading compared with as-prepared PSi. This is also not surprising, because of the relatively short diffusion length of the molten triclosan into the shallow pits/pores of the stain etched PSi.

All XRD spectra of triclosan loaded anodized PSi samples present no or very weak signals of crystalline triclosan compared with spectrum of the solid crystalline triclosan (see Figures 40a, b, and c in Chapter III). However, stain etched PSi exhibits relative stronger X-ray signals than that of anodized PSi. This is also likely a consequence of the more open, shallow pits/pores of the stain etched material, permitting some crystallization of the molten triclosan upon cooling, albeit with a higher surface area.

As discussed earlier, the reason is that in addition to triclosan located on the surface, part of nanostructured triclosan confined in the shallow pits or pores can still be detected by EDX.

During the release process, for as-prepared PSi, although the pores in stain etched PSi are shallow and random, the pits with 5 nm diameter did not influence the nanostructuring effect so the maximum of released triclosan concentration (13.23 μg/mL) was still up to the 10 μg/mL, enhancing the solubility of triclosan. Furthermore, the higher surface area of stain etched PSi (402 m^2/g) and the associated higher dissolution rate make more triclosan released in the first 2 days, even giving a little bit higher maximum triclosan concentration in as-prepared stain etched PSi than that of anodized PSi (13.23 μg/mL for as-prepared stain etched PSi versus 12.28 μg/mL for as-prepared anodized PSi). Subsequently, because of the following significantly dropped dissolution rate of stain etched PSi, the triclosan release is decreased resulting in the lower average concentration than anodized PSi (4.05 μg/mL for as-prepared stain etched PSi versus 6.73 μg/mL for as-prepared anodized PSi). The total released amount is associated with the total loading amount.

In terms of triclosan release behaviors, due to the significantly lower dissolution rate of oxidized PSi compared to that of as-prepared PSi materials (Figure 47), all concentrations and total amounts of released triclosan from oxidized PSi samples are much lower than that in as-prepared PSi sample. In the comparison between oxidized stain etched PSi and oxidized anodized PSi, the maximum concentration of triclosan released from oxidized stain etched PSi (5.71 μg/mL) is higher than that in oxidized anodized PSi (1.92 μg/mL), because of the higher dissolution rate of oxidized stain etched PSi on the first day (104.1 μg/mL for oxidized stain etched PSi versus 73.1 μg/mL for oxidized anodized PSi on silicic acid concentration on 1st day). However, although the average dissolution rate of oxidized stain etched PSi is lower than that of oxidized anodized PSi, the average concentration and total amount of triclosan released from oxidized stain etched PSi is higher than those in oxidized anodized PSi. These results are due to the relatively higher loading of triclosan (compared with oxidized anodized PSi) located in shallow pores of oxidized stain etched PSi instead of deep pores in oxidized anodized PSi.

4.4 Summary

Stain etched PSi employed in this study gives us a new option for drug delivery. The unique morphology of stain etched PSi, with a high dissolution rate in the first 48 h of aqueous exposure provides a different triclosan loading and release behavior from that of anodized material. Triclosan can be released at similarly high concentrations as anodized PSi, followed by a steady and sustained release at a lower concentration. Furthermore, the shallow pits and pores in stain etched PSi facilitate the triclosan loading

in the oxidized form and the high dissolution rate of oxidized PSi on the first day gives higher maximum concentration of released triclosan than that of oxidized anodized PSi. This may expand the applications of oxidized PSi in drug delivery.

V. Incorporation of Ciprofloxacin and Ciprofloxacin HCl into Different Porous Silicon Materials

5.1 Introduction

In the previous studies, a systematic investigation of the properties of PSi materials affecting triclosan delivery has been done, including porosity, pore size, surface chemistry, and particle size, along with an investigation of the loading methods. An understanding of the incorporation of triclosan in different porous silicon materials prompted us to try other drugs in order to broaden their potential usefulness.

In this study, ciprofloxacin (Cipro) and its hydrochloride salt (Cipro HCl) are chosen as the drugs to be studied. The structures of these two antibiotics are presented in Figure 50. As introduced in Chapter I, Cipro is a synthetic broad-spectrum antibiotic of the fluoroquinolone drug class, which has poor aqueous solubility of 67 μg/mL,[147] and a high decomposition point at 257-268 °C; in contrast, Cipro HCl is hydrophilic, with an aqueous solubility of 30 mg/mL and a decomposition point of 314-330 °C.[148] In terms of drug carriers, two types of anodized PSi and one stain etched PSi are investigated in this chapter: 1) anodized PSi with porosity of 81% and particle size in the range of 38-75 μm, referred to herein as PPK 1405; 2) anodized PSi with porosity of 64.2% and the average particle size of 20.5 μm, herein referred to as QNA 3489; and 3) stain etched PSi with porosity of 55.4% and an average particle size of 2.2 μm. Cipro and Cipro HCl are loaded into PSi materials PPK 1405, QNA 3489, and stain etched PSi in both as-prepared and oxidized forms in this study.

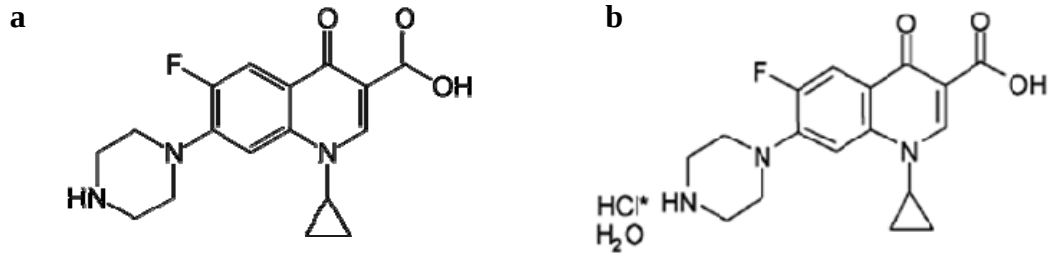

Figure 50. The structures of (a) Cipro and (b) Cipro HCl.

The aim of these investigations is to look for the Cipro and Cipro HCl loading capacity of various PSi materials, and delivery behaviors of these loaded samples involving duration, concentration, and inhibition zone, and finally to analyze the factors that dominate these behaviors with regard to PSi carrier and/or drug.

5.2 Experimental

5.2.1 The Preparation of Cipro and Cipro HCl Loaded PSi Samples

Table 10. Cipro and Cipro HCl loaded PSi samples.

	Sample ID	Particle size (μm)	Porosity	surface area (m^2/g)	loading method
Group I	Cipro in stain etched PSi	D_{50} = 2.2	55.4%	402	Melt loading: Loading target: 40% Heating temperature: ~250 °C for Cipro; ~260 °C for Cipro HCl
	Cipro HCl in stain etched PSi				
Group II	Cipro HCl in QNA 3489	D_{50} = 20.5	64.2%	275	
	Cipro HCl in QNA 3489 Ox				
Group III	Cipro in oxidized PPK 1405	38 – 75 µm (range)	81%	200	
	Cipro in PPK 1405				
	Cipro HCl in PPK 1405				

Table 10 lists the samples prepared in this study, including Cipro and Cipro HCl loaded in stain etched PSi in Group I; Cipro HCl in anodized PSi QNA 3489 and oxidized QNA 3489 in Group II; Cipro loaded in anodized PSi PPK 1405 and oxidized PPK 1405, and Cipro HCl loaded in anodized PSi PPK 1405 in Group III. Some

properties such as particle size, porosity and surface area are also listed in Table 10. Cipro and Cipro HCl were loaded by heating the premixed drug and PSi materials in an oven for 30 min (melt method). Because of the relatively higher decomposition points of Cipro HCl and Cipro, Cipro HCl was loaded at around 260 °C and Cirpo at 250 °C. The loading targets for both Cipro and Cipro HCl are 40% by mass.

5.2.2 Characterization of the Loaded PSi Samples

Because the light elements carbon and hydrogen in Cipro cannot be detectable by EDX in our SEM, the Cipro loaded PSi samples were not characterized by SEM and related analysis. Samples loaded with Cipro HCl were characterized by SEM, EDX and EDX mapping by the detection of chlorine as the characteristic element. Cipro HCl loaded in anodized PSi PPK 1405 was chosen as a representative sample for illustration (Figure 51) which confirms the uniform presentation of chlorine in the PSi.

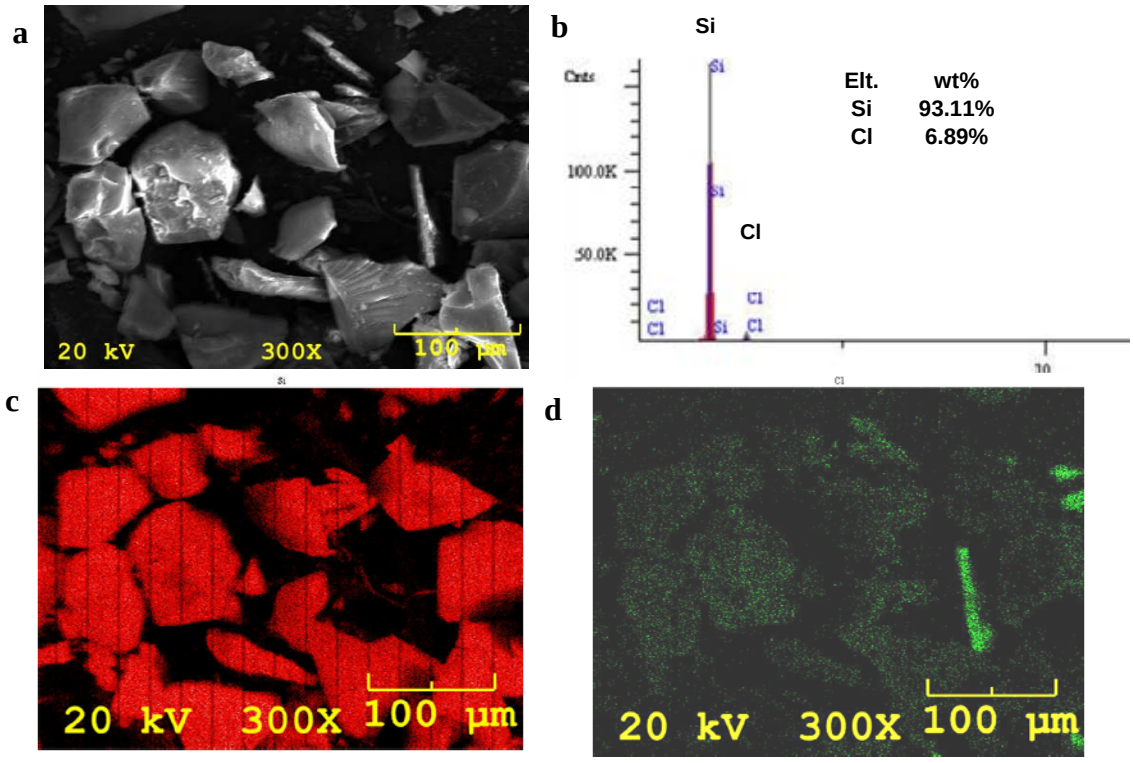

Figure 51. Cipro HCl loaded anodized PSi PPK characterized by SEM (a), EDX and element analysis (b), EDX mapping (c) for element Si and (d) for element Cl.

After SEM analysis, all loaded samples were characterized by TGA and XRD. Figure 52 shows the TGA results of both Cipro and Cipro HCl loaded PSi samples. Cipro and Cipro HCl loadings were all ~17% or less. The average loadings of different trials for each sample are labeled in Figure 52.

Even though the decomposition point of Cipro HCl is slightly higher than that of Cipro, TGA graphs illustrate that both Cipro and Cipro HCl are eliminated from PSi carriers beginning at around 250 °C and lasting for 30 min (from 30 min to 60 min), with the exception of the loaded anodized PSi (PPK 1405) sample. This exception can possibly be explained by the two stages of Cipro elimination. In Figure 52e, initial mass loss begins at around 125 °C after 12 min, then after the temperature reaches ~250 °C, Cipro is eliminated at a different rate from 30 min to 60 min. The second stage is the same as the observations in other samples, where the drugs are eliminated from pores, but it is difficult to explain the mass loss in the first lower temperature stage for this sample.

Given the high decomposition temperatures, Cipro and Cipro HCl cannot be completely eliminated from pores after 60 min. This is consistent with the lack of flat baseline at the end of a given experiment, indicating that no steady weight was achieved at the practical temperature limit of this instrument. In addition, compared with the results of release assays, the weight losses measured by TGA are smaller than the total released amounts of Cipro (or Cipro HCl) for some samples. For example, the weight loss of Cipro HCl loaded stain etched PSi is 16.7% (Figure 52b), which means there is 0.835 mg Cipro in a 5 mg loaded PSi sample. However, in the real release behavior, there is 1.7 mg Cipro HCl released from this sample (Table 11). Thus, the TGA-derived loading values clearly underestimate the true amount of cipro/Cipro HCl present in these porous

Si samples.

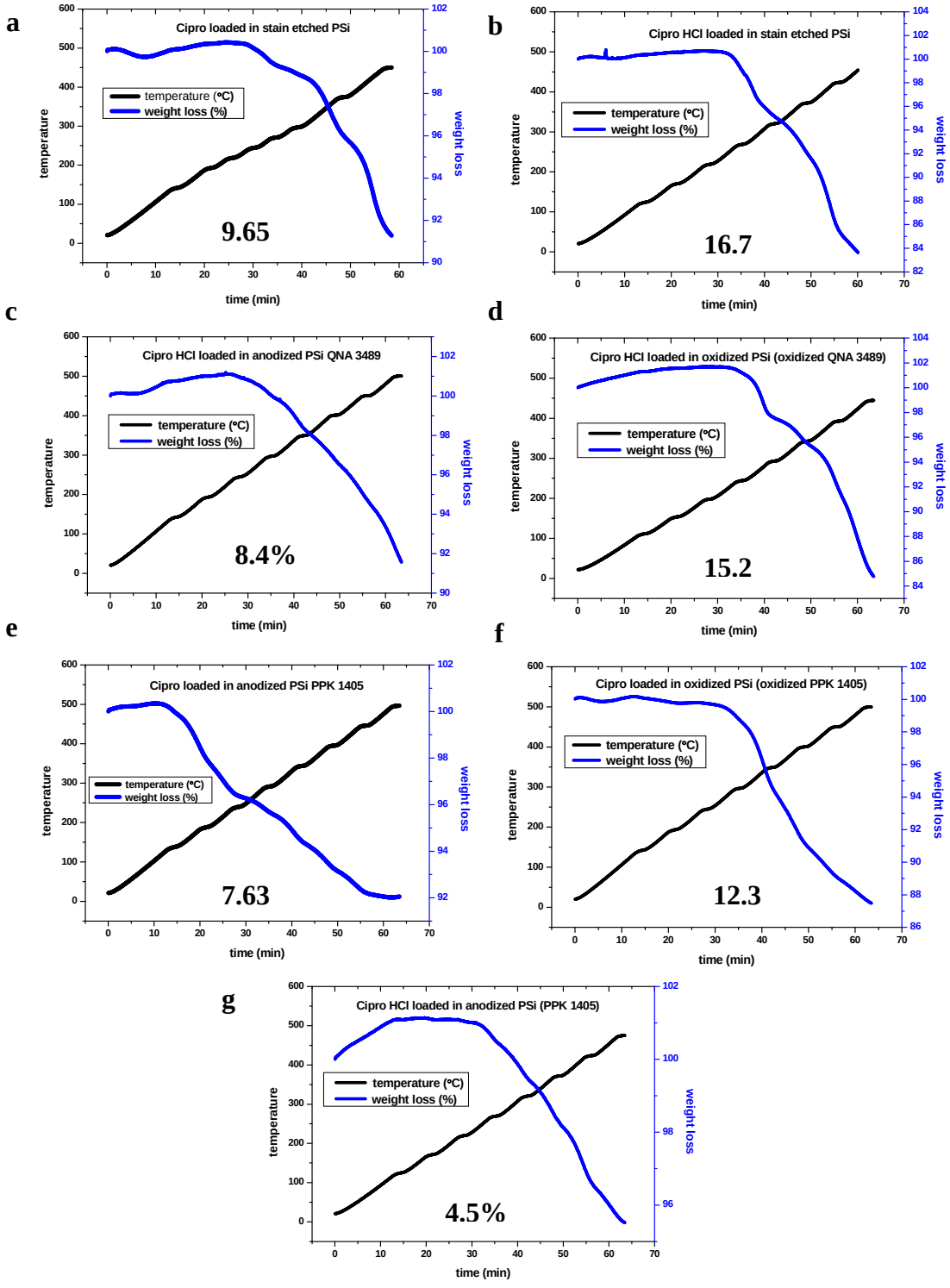

Figure 52. TGA measurements for Cipro and Cipro HCl loaded samples.

Figure 53 shows the XRD spectra of pure Cipro and all loaded samples. Figure 53a is the spectrum of Cipro itself, which has identical characteristic peaks with Cipro HCl, with the most significant peaks appearing near 14°, 20° and 25°. Compared with the spectrum of pure Cipro, Cipro-loaded stain etched PSi (Figure 53b) has obvious characteristic peaks of Cipro at 14°, 20° and 25°, but the intensities are much weaker than that of pure Cipro, which illustrates some Cipro with limited crystallinity existing in the sample. For the Cipro HCl-loaded stain etched PSi, there are also some visible peaks of Cipro HCl, but the original significant peaks at 14°, 20° and 25° are too weak to stand out from the other small peaks shown in the spectrum of the pure drug.

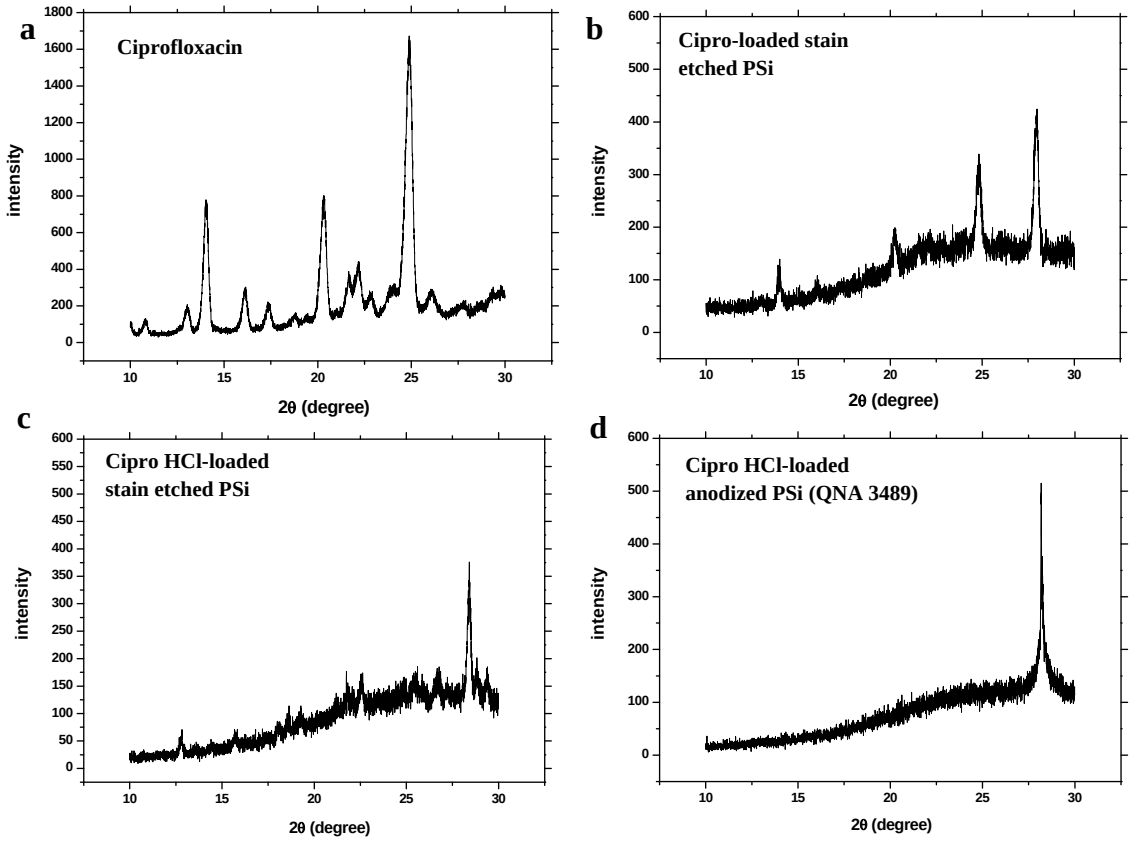

Figure 53. X-ray diffraction spectra for Cipro and Cipro/Cipro HCl loaded samples.

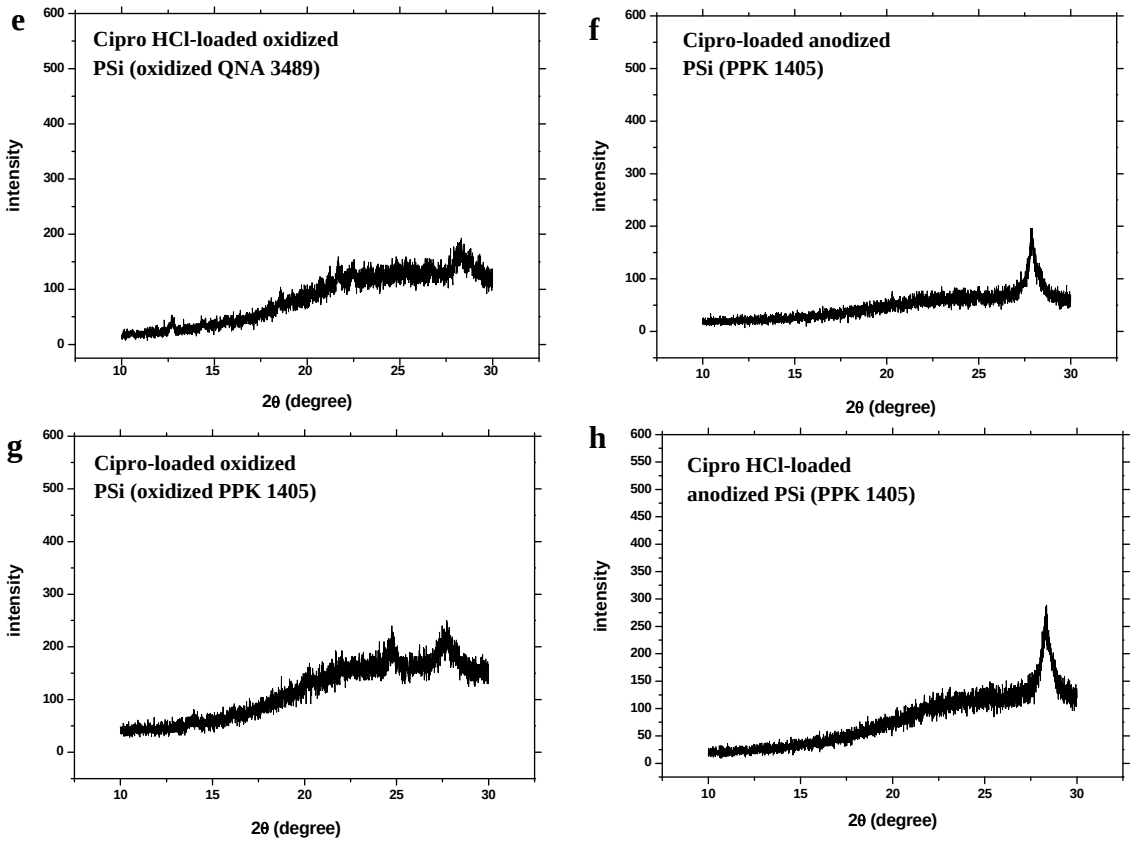

Figure 53 (cont'd). X-ray diffraction spectra for Cipro and Cipro HCl loaded samples.

For loaded as-prepared anodized PSi (Figures 53d, f and h), no crystalline Cipro or Cipro HCl is detected but the peak of PSi located near 28°. Only some very weak characteristic peaks exist in the spectra of oxidized anodized PSi (Figures 53e and g). In short, all Cipro and Cipro HCl loaded in the PSi samples lose their original crystallinity in some degree by nanostructuring or amorphization.

5.2.3 Silicon Dissolution Assays of Anodized PSi with Porosity of 64.2% and Average Particle Size of 20.5 μm

The dissolution behavior of PPK 1405 (porosity of 81% and particle size in the range of 38-75 μm), as-prepared and oxidized, along with a stain etched sample (porosity

of 55.4% and average particle size of 2.2 μm) has been described previously in Chapter IV. As anodized PSi QNA 3489 with porosity of 64.2% and average particle size of 20.5 μm was first used in this study, silicon dissolution assays and a comparison with other PSi samples are necessary. Figure 54 shows that as-prepared anodized PSi QNA 3489 has the highest rate of dissolution (467 μg/mL per 24h), and oxidized QNA 3489 has a lower rate (237 μg/mL) than the as-prepared form, only slightly less than PPK 1405 (266 μg/mL). Stain etched PSi has very low average dissolution rate (average silicic acid concentration of 141 μg/mL), but extremely high rate on the first two days. Oxidized PPK 1405 has lowest average silicic acid concentration, of only 62 μg/mL.

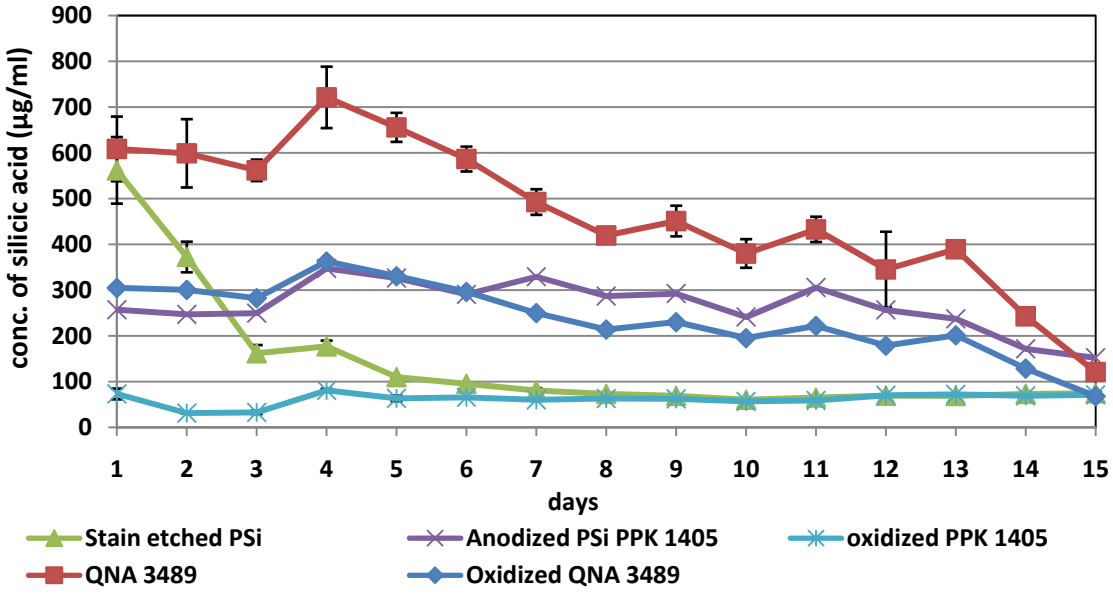

Figure 54. Silicon dissolution assays of anodized PSi (QNA 3489) and oxidized QNA 3489, compared with anodized PSi PPK 1405 and stain etched PSi.

5.2.4 Antibacterial Assays

For the antibacterial assays, Cipro and Cipro HCl standard solutions are prepared and characterized by UV/visible spectrophotometry in order to calculate the concentrations of Cipro and Cipro HCl released from these PSi samples. Figure 55 gives

the standard curves of Cipro and Cipro HCl, showing that the absorbance is linear with the concentration in the range of 0.1-1.0 μg/mL for Cipro and 0.001-0.02 mg/mL (1-20 μg/mL) for Cipro HCl. The released Cipro or Cipro HCl solutions from loaded PSi samples are diluted until the concentrations are in the range of standard solutions, when the samples are evaluated by UV/Vis spectrophotometry. The equation y = 0.1x is employed for Cipro concentration calculations, and y = 92.82x is used for Cipro HCl, where y refers to absorbance and x refers to concentration in μg/mL for Cipro and mg/mL for Cipro HCl.

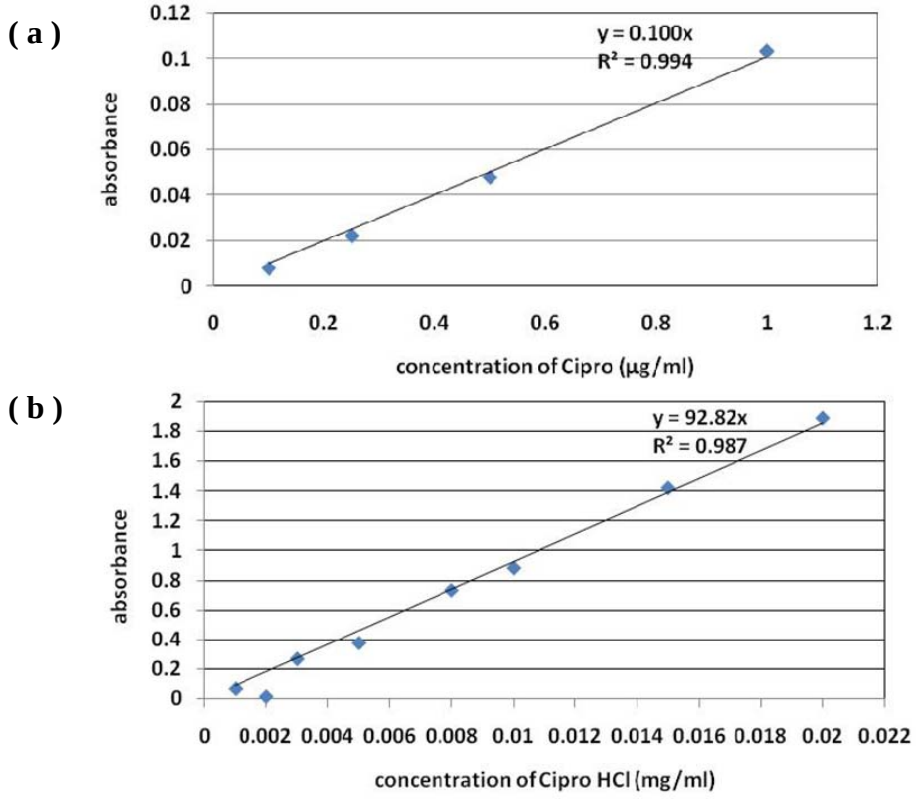

Figure 55. Standard curve of (a) Cipro and (b) Cipro HCl.

Figure 56 shows the concentrations of Cipro or Cipro HCl released from all types of PSi samples and their bacterial inhibition zones. Because of the low loadings of Cipro and Cipro HCl, the activity duration does not last as long as that observed for triclosan.

While the activity associated with Cipro or Cipro HCl release lasts only a few days for anodized PSi, in the case of stain etched material, this is extended for up to two weeks. Although the activity durations are short, the concentration of Cipro has been much enhanced by loading into these PSi matrices, from ~120 μg/mL (solubility in water) at 37 °C[147] up to 500 μg/mL (in Cipro loaded stain etched PSi, 56a), indicating that the dissolution of Cipro is enhanced 4-fold. The enhanced concentrations of Cipro (500 μg/mL from Cipro loaded stain etched PSi; 250 μg/mL from Cipro loaded anodized PPK 1405) are comparable to the concentration of Cipro HCl released from PSi (450 μg/mL from Cipro HCl loaded anodized QNA 3489; 200 μg/mL from loaded anodized PPK 1405).

For the associated antibacterial activities, the maximum inhibition zones formed from these loaded samples are relatively large in their initial period of measurement, reflecting the significant antibacterial activity of Cipro/Cipro HCl. Most of the maximum inhibition zones are around 25 mm; for example, 29 mm, 27 mm, 24 mm and 22 mm for Cipro loaded stain etched PSi, Cipro HCl loaded stain etched PSi, Cipro loaded PPK 1405, and Cipro HCl loaded PPK 1405, respectively. Only Cipro loaded oxidized PPK 1405 has a much smaller inhibition zone, with 16 mm. This is definitely due to the much lower concentration of Cipro released from oxidized PPK 1405 (only ~ 124 μg/mL on the first day) than that from all other samples. Recall that the concentrations of Cipro or Cipro HCl released from other samples are all higher than 200 μg/mL. Overall, the decreases in inhibition zones are consistent with the decreases of concentration of the given drugs released from these PSi materials.

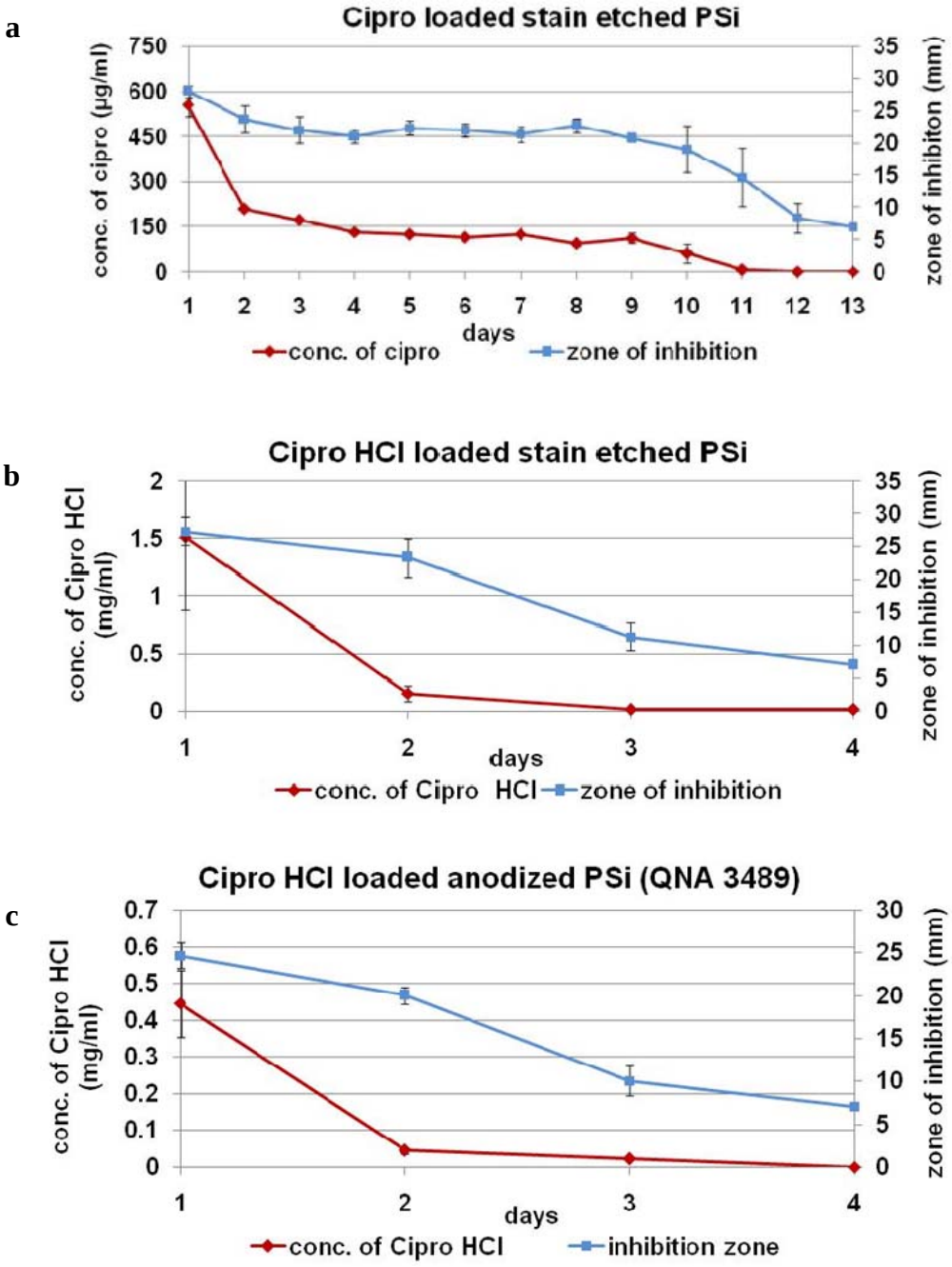

Figure 56. Combined zone inhibition assay/triclosan concentration release assays for Cipro and Cipro HCl loaded samples.

d

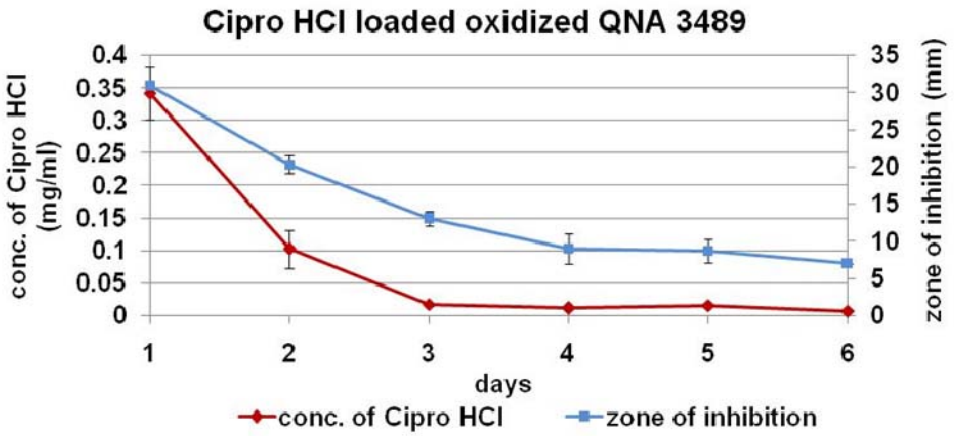

e

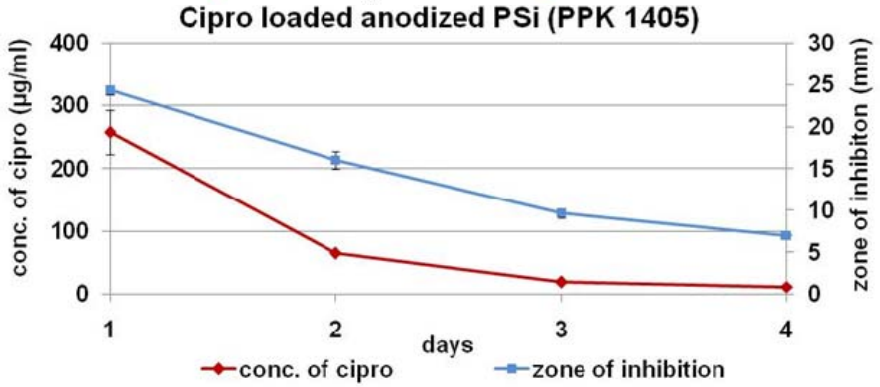

f

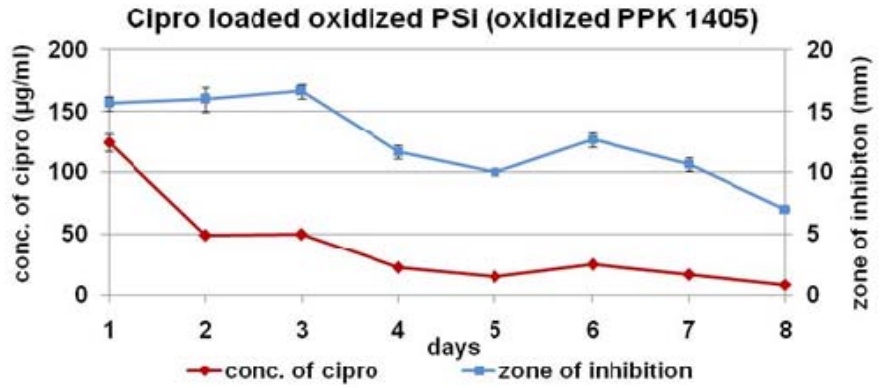

g

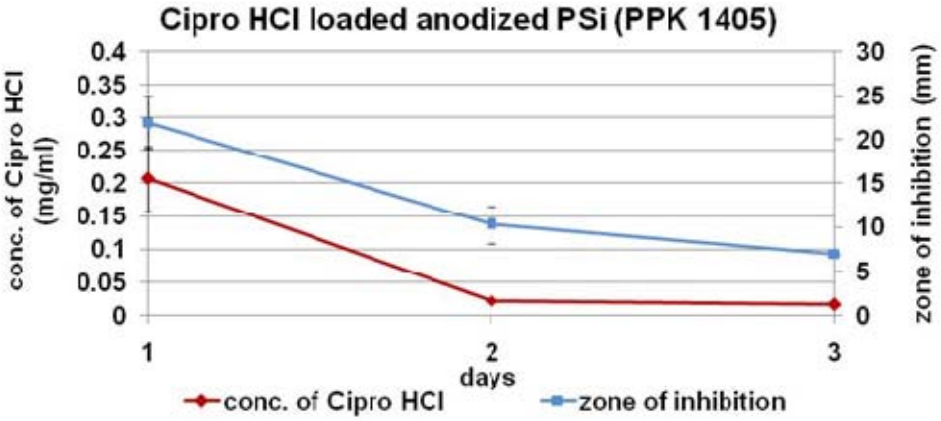

Figure 56 (cont'd). Combined zone inhibition assay/triclosan concentration release assays for Cipro and Cipro HCl loaded samples.

5.3 Results and Discussion

Table 11. Comparison of Cipro and Cipro HCl loaded PSi samples.

	Sample ID	Particle size	Porosity	Signal of cryst. Cipro/ Cipro HCl on surface (XRD)	Duration of activity (days)	Max conc. of Cipro / Cipro HCl (μg/mL)	Total amount of released drug (μg)	Max inhibition zone (mm)
Group I	Cipro in stain etched PSi	D_{50} = 2.2 μm	55.4%	yes	13	553.12	1709.97	28
	Cipro HCl in stain etched PSi			yes	4	1513.24	1702.25	27
Group II	Cipro HCl in QNA 3489	D_{50} = 20.5 μm	64.2%	no	4	445.39	512.31	25
	Cipro HCl in oxidized QNA 3489			yes	6	341.93	493.77	31
Group III	Cipro in oxidized PPK 1405	38 – 75 μm	81%	yes	8	124.18	308.65	16
	Cipro in PPK 1405			no	4	257.60	353.35	24
	Cipro HCl in PPK 1405			no	3	207.82	235.54	22

Surface areas: 402 m^2/g for stain etched PSi; 275 m^2/g for anodized PSi (QNA 3489); and 200 m^2/g for anodized PSi (PPK 1405).

Table 11 summarizes the properties of PSi samples and Cipro and Cipro HCl released from these PSi carriers. Compared with anodized PSi samples, drug-loaded stain etched PSi samples have the highest maximum concentration and total loading amount of these drugs. This is due to both the unique morphology of stain etched PSi and the properties of Cipro and Cipro HCl. As mentioned earlier, Cipro and Cipro HCl have high decomposition points and are not stable when the temperature is above these points, which is challenging to diffuse molten Cipro and Cipro HCl in an intact form deeply into the porous network. Meanwhile, the shallow, roughened morphology of stain etched PSi (see Figure 44 in Chapter IV) provides a more facile framework for Cipro and Cipro HCl loading. Thus, in this case, more Cipro or Cipro HCl can be loaded in the pores than can be loaded into the deep pores of anodized PSi, leading to an overall greater amount of

total drug released. In addition, the extremely high dissolution rate of stain etched PSi in the first two days is also a factor in obtaining a high maximum concentration of Cipro and Cipro HCl. It is noted that anodized PSi QNA 3489 has an extremely high dissolution rate; however, in such comparisons, given the short antibacterial activity duration and high dissolution rate of Cipro-loaded stain etched PSi during the first two days, the long-term dissolution behavior of QNA 3489 does not come into play.

Anodized PSi PPK 1405 and QNA 3489 have similar morphologies. Although QNA 3489 has a slightly lower porosity than PPK 1405, the smaller particle size of QNA 3489 creates a relatively high surface area, leading to a higher dissolution rate (the average dissolution rate of QNA 3489 is 467 μg/mL per 24 h, compared with an average dissolution rate of PPK 1405 of 266 μg/mL). This is why Cipro and Cipro HCl loaded QNA 3489 have slightly higher maximum concentration and total loaded amount values than those of PPK 1405.

As mentioned in Chapter III, there are two factors affecting drug release; one is PSi dissolution rate, and another is drug diffusion from pores influenced by the interaction between drug and PSi surface. In the comparison between oxidized QNA 3489 and as-prepared PPK 1405, it is expected that the drug release behaviors are influenced by both factors. However, in the cases of Cipro HCl loaded oxidized QNA 3489 and Cipro HCl loaded as-prepared PPK 1405, although the dissolution rate of oxidized QNA 3489 (237 μg/mL per 24 h) is slightly lower than that of anodized PPK 1405 (266 μg/mL per 24 h) in the 15 days duration, during activity (3-6 days) of the loaded samples (Cipro HCl in QNA 3489 with as-prepared and oxidized form and Cipro HCl in PPK 1405) , the dissolution rate of oxidized QNA 3489 is still higher than that of

as-prepared PPK 1405. Thus, regardless of the influence of PSi surface chemistry, the higher dissolution rate of oxidized QNA 3489 during the 3-6 day period still plays a more important role than the surface chemistry properties.

For the samples in each group based on the same PSi carrier, the drug loading and release are predominantly affected by the interaction between the drug and the PSi surface. However, this interaction between hydrophobic Cipro or hydrophilic Cipro HCl and as-prepared PSi or oxidized PSi does not give significant differences in the released concentration (per 24h interval) or total amount released. For example, in Group I, both samples give ~ 1700 μg for the total amount of released drug. The difference is only ~ 7 μg. Also, in Group II, the total amount of released drugs are 512 μg and 494 μg for Cipro HCl loaded QNA 3489 and Cipro HCl in oxidized QNA 3489, respectively. The difference is only ~ 9 μg. Again, in Group III, the total amounts are all ~ 300 μg. The weak influence of interaction between the drug and the PSi surface is mainly due to the properties of Cipro and Cipro HCl. As mentioned before, both of these two drugs do not easily diffuse into deep pores of PSi, especially for the anodized PSi. This short –length diffusion decreases the attachment area between the drug and the PSi surface, which is why the effect of interactions between Cipro/Cipro HCl and PSi surface is small. Therefore, for Cipro and Cipro HCl loading and release based on the same PSi carrier, surface properties of PSi materials do not play an important role.

In conclusion, the differences between samples in different groups are mainly caused by the morphology of the pores in stain etched PSi and anodized PSi. For PSi samples with similar morphology, the PSi dissolution rate plays a more important role

than the surface chemistry of PSi. When the PSi carriers are the same, surface chemistry does not apparently impact the delivery of Cipro and Cipro HCl.

5.4 Summary

In this study, the high decomposition point of Cipro and Cipro HCl inhibits significant loading in PSi using molten infiltration; however some modest amounts incorporated provide another example of the role of the porous Si carrier on drug release and activity. This system also highlights the significant differences between the use of anodized and stain etched PSi.

As different drugs from triclosan, Cipro and Cipro HCl are more readily loaded in the shallow pores of stain etched PSi, compared with deep pores of anodized PSi. Thus, stain etched PSi gives higher Cipro/Cipro HCl release amounts than that of anodized PSi. However, for PSi samples with the same morphology, QNA 3489 gives a slightly higher release amount than PPK 1405 due to their significant differences in dissolution rate, regardless of the surface interaction between a given drug and PSi. For QNA 3489 and PPK 1405 both as anodized PSi, the interaction between PSi surface and given drugs do not play an important role, either. Hydrophobic Cipro and hydrophilic Cipro HCl loaded into as-prepared PSi or oxidized PSi do not give obvious difference on the release behavior.

Overall, this study is a good example of the importance of the different factors affecting drug release, including dissolution rate and interaction between PSi surface and a given drug, by using Cipro and Cipro HCl loading in different PSi samples. In the case of Cipro and Cipro HCl loading, the morphology of PSi is the most important parameter

affecting the drug loading and release behavior. Under similar morphologies, the PSi dissolution rate perhaps plays a more important role than the surface chemistry.

VI. Inorganic Surface Coatings on Porous Silicon: Impact on Release

6.1 Introduction

In this section, our attention turns to PSi surface coatings. Once PSi materials are loaded with a variety of drugs, their long-term storage and stability should be considered. For example, the premature diffusion of drug molecules from the carriers before use must be suppressed. Due to considerations such as these, the goal of this study is to develop inorganic surface modification reactions for long term stabilization of the loaded PSi.

The most common inorganic candidates for coating or packaging are those of silicon and titanium compositions. The usefulness of silica as a coating material mainly lies in its high stability, especially in aqueous media, and other reasons including easy regulation of the coating process, chemical inertness, rich surface chemistry, controlled porosity, optical transparency and high biocompatibility.[149] These advantages render silica an ideal, low-cost material to tailor surface properties. So far, silica coatings have been used to form encapsulated or core shell structures to improve physical and chemical properties that can be introduced for a broad range of applications. For example, Iler's patent involves silica coatings on TiO_2.[150] Because the identity of the TiO_2 surface is completely masked by a shell of silica, the light-scattering properties of the TiO_2 can be fully utilized but the silica suppresses surface reactions between TiO_2 and the embedding matrix (resins and polymers).[150] Also, coating magnetic nanoparticles with silica is another important approach. Silica formed on the surface of magnetic nanoparticles could screen the magnetic dipolar attraction between magnetic nanoparticles and protect them from leaching in an acidic environment.[151] Due to the existence of abundant silanol groups on the silica layer, silica-coated magnetic nanoparticles can be easily activated to

be modified with various functional groups; and the silica layer provides a chemically inert surface for magnetic nanoparticles in biological systems.

Titania is considered as a common coating material because of its chemical and biological inertness, mechanical toughness, high photocatalytic activity, favorable redox potential, and low cost.[152] Applications in which TiO_2 photocatalysis can be used include self-cleaning products, air and water purification, and degradation of toxic organic waste.[152] Some commercial products, such as self-cleaning windows, are already in everyday use. Titanium also has been widely used in medical devices in oral implantology and in orthopedics. For example, in Arai's work, the effect of coating denture base acrylic resin with TiO_2 was investigated in the inhibition of oral microbial adhesion and it was confirmed that the TiO_2 coating inhibited biofilm formation.[153]

In my research, such relatively inert coatings may be applied not only to form a barrier for the drug diffusion to the environment by itself, but also to protect PSi nanoparticles from oxidation or degradation. The silanol groups on the surface of the silica layer may have the potential for further surface treatment for subsequent processes such as biomolecular attachment.

6.2 Experimental

6.2.1 Organosilica Coatings on Triclosan Loaded PSi Samples

The sol-gel process is a commonly used method for coating fine particles. The coating is performed based on the hydrolysis of the precursors, such as tetraethoxy silane (TEOS), in the presence of water and a catalyst, and the subsequent condensation of hydrolyzed TEOS on a given surface.[154]

In the experiments described in this chapter, tetramethoxysilane (TMOS), tetraethoxysilane (TEOS), and n-octyltriethoxysilane are employed for silica coatings on a given PSi surface. The reaction is shown as Figure 57, where a Si-O-Si chemical linkage is established between surface Si atoms and silica reagents, followed by lateral polymerization, and finally formation of a three –dimensional network via siloxane bond formation with varying degrees of hydrolysis.

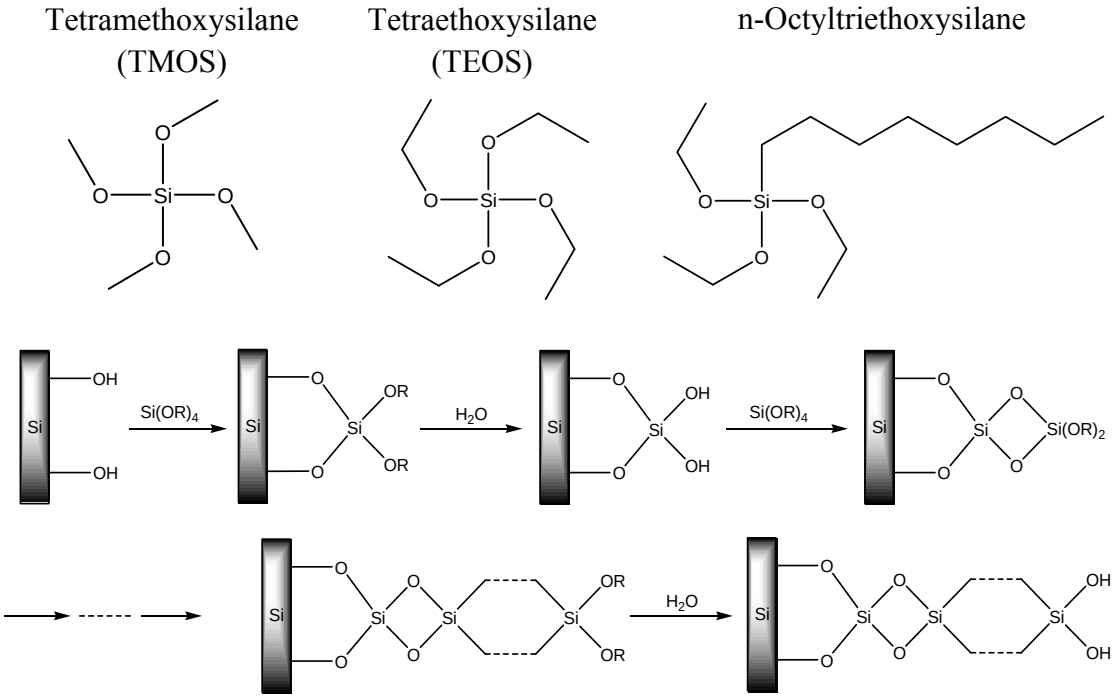

Figure 57. Reagents and reaction mechanism for an organosilica coating on a PSi surface.

In an effort to control the structure of such coatings, different reaction times (2 min, 6 min, or 12 min at room temperature with a 1:1 ratio of reagents to water), ratios of reagent to water (1:1, 2:1, and 2:0.5 at room temperature for 10 min), and reaction temperatures (room temperature, and 70 °C) were all evaluated. Relevant details will be shown at appropriate locations in the Results and Discussion section.

In some cases, triclosan loaded PSi samples were used because the element Cl is detectable by EDX. This tracking of triclosan is helpful in evaluating the effect of a given coating process. In addition to this technique, FTIR and TEM were also employed for characterization, followed by antibacterial assay in selected cases.

6.2.2 Organotitania Coatings on Cipro HCl loaded PSi Samples

The sol-gel technique is also suitable for titania coatings starting from suitable organic precursors.[155] In these studies, titanium(IV) propoxide was employed. The mechanism of reaction is shown in Figure 58. The hydroxyl groups on the surface of silicon attack titanium propoxide and displace the propoxy groups, attaching a layer of titanium propoxide. Continuing reactions occur between coated PSi and titanium propoxide, putting more layers of titanium oxide on the surface through Ti-O-Ti bonds.

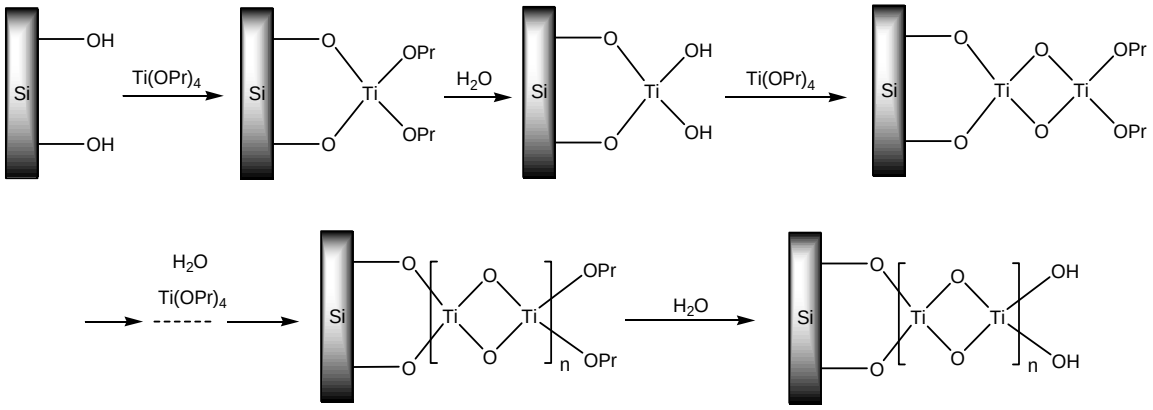

Figure 58. The reaction mechanism of an organotitania coating on PSi surface.

In organotitania coating experiments, Cipro HCl loaded PSi samples were used for tracking the impact of these surface modification reactions on drug detection in the PSi. In the first several trials, undiluted Ti(IV) propoxide is used. However, once Ti(IV)

propoxide is directly mixed with water, Ti(IV) propoxide reacts with water too vigorously to produce bulk titania particles. An alternative method is to add water directly to a given PSi sample located on filter paper (to remove the PSi particles from the undiluted Ti(IV) propoxide solution). In this way, it is expected that PSi particles surface will be covered by a layer of Ti(IV) propoxide after filtration, and only this layer of Ti(IV) propoxide reacts with water on the PSi surface. However, it is found that this method does not work either, because of high viscosity and hydrophobicity of Ti(IV) propoxide. Viscous Ti(IV) propoxide cannot go through a filter paper very well, and also too much Ti(IV) propoxide mixed with PSi particles remains on the filter paper and readily reacts with water. Therefore, in the following experiments, Ti(IV) propoxide is diluted with hexane in the ratio of 1:1 by volume.

Finally, a thin and uniform organotitania coating is achieved by the following typical procedure: Cipro HCl loaded PSi samples were first mixed with 1:1 diluted Ti(IV) propoxide at room temperature for 30 min for fully covering PSi with a thin layer of diluted Ti(IV) propoxide. After separating the solid products from the solvent by filtration, 20 drops of water were then added to the PSi particles located on the filter paper. Because of the hydrophobic Ti(IV) propoxide covered PSi surface, a big droplet of water formed on the surface of PSi. Then 10 drops of ethanol were added in order to wet the surface and allow the Ti(IV) propoxide layer react with water, thereby forming a thin organotitania coating. The final product was dried in vacuum, and characterized by SEM, EDX and FTIR, followed by antibacterial assays.

6.3 Results and Discussion

In this section, specific examples will be selected to illustrate the coating produced by different reagents and conditions, and the corresponding barrier effect on active drug diffusition.

6.3.1 Organosilica Coatings

Example 1: Organosilica coating by TMOS on PSi at room temperature.

In this case, PSi with 74% porosity, 25-45 μm in particle size and melt-doped with 54% triclosan (herein referred to as PPK 1877) was employed. PSi samples (10 mg in size) were dispersed in a mixture of TMOS and water in a volume ratio of 1:2 and stirred at room temperature for 10 min. In comparing the SEM images shown in Figure 59a and 59b for uncoated PSi under 100X magnification and 500X magnification, the morphology of an organosilica coated PSi sample (Figure 59c and d) taken under the same magnification does not appear significantly different, especially in terms of particle size. However, slight differences in the Cl wt % were detected by EDX before and after coating. Before coating, the lowest Cl wt % in all examined microscopic areas was 4.279%, but after coating, the highest Cl wt % was just 0.81%.

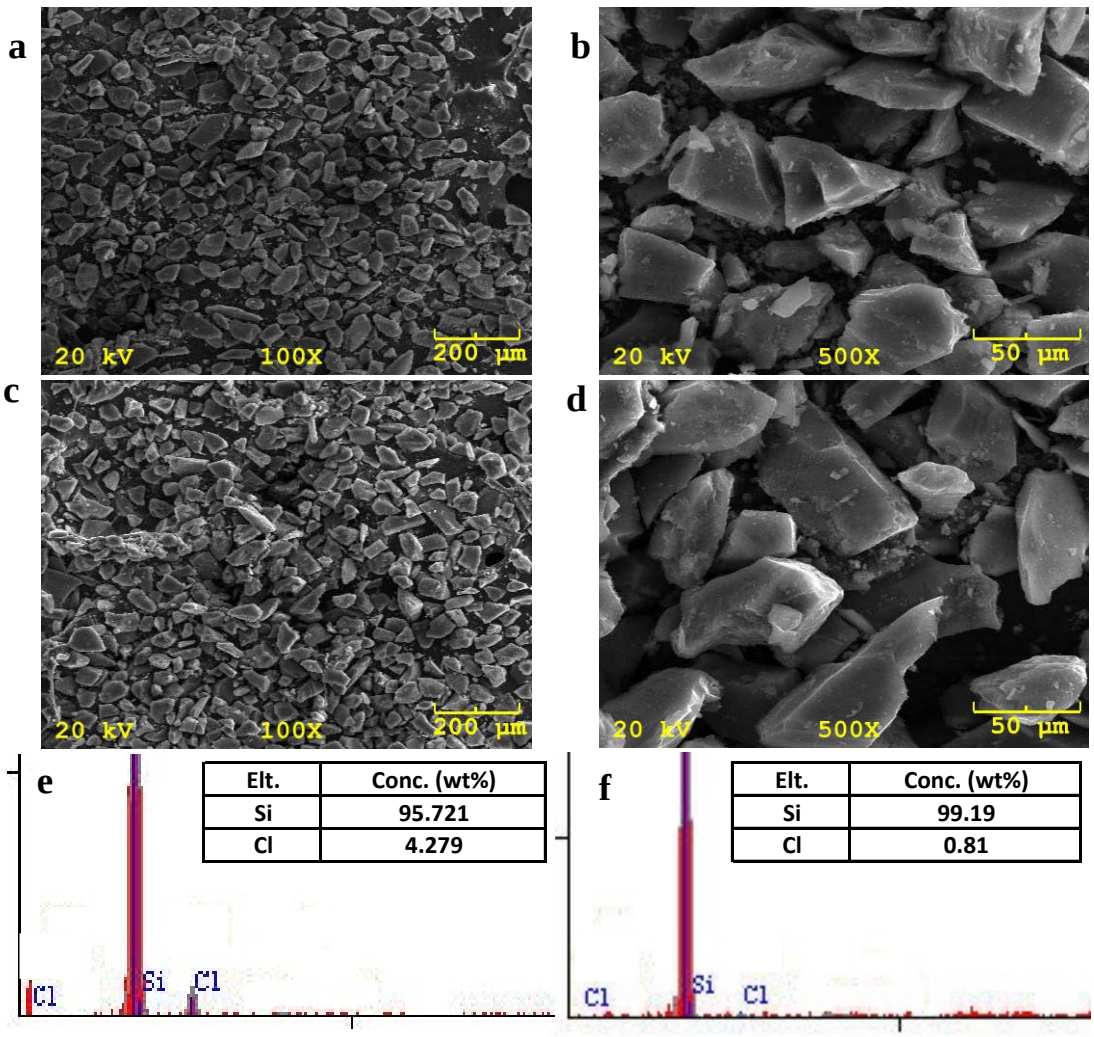

Figure 59. SEM images of triclosan loaded PSi before (a, b) and after (c, d) organosilica coating by TMOS. EDX spectrum and elemental analysis before (e) and after (f) coating.

Figure 60 exhibits the FTIR spectra before and after coating. Before coating (Figure 60a), the characteristic peaks of triclosan located in the range of 500-1500 cm^{-1} are obvious, but after coating (Figure 60b), these triclosan peaks disappear and the strong peak of ν(Si-O-Si) located at 1095 cm^{-1} is observed, corresponding to the silica coating. Meanwhile, the peaks for ν(Si-Si) located at 630 cm^{-1} and ν(Si-H) located at 2090 cm^{-1} are still detectable, which indicates the organosilica layer is thinly formed.

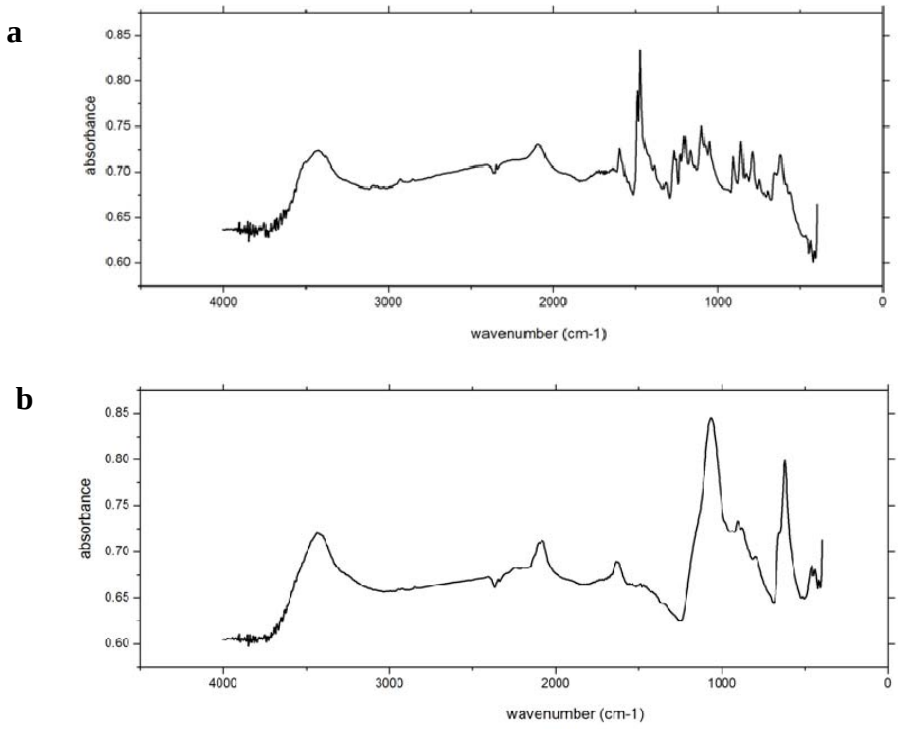

Figure 60. FTIR spectra for triclosan loaded PSi before (a) and after (b) organosilica coating.

Example 2: Organosilica coating by n-octyltriethoxysilane on PSi at room temperature.

In this case, a hydrophobic organosilica coating is achieved by the use of n-octyltriethoxysilane. 8 mg of anodized PSi powder with 74% porosity and 60-64% triclosan loading (herein referred to as PPK 1935) was soaked in 2 mL n-octyltriethoxysilane and 2 mL D. I. water; the mixture was stirred at room temperature for 10 min. The final product was obtained by filtration and drying.

Figure 61 shows the SEM images of PSi particles before and after coating. In a manner different from Example 1, PSi particles coated by n-octyltriethoxysilane (Figures 61c and d) exhibit a significantly bigger particle size than that before coating (Figure 61a and b) under the same magnifications. However, FTIR spectra (Figure 62) give the same results as PSi coated by TMOS in Example 1, where significant ν(Si-O-Si) peak and ν(Si-

Si), ν(Si-H) peaks in the spectrum (Figure 62b) taken after coating appear instead of the peaks of triclosan in the spectrum (Figure 62a). The main difference is there is a strong peak near 2900 cm^{-1} corresponding to the ν(C-H) vibration, which is a consequence of the presence of n-octyl groups on the PSi surface.

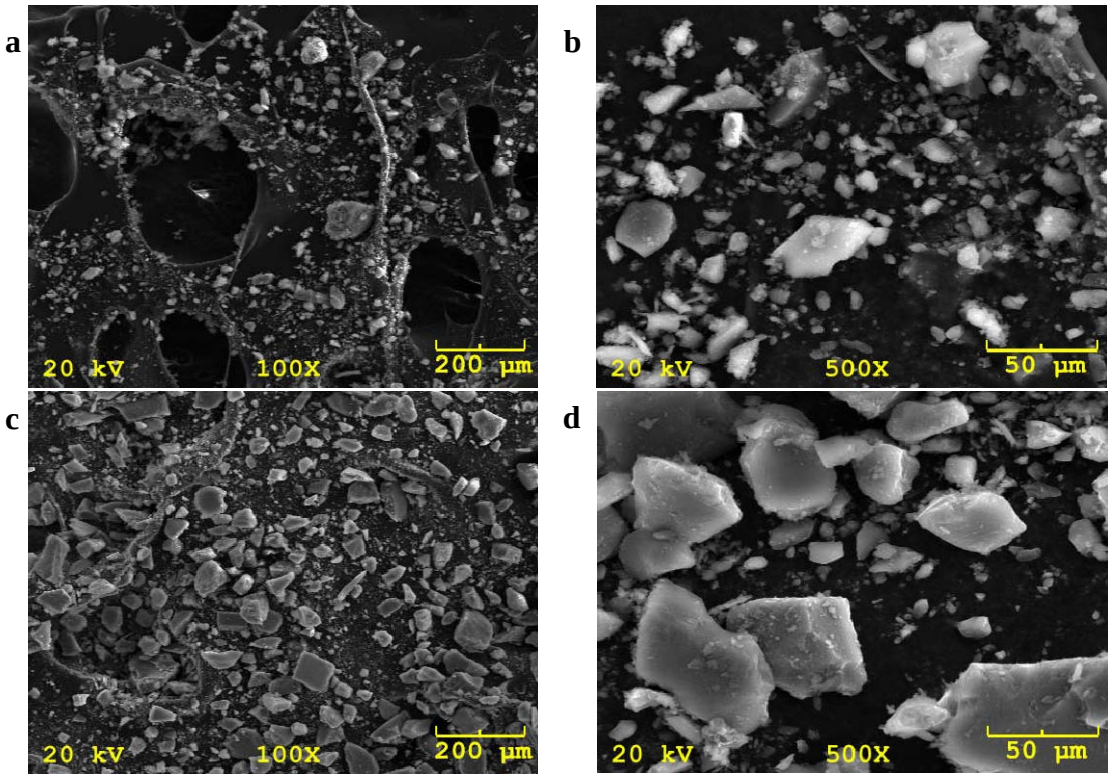

Figure 61. SEM images of triclosan loaded PSi before (a, b) and after (c, d) coating by n-octyltriethoxysilane.

These two examples were selected from the overall trials performed, involving different reaction times, and ratios of reagent to water reacted at room temperature. It is found that different reaction times and ratios give a similar result in that thin, but measurable organosilica coatings are formed on the PSi surface. However, all FTIR spectra exhibit ν(Si-H) peaks that are still detectable indicating that the Si-H species have not been fully replaced by covalent Si-O species, but rather a physical coating of SiO_2. In order to accelerate the hydrolysis of Si precursors and the transition of Si-H species to Si-

OH, the system was heated. Hence, the temperature in the following trials was set at 70 °C.

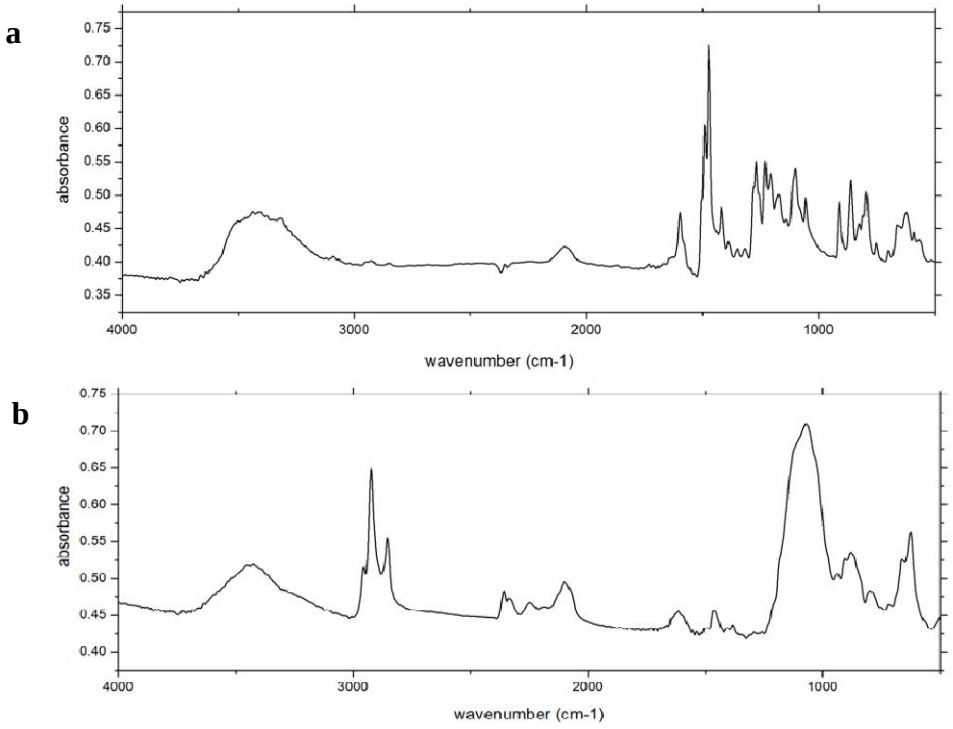

Figure 62. IR spectra for triclosan loaded PSi before (a) and after (b) organosilica coating by n-octyltriethoxysilane.

Example 3: Organosilica coating by TMOS and TEOS at 70 °C.

In these two trials, 10 mg of unloaded PSi with 81% porosity, and 38-75 μm in size (referred herein as PPK 1405) were mixed with 2 mL of a given Si reagent (TMOS or TEOS), 2 mL of water, and 20 drops of ethanol, and the mixture was heated and stirred in a water bath at 70 °C. For TMOS, the mixture was heated until the system reached the highest viscosity (prior to gel stage) which took about 13 min. After centrifugation, PSi was allowed to settle then the top liquid layer turned to gel (see Figure 63a). For TEOS, it took a longer time to achieve a suitable viscosity, but after heating around 47 min, the system still lacked significant viscosity, and TEOS and water were separated after

centrifugation because of the hydrophobicity of TEOS (See Figure 63b). Because of the low degree of TEOS hydrolysis compared with TMOS, the final product coated by TEOS was heated at 200 °C in an oven for one day to drive the residual TEOS on the PSi surface to silica.

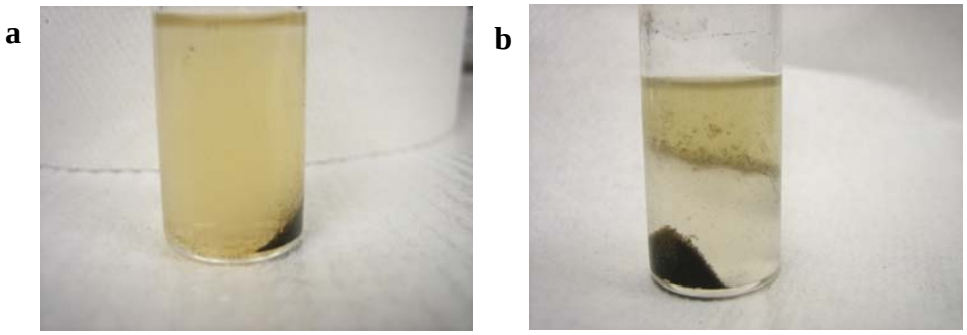

Figure 63. PSi particles (PPK 1405) in the system of TMOS (a) and TEOS (b) with water after centrifuging.

Figure 64 illustrates the FTIR results of PSi before and after coating by TMOS and TEOS. Compared with uncoated PSi (Figure 64a), both FTIR spectra of coated PSi with TMOS and TEOS (Figure 64b and c) exhibit a strong ν(Si-O-Si) vibration around 1095 cm^{-1}, but no distinct ν(Si-Si) vibration around 630 cm^{-1}. For the coated PSi after heating at 200 °C, the intensity of the Si-H species near 2090 cm^{-1} has disappeared (Figure 64c). These observations seem to suggest that the organosilica coating in this case is perhaps slightly thicker than that achieved in the first two examples, and is consistent with a transformation of Si-H species to Si-O bonds. Heat does facilitate thicker coatings.

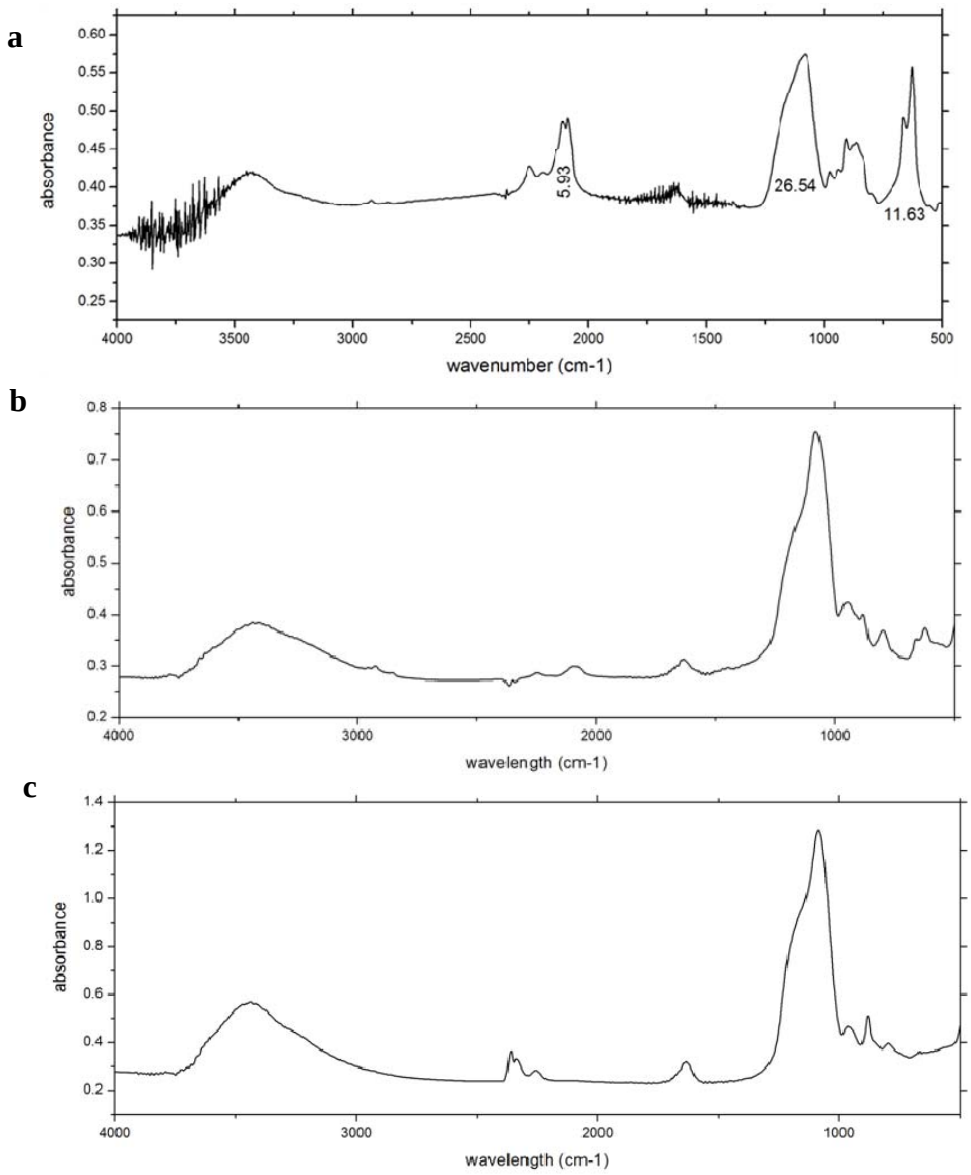

Figure 64. IR spectra of unloaded as-prepared PSi particles (PPK 1405) (a) and coated PSi by TMOS (b) and TEOS (c) after heating.

The coating of PSi by TMOS was also characterized by TEM. Recall that in Chapter III, TEM images of as-prepared anodized PSi with deep ordered columnar pore channels were shown. After coating, this characteristic morphology disappears, but the lattice planes associated with crystalline silicon can still be observed after TMOS

treatment (Figure 65b, 65c). This evidence confirms that a thin organosilica layer is successfully and uniformly coated.

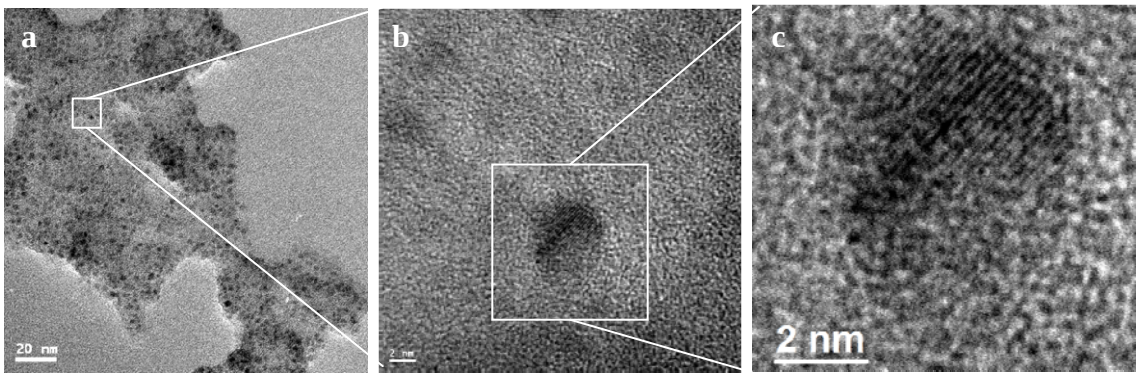

Figure 65. TEM images of organosilica coated triclosan loaded PSi sample. (a) an entire particle; (b) and (c) enlarged from image a.

Example 4. Organosilica coatings of PSi by TMOS for antibacterial assays.

Organosilica coatings in this example are achieved by mixing PSi of 74% porosity and 60-64% triclosan loading (referred herein as PPK 1935), 2 mL TMOS, 2mL H_2O and 20 drops of ethanol at 70 °C until the system is slightly viscous.

Figure 66 shows FTIR spectra taken before and after coating with TMOS. Similar observations with the coating in the case of TEOS of example 3, including a strong ν(Si-O-Si) vibration and an absence of ν(Si-Si) and ν(Si-H) vibrations after TMOS exposure, indicate a relatively thicker coating is successfully formed on the PSi surface.

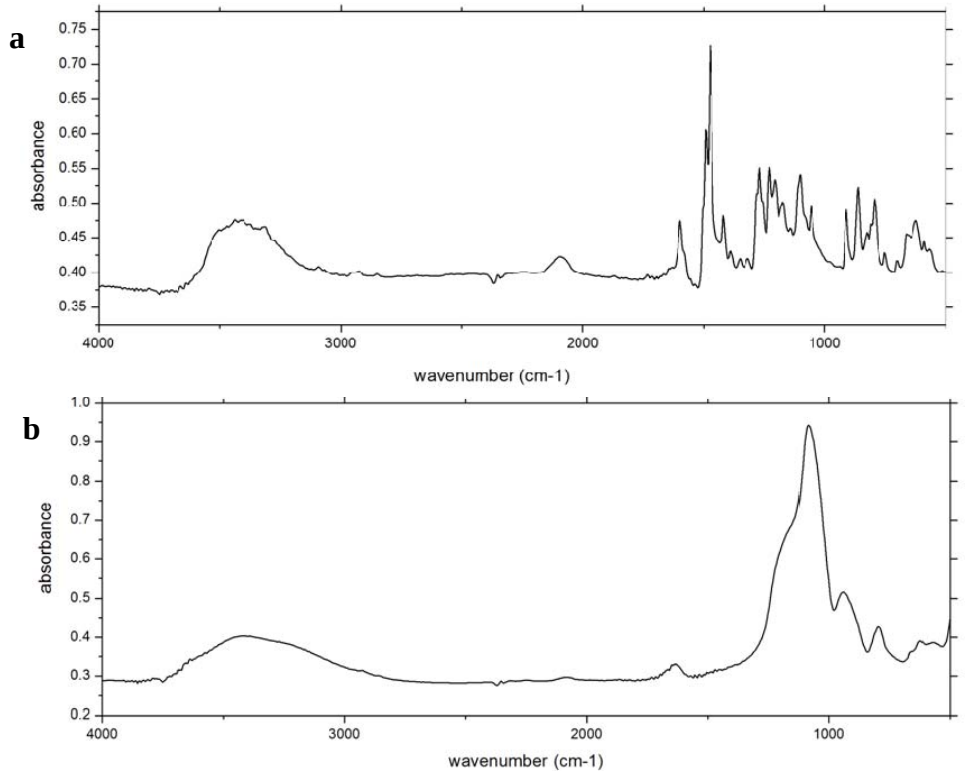

Figure 66. IR spectra for triclosan loaded PSi before (a) and after (b) organosilica coating by TMOS.

Antibacterial assays were carried out to evaluate the impact of an organosilica coating on triclosan release from PSi. Figure 67 shows the antibacterial assay results of a coated PSi sample. In Chapter III, triclosan loaded anodized PSi is shown to release triclosan over 90 days (see Figure 41). This type of sample (triclosan loaded anodized as-prepared PSi) can release triclosan with the highest concentration around 10-12 μg/mL and the inhibition zone can reach over 30 mm during the first 48 hr of release (Figures 41g and f). However, after an organosilica coating, triclosan was only released for 7 days from the anodized as-prepared PSi, and the highest released triclosan concentration is ~1 μg/ml, with an associated inhibition zone of only 18 mm. This antibacterial assay suggests that the organosilica coating does form a barrier to prevent drug molecules diffusing from the carriers. The other possibility for this system is that the alkoxy silane

reagent extracts significant quantities of the loaded triclosan from the porous Si in an adverse manner.

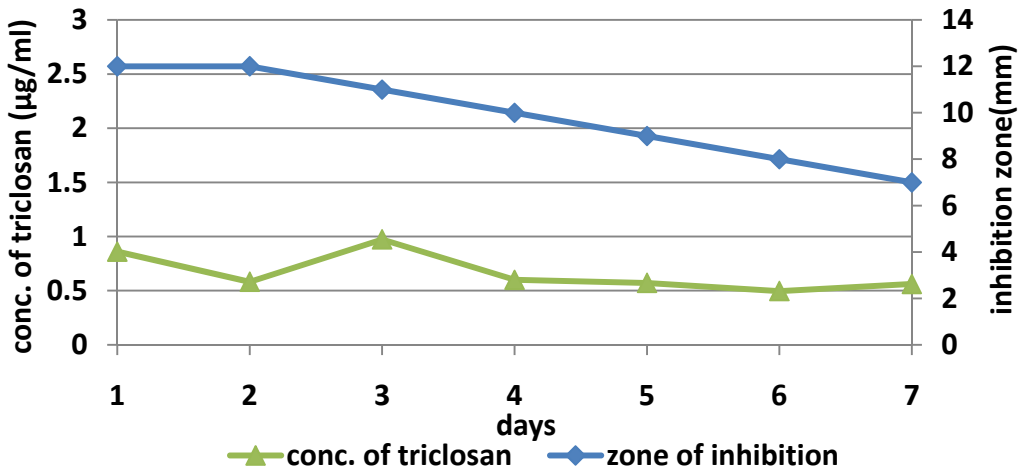

Figure 67. Combined zone inhibition assay/triclosan concentration release assay for organosilica coated PSi by TMOS.

6.3.2 Organotitania Coatings

As mentioned before, in the first several trials, when undiluted Ti(IV) propoxide was used, excess bulk titania powder was formed (as shown in Figure 68). Figures 68a, b, c and Figures 68d, e, f are the SEM images and EDX mapping results of products generated from two trials using by undiluted Ti(IV) propoxide. EDX mapping images represent the distribution of titanium (Figure 68b, e) and silicon (Figure 68c, f) corresponding to these SEM images. It is obvious that many particles shown in the SEM image are composed solely of titanium (Figure 68b, e) and only a few bright red spots (Figure 68c, f) demonstrate the presence of silicon.

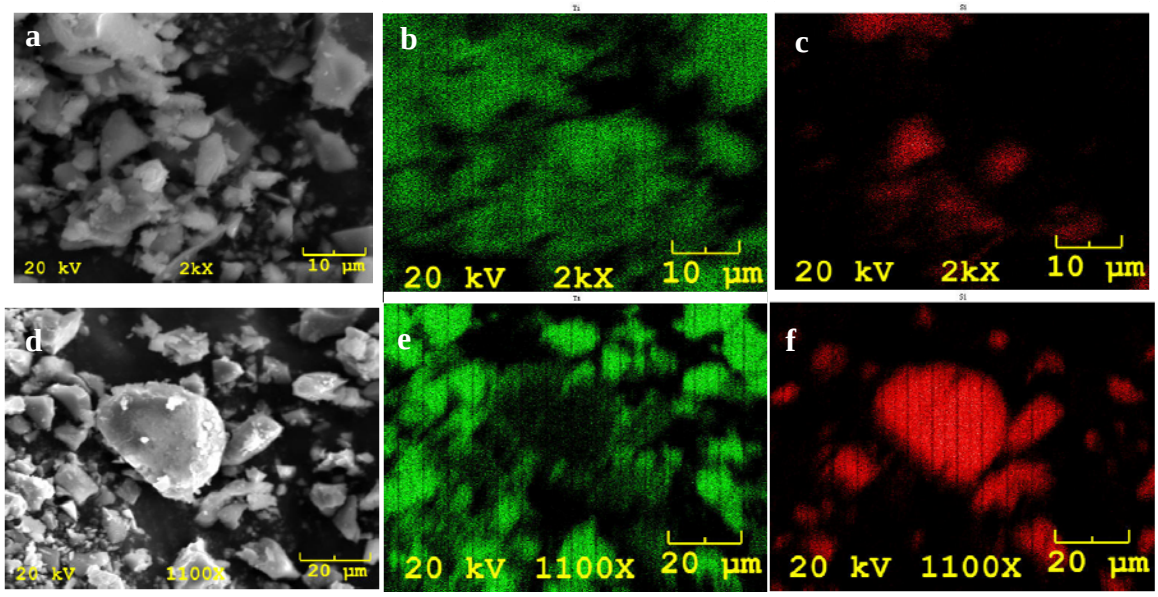

Figure 68. SEM (a, d) and EDX mapping images (b, c, e, f) of two examples of organotitania coated PSi, where b, e are for titanium and c, f are for silicon.

In order to coat an uniformly thin layer of organotitania material on the PSi particle surface, diluted Ti(IV) propoxide was used. In this case, Cipro HCl was first loaded into PSi with 81% porosity and 38-75 μm in size (referred to herein as PPK 1405) by the method described in section 5.2.1. The coated samples were characterized by FTIR, SEM, and EDX mapping, and followed by antibacterial assays.

Figure 69 presents FTIR spectra of Cipro HCl loaded PSi, taken before (a) and after (b) coating, and Figure 68c is a spectrum of a control sample prepared from the reaction of Ti(IV) propoxide with D. I. water. From Figure 69c, the multiple peaks in the range of 500-1000 cm^{-1} can be considered as characteristic of the organotitania product. Thus, in Figure 69b, the increased absorbance in the range of 500-1000 cm^{-1} compared with the uncoated PSi sample shown in Figure 68a is presumably due to the organotitania coating.

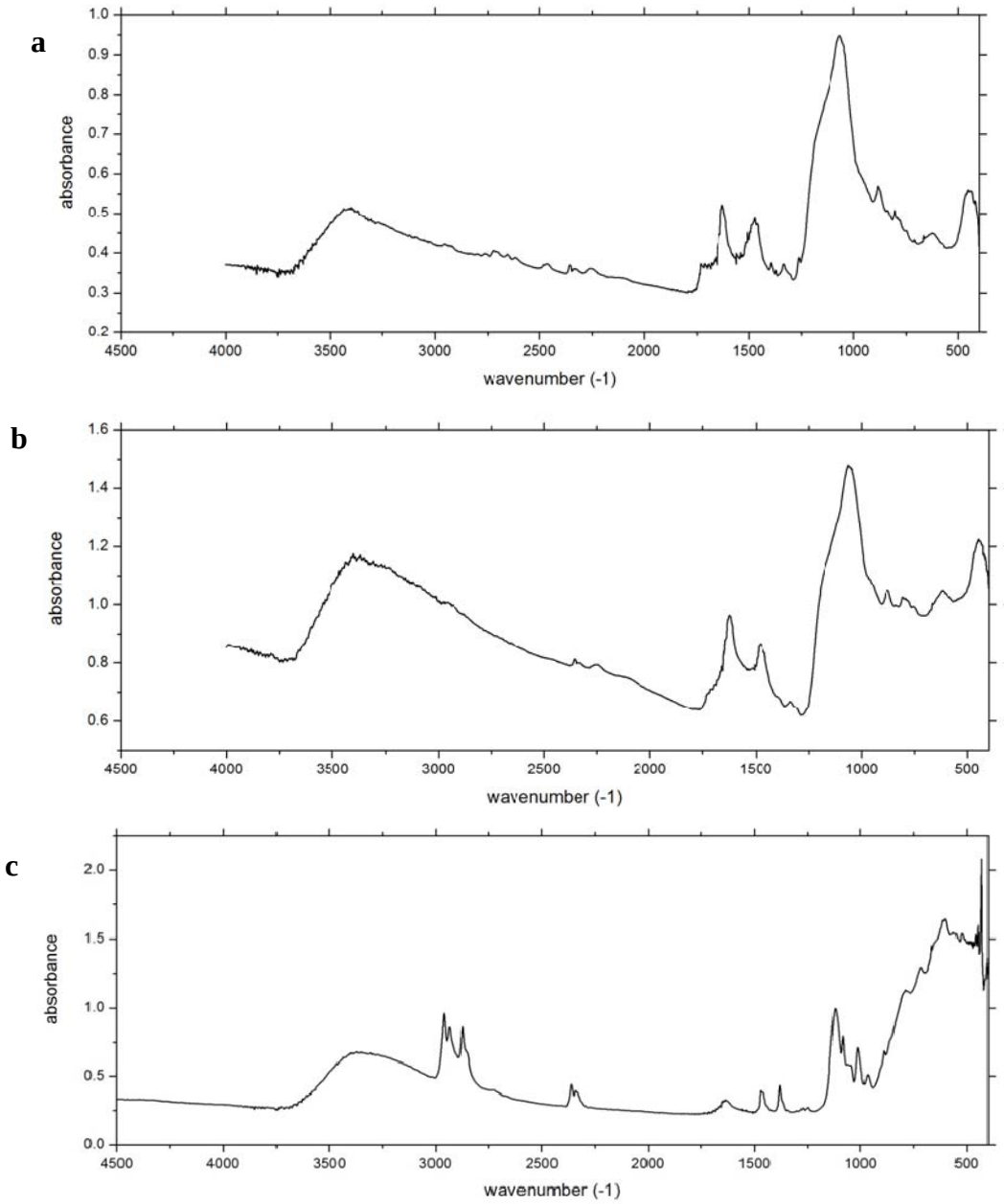

Figure 69. IR spectra of Cipro HCl loaded PSi (a), coated PSi (b) and product from Ti(IV) propoxide reacting with water (c) as control.

Further characterization was carried out by SEM and EDX. Figure 70 shows the SEM, and EDX mapping images and the associated elemental analysis of Cipro HCl loaded PSi before coating with Ti(IV) propoxide. Figure 70a was taken at low magnification and shows the relatively uniform size of PSi particles used in this

experiment. There is 6.4 wt% Cl in this microscopic area (Figure 70b). A SEM image from another area under a higher magnification is shown in Figure 70c. The corresponding Cl in this area is 6.89 wt%, and the silicon and triclosan are all distributed evenly.

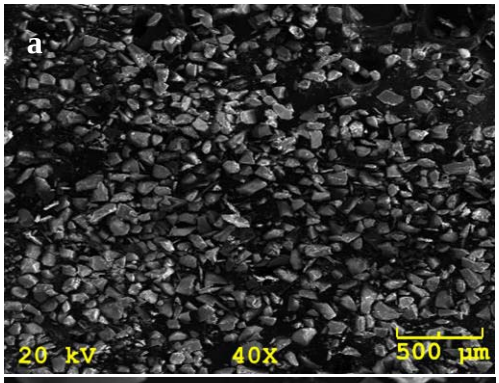

b

Elt.	Line	Intensity (c/s)	Atomic %	Atomic Ratio	Conc		
Si	Ka	879.36	94.855	1.0000	93.591	wt.%	
Cl	Ka	29.87	5.145	0.0542	6.409	wt.%	
			100.000		100.000	wt.%	Total

kV	20.0
Takeoff Angle	35.0°
Elapsed Livetime	60.0

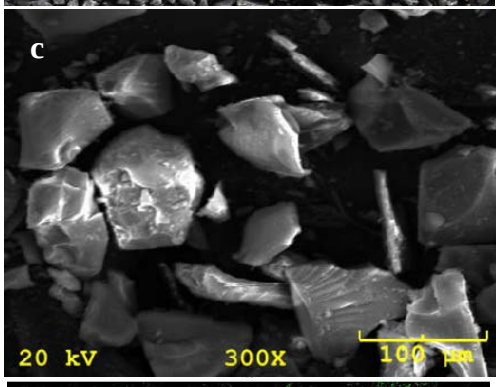

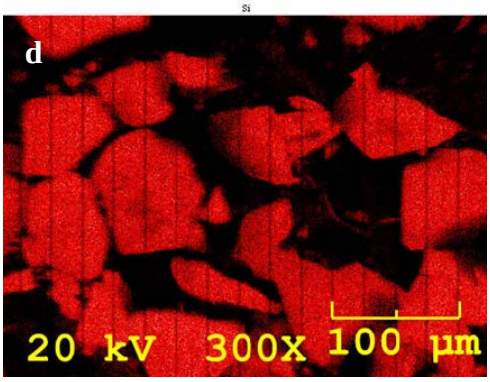

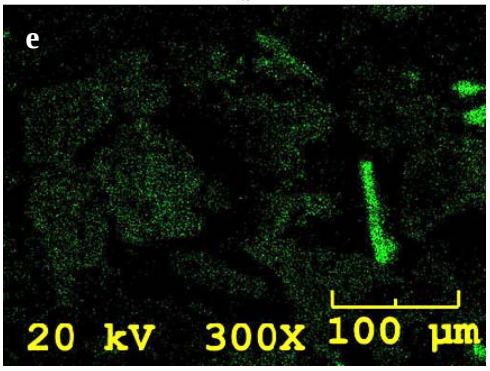

f

Elt.	Line	Intensity (c/s)	Atomic %	Atomic Ratio	Conc		
Si	Ka	17,802.08	94.461	1.0000	93.108	wt.%	
Cl	Ka	655.66	5.539	0.0586	6.892	wt.%	
			100.000		100.000	wt.%	Total

kV	20.0
Takeoff Angle	35.0°
Elapsed Livetime	98.0

Figure 70. SEM image of a Cipro HCl loaded PSi sample before coating at low magnification (a) and its elemental analysis (b). SEM image of another area at high magnification (c) and its EDX mapping (d for Si and e for Cl) and its elemental analysis (f).

Compared with samples before coating, an SEM image at low magnification (Figure 71a) shows the particle size is still uniform after coating. The most significant

difference compared with the samples produced by the undiluted Ti(IV) propoxide is the uniform signal for titanium distributed on the PSi particle surface and an absence of extra titania particles. Meanwhile, the Cl percentages are lower than those before coating (Figure 71b, d compared with Figure 70b and f).

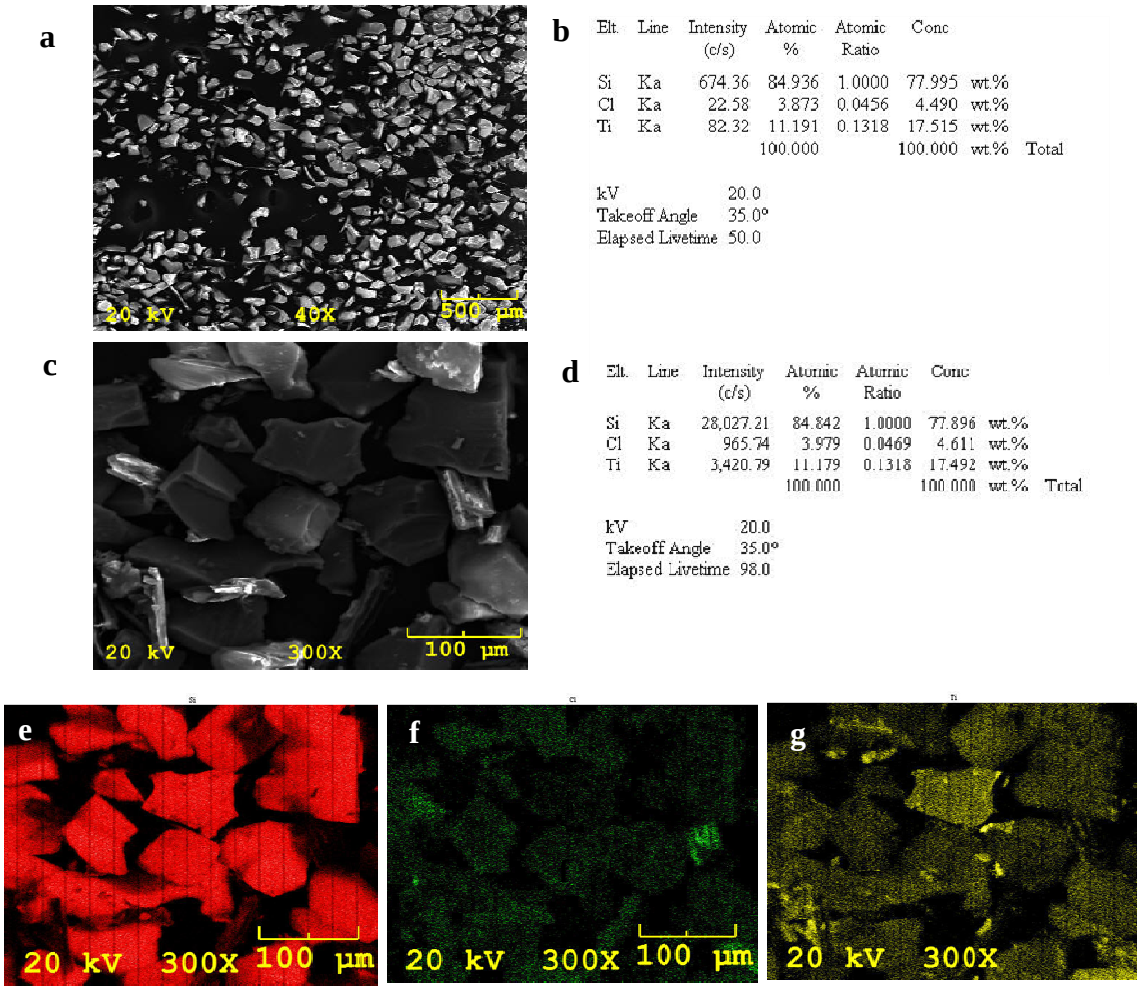

Figure 71. SEM image of a Cipro HCl loaded PSi sample after coating at low magnification (a) and its elemental analysis (b). SEM image of another area at high magnification (c), elemental analysis (d) and its EDX mapping (e for Si, f for for Cl and g for Ti).

Finally, the antibacterial assay results (Figure 72) reveal that after an organotitania coating, the highest concentration of released Cipro HCl decreases from 0.2

mg/mL to 0.017 mg/mL, inhibition zone decreases from 22 mm to 10 mm on the first day, and the activity duration is reduced by one day relative to the uncoated sample. The significant decreases in concentration of released Cipro HCl and associated inhibition zone confirm that an organotitania coating on these PSi particles also provides a barrier for payload diffusion.

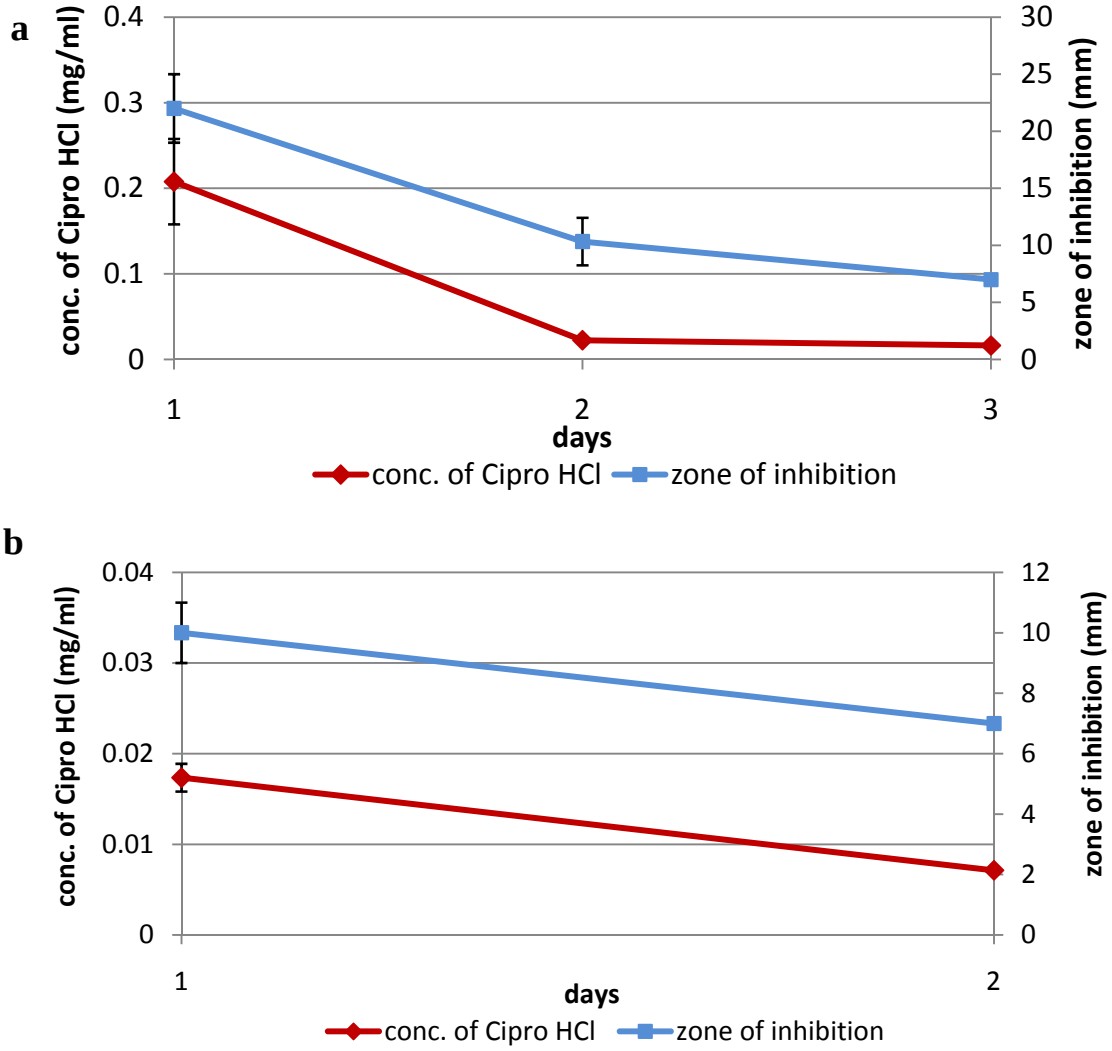

Figure 72. Combined zone inhibition assay/Cipro HCl concentration release assay for PSi before (a) and after (b) organotitania coating.

6.4 Summary

In this study, the goal of developing surface coatings through organosilica and organotitania film has been successfully achieved. These coatings can be produced with rather simple procedures in a uniform manner, and they do prevent payload diffusion to the surroundings, or alternatively extracts the active drug from the pores during the coating process. Further refinements, including the role of annealing and the use of other silicon and titanium alkoxide reagents, remain to be evaluated.

References

1. (a) Han, C.; Wang, B. In *Drug delivery: principles and applications*. Wiley-Interscience, **2005**, p 1. (b) Kuhlmann, J. *Int. J. Clin. Pharmacol. Ther.* **1997**, *35*, 541-552.
2. Prentis, R. A.; Lis, Y.; Walker, S. R. *Br. J. Clin. Pharmacol*. **1988**, *25*, 387-396.
3. Kubinyi, H. *Nat. Rev. Drug Discov.* **2003**, *2*, 665-668.
4. Merisko-Liversidge, E. M.; Liversidge, G. G. *Toxicol Pathol* **2008**, *36*, 43-48.
5. Lipinski, C. A. *J. Pharmacol. Toxicol. Methods* **2000**, *4*, 235-249.
6. Lee, T. W. L.; Robinson, J. R. In *Remington: The Science and Practice of Pharmacy*, Limmer, D., Ed.; Lippincott Williams & Wilkins: Baltimore, **2000**, p 2077.
7. Hancock, B. C.; Parks, M. *Pharm. Res*. **2000**, *17*, 397-404.
8. Zhou, D.; Zhang, G. Z.; Law, D.; Grant, D. J. W.; Schmitt, E. A. *J. Pharm. Sci* **2002**, *91*, 1863-1872.
9. Martinez, M. N.; Amidon, G. L. *J. Clin. Pharmacol.* **2002**, *42*, 620-643.
10. Allen, T. M.; Cullis, R. R. *Science* **2004**, *303*, 1818-1822.
11. Kaparissides, C.; Alexandridou, S.; Kotti, K.; Chaitidou, S. *J. Nanotech. Online* **2006**, *2*, 1-11.
12. Desail, D.; Kothari, S.; Chen, W.; Wang, J.; Huang, M.; Sharma, L. *J. Pharm. Sci.* **2011**, *100*, 1900-1912.
13. Zhou, Y.; Huang, W.; Liu, J.; Zhu, X.; Yan, D. *Adv. Mater.* **2010**, *22*, 4567-4590.
14. Jeong, B.; Bae, Y. H.; Lee, D. S.; Kim, S. W. *Nature* **1997**, *388*, 860-862.

15. (a) Kratz, K.; Narasimhan, A.; Tangirala, R.; Moon, S.; Revanur, R.; Kundu, S.; Kim, H. S.; Crosby, A. J.; Russell, T. P.; Emrick, T.; Kolmakov, G.; Balazs, A. C. *Nat. Nanotech.* **2012**, *7*, 87–89. (b) Liu, X.; Gao, C.; Shen, J.; Mohwald, H. *Macromol. Biosci*. **2005**, *5*, 1209–1219.

16. Lian, T.; Ho, R. J. Y. *J. Pharm. Sci.* **2001**, *90*, 667-680.

17. (a) Lasic, D. *Nature* **1992**, *355*, 279-280. (b) Huang, C. K.; Lo, C. L.; Chen, H. H.; Hsiue, G. H. *Adv. Funct. Mater.* **2007**, *17*, 2291-2297.

18. Gao, W.; Chan, J. M.; Farokhzad, O. C. *Mol. Pharmaceut.* **2010**, *7*, 1913-1920.

19. Chandna, P.; Saad, M.; Wang, Y.; Ber, E.; Khandare, J.; Vetcher, A. A.; Soldatenkov, V. A.; Minko, T. *Mol. Pharmaceut.* **2007**, *4*, 668-678.

20. Wang, C.; Chen, J.; Talavage, T.; Irudayaraj, J. *Angew. Chem.* **2009**, *121*, 2797-2801.

21. Peng, G.; Tisch, U.; Adams, O.; Hakim, M.; Shehada, N.; Broza, Y. Y.; Billan, S.; Abdah-Bortnyak, R.; Kuten, A.; Haick, H. *Nat. Nanotech.* **2009**, *4*, 669-673.

22. Pornpattananangkul, D.; Zhang, L.; Olson, S.; Aryal, S.; Obonyo, M.; Vecchio, K.; Huang, C.; Zhang, L. *J. Am. Chem. Soc.* **2011**, *133*, 4132-4139.

23. Norman, R. S.; Stone, J. W.; Gole, A.; Murphy, C. J.; Sabo-Attwood, T. L. *Nano Lett.* **2008**, *8*, 302-306.

24. Zhang, X.; Chen, M.; Lam, R.; Xu, X.; Osawa, E.; Ho, D. *ACS Nano* **2009**, *3*, 2609-2616.

25. Ghosh, P.; Kim, C.; Han, G.; Forbes, N. S.; Rotello, V. M. *ACS Nano* **2008**, *2* 2213-2218.

26. Farokhzad, O. C.; Langer, R. *ACS Nano* **2009**, *3*, 16-20.

27. Lenk, C.; Biller-Andorno, B. *Med. Health Care Philos.* **2007**, *10*, 173-184.

28. Park, K. *J. Control Release* **2007**, *120*, 1–3.

29. (a) Wagner, V.; Dullaart, A.; Bock, A. K.; Zweck, A. *Nat. Biotechnol.* **2006**, *24*, 1211–1217. (b) Zhang, L.; Gu, F. X.; Chan, J. M.; Wang, A. Z.; Langer, R. S.; Farokhzad, O. C. *Clin. Pharmacol. Ther.* **2008**, *83*, 761–769. (c) Davis, M. E.; Chen, Z.; Shin, D. M. *Nat. Rev. Drug Discovery* **2008**, *7*, 771–782.

30. Shi, J.; Votruba, A. R.; Farokhzad, O. C.; Langer, R. *Nano Lett*. **2010**, *10*, 3223–3230.

31. Zhang, L.; Gu, F. X.; Wang, A. Z.; Langer, R. S.; Farokhzad, O. C. *Clin. Pharmacol. Ther.* **2008,** *83*, 761-769.

32. Duncan, R. *Nat. Rev. Drug Discov.* **2003**, *2*, 347-360.

33. (a) Zhang, L.; Granick, S. *Nano Lett.* **2006**, *6*, 694–698. (b) Bangham, A. D.; Horne, R. W. *J. Mol. Biol.* **1964**, *8*, 660–668. (c) Horne, R. W.; Bangham, A. D.; Whittaker, V. P. *Nature* **1963**, *200*, 1340. (d) Bangham, A. D.; Horne, R. W.; Glauert, A. M.; Dingle, J. T.; Lucy, J. A. *Nature* **1962**, *196*, 952–955.

34. Torchilin, V. P. *Nat. Rev. Drug Discov*. **2005**, *4*, 145–159.

35. Northfelt, D. W.; Dezube, B. J.; Thommes, J. A.; Miller, B. J.; Fischl, M. A.; Friedman-Kien, A.; Kaplan, L. D.; Mond, C. D.; Mamelok, R. D.; Henry, D. H. *J. Clin. Oncol.* **1998**, *16*, 2445–2451.

36. Francis, M. F.; Cristea, M.; Winnik, F. M. *Pure Appl. Chem*. **2004**, *76*, 1321-1335.

37. Haag, R.; Kratz, F. *Angew. Chem. Int. Ed.* **2006**, *45*, 1198 – 1215.

38. Dykes, G. M. J. *Chem. Technol. Biotechnol.* **2001**, 76903-76918.

39. Klanjnert, B.; Bryszewska, M. *Acta Biochim. Pol.* **2001**, *48*, 199-208.

40. Kukowska-Latallo, J. F.; Candido, K. A.; Cao, Z. *Cancer Res.* **2005**, *65*, 5317–5324.

41. Zhu, Y.; Shi, J.; Shen, W.; Chen, H.; Dong, X.; Ruan, M. *Nanotechnology* **2005**, *16*, 2633-2638.

42. Jurgon, R.; Seliger, C.; Hilpert, A. Trahms, L.; Odenbach, S.; Alexiou, C. *J. Phys.: Condens. Matter*. **2006**, *18*, S2893–S2902.

43. Kim, D. K.; Mikhaylova, M.; Zhang, Y.; Muhammed, M. *Chem. Mater.* **2003**, *15*, 1617-1627.

44. Wang, Q.; Liu, J. *Fundam. Biomed. Technol.* **2011**, *5,* 567-598.

45. Zhao, Q.; Wang, L.; Cheng, R.; Mao, L.; Arnold, L. D.; Howerth, E. W.; Chen, Z. G.; Platt, S. *Theranostics* **2012**, *2,* 113-121.

46. (a) Giljohann, D. A.; Seferos, D. S.; Daniel, W. L.; Massich, M. D.; Patel, P. C.; Mirkin, C. A. *Angew. Chem., Int. Ed*. **2010,** *49*, 3280 – 3294. (b) Daniel, M.-C.; Astruc, D. *Chem. Rev.* **2004**, *104*, 293-346.

47. (a) El-Ghannam, A.; Jahed, K.; Govindaswami, M. *J. Biomed. Mater. Res. Part A* **2010**, *94A*, 308-316. (b) Sabetrasekh, R.; Tianined, H.; Lyngstadaas, S. P.; Reseland, J.; Haugen, H. *J. Biomater. Appl.* **2011**, *25*, 559-580.

48. (a) Vitale-Brovarone, C.; Ciapetti, G.; Leonardi, E.; Baldini, N.; Bretcanu, O.; Verné, E.; Baino, F. *J. Biomater. Appl.* **2011,** *26*, 465-489. (b) Balagna, C.; Vitale-Brovarone, C.; Miola, M.; Verné, E.; Canuto, R. A.; Saracino, S.; Muzio, G.; Fucale, G.; Maina, G. *J. Biomater. Appl*. **2011**, *25*, 595-617. (c) Vallet-Regí, M.; Ruiz-Hernández, E. *Adv. Mater.* **2011,** *23*, 5177–5218.

49. Paul, W.; Sharma, C. P. *J. Biomater. Appl.* **2003**, *17*, 253-264.

50. Palazzo, B.; Iafisco, M.; Laforgia, M.; Margiotta, N.; Natile, G.; Bianchi, C. L.; Walsh, D.; Mann, S.; Roveri, N. *Adv. Funct. Mater.* **2007**, *17*, 2180–2188.

51. Espanol, M.; Perez, R. A.; Montufar, E. B.; Marichal, C.; Sacco, A.; Ginebra, M. P. *Acta Biomater.* **2009**, *5*, 2752–2762.

52. Colilla, M.; Manzano, M.; Vallet-Regí, M. *Int. J. Nanomedicine* **2008**, *3*, 403–414.

53. Popovici, R. F.; Seftel, E. M.; Mihai, G. D.; Popovici, E.; Voicu, A. A. *J. Pharm. Sci.* **2011**, *100*, 704-714.

54. Reffitt, D. M.; Jugdaohsingh, R.; Thompson, R. P.; Powell. J. J. *J. Inorg. Biochem.* **1999**, *76*, 141-147.

55. Uhlir, A., Jr. A. *Bell. Syst. Tech. J.* **1956**, *35*, 333-347.

56. Torres-Costa, V.; Martín-Palma, R. J. *J. Mater. Sci.* **2010**, *45*, 2823-2838.

57. Watanabe, Y.; Sakai, T. *Rev.Elec. Commun. Lab.* **1971**, *19*, 899-905.

58. Canham, L. T. *Appl. Phys. Lett.* **1990**, *57*, 1046-1048.

59. (a) Canham, L. T. *Adv. Mater.* **1995**, *7*, 1033-1037. (b) Canham, L. T.; Newey, J. P.; Reeves, C. L.; Houlton, M. R.; Loni, A.; Simons, A. J.; Cox, T. I. *Adv. Mater.* **1996**, *8*, 847-849. (c) Canham, L. T.; Reeves, C. L.; King, D. O.; Branfield, P. J.; Crabb, J. G.; Ward. M. C. L. *Adv. Mater.* **1996**, *8*, 850-852. (d) Bowditch, P.; Waters, K.; Gale, H.; Rice, P.; Scott, E. A. M.; Canham, L. T.; Reeves, C. L.; Loni, A.; Cox, T. I. *Mat. Res. Soc. Symp. Proc.* **1999**, *536*, 149-154.

60. Salonen, J.; Kaukonen, A. M.; Hirvonen, J.; Lehto, V. *J. Pharm. Sci*, **2008**, *97*, 632-653.

61. Halimaoui, A. In *Porous Silicon Science and Technology*. Vial, J. C.; Derrien, J., Ed.; Springer-Verlag New York Inc.: France, **1994**, p 33.

62. Halimaoui, A. In *Properties of Porous Silicon.* Canham, L. T., Ed.; INSPEC, The Institution of Electrical Engineers: London, United Kingdom, **1997**, p 12.

63. Coffer, J. L. In *Properties of Porous Silicon.* Canham, L. T., Ed.; INSPEC, The Institution of Electrical Engineers: London, United Kingdom, **1997**, p 23.

64. (a) Fathauer, R. W.; George, T.; Ksendzov, A.; Vasquez, R. P. *Appl. Phys. Lett*. **1992**, *60*, 955-997. (b) Shih, S.; Jung, K. H.; Hsieh, T. Y.; Sarathy, J.; Campbell, J. C.; Kwong, D. L. *Appl. Phys. Lett.* **1992**, *60*, 1863-1865.

65. Smith, R. L.; Collins, S. D. *J. Appl. Phys*. **1992**, *71*, R1-R22.

66. Lehmann, V.; Gösele, U. *Appl. Phys. Lett.* **1991**, *58*, 856-858.

67. Heinrich, J. L.; Curtis, C. L.; Credo, G. M.; Kavanagh K. L.; Sailor, M. J. *Science*, **1992**, *255*, 66–68.

68. (a) Salonen, J.; Laitinen, L.; Kaukonen, A. M.; Tuura, J.; Björkqvist, M.; Heikkilä, T.; Vähä-Heikkilä, K.; Hirvonen**,** J.; Lehto, V.-P. *J. Controlled Release* **2005**, *108*, 362-374. (b) Dorvee, J. R.; Sailor, M. J.; Miskelly, G. M. *Dalton Trans.* **2008**, 721-730.

69. Chiappini, C.; Tasciotti, E.; Fakhoury, J. R.; Fine, D.; Pullan, L.; Wang, Y.-C.; Fu, L.; Ferrari, M. *Chem. Phys. Chem.* **2010**, *11*, 1029-1035.

70. Fekih, Z.; Otmani, F. Z.; Ghellai, N.; Chabanne-Sari, N. E. *M. J. Condensed Mate.* **2006**, *7*, 35-37.

71. (a) Canham, L. T. In *Properties of Porous Silicon*. Canham, L. T., Ed.; INSPEC, The Institution of Electrical Engineers: London, United Kingdom, **1997**, p 83. (b) du Plessis, M. *Mater. Sci. & Eng. B* **2008**, *147*, 226-229.

72. Herino, R.; Bomchil, G. Bertrand, C.; Ginoux, J. L. *J. Electrochem. Soc.* **1987**, *134*, 1994-2000.

73. Zhang, X. G. *J. Eletrochem. Soc.* **2004**, *151*, C69-C80.

74. Bradley D. F.; Ramírez-Porras, A. In *Advances in Chemical Sensors*. Wang, W., Ed.; InTech, **2012**, p 153.

75. Song, J. H.; Sailor, M. J. *J. Am. Chem. Soc.* **1998**, *120*, 2376-2381.

76. Buriak, J. M. *Chem. Rev.* **2002**, *102*, 1271-1308.

77. Gupta, P.; Colvin, V. L.; George, S. M. *Phys. Rev. B*, **1988**, *37*, 8234-8243.

78. Canham, L. T. In *Properties of Porous Silicon.* Canham, L. T., Ed.; INSPEC, The Institution of Electrical Engineers: London, United Kingdom, **1997**, p 145.

79. Earwaker, L. G.; Farr, J. P. G.; Grzeszczyk, P. E.; Sturland, I. *Nucl. Instrum. & Methods Phys. Res. B* **1985**, *B9*, 317-320.

80. Loni, A.; Simons, A. J.; Canham, L. T.; Philips, H. J.; Earwaker, L. G. *J. Appl. Phys.* **1993**, *76*, 2825-2832.

81. Canham, L. T.; Houlton, M. R.; Leong, W. Y.; Peckering, C.; Keen, J. M. *J. Appl. Phys.* **1991**, *70*, 422-431.

82. Stutzmann, M.; Brandt, M. S. *Phys. Status Solidi B* **1995**, *190*, 97-106.

83. Banerjee, S.; Narasimhan, K. L.; Sardesai, A. *Phys. Rev. B* **1994**, *49*, 2915-2918.

84. Konishi, T.; Yao, T.; Tajima, M.; Ohshima, H.; Ito, H.; Hattori, T. *Jpn. J. Appl. Phys.* **1992**, *31*, L1216-1218.

85. Grosman, A.; Orgega, C.; Siejka, J.; Chamarro, M. *J. Appl. Phys.* **1993**, *74*, 1992-1996.

86. Anderson, R. C.; Muller, R. S.; Tobias, C. W. *J. Electrochem. Soc*. **1993**, *140*, 1393-1396.

87. Bowditch, A. P.; Waters, K.; Gale, H.; Rice, P.; Scott, E. A. M.; Canham, L. T.; Reeves, C. L.; Loni, A.; Cox, T. I. *Mater. Res. Soc. Symp. Pro.* **1999**, *536*, 149-154.

88. Decuzzi, P.; Pasqualini, R.; Arap, W.; Ferrari, M. *Pharm. Res.* **2009**, *26*, 235-243.

89. Anderson, S. H. C.; Elliott, H.; Wallis, D. J.; Canham, L. T.; Powell, J. J. *Phys. Stat. Sol. (a)* **2003**, *197*, 331-335.

90. (a) Armstrong, F. A. J. *J. Mar. Biol. Assoc. U. K.* **1951**, *30*, 149-160. (b) Tůma, J. *Microchimica Acta* **1961**, *50*, 513-523.

91. Salonen, J.; Lehto, V.-P.; Laine, E. *Appl. Phys. Lett.* **1997**, *70*, 637-639.

92. Takahagi, T.; Ishitani, A.; Kuroda, H.; Nagasawa, Y.; Ito, H.; Wakao, S. *J. Appl. Phys.* **1990**, *68*, 2187.

93. Bisi, O.; Ossicini, S.; Pavesi, L. *Surf. Rep.* **2000**, *38*, 1-126.

94. Canham, L. T. In *Properties of Porous Silicon.* Canham, L. T., Ed.; INSPEC, The Institution of Electrical Engineers: London, United Kingdom, **1997**, p 60.

95. Morazzani, V.; Ganem, J. J.; Cantin, J. L. In *Optoelectronic Properties of Semiconductors and Superlattices Volume 5: Structural and Optical Properties of Porous Silicon Nanostructures*, Amato, G.; Delerue, C.; von Bardeleben, H.-J. Eds., Gordon and Breach Science Publishers: Amsterdam, Netherlands, **1997**, p 526.

96. Canham, L. T. In *Properties of Porous Silicon.*Canham, L. T., Ed.; INSPEC, The Institution of Electrical Engineers: London, United Kingdom, **1997**, p 160.

97. Hou, X. Y.; Shi, G.; Wang, W.; Zhang, F. L.; Hao, P. H.; Huang, D. M.; Wang, X. *Appl. Phys. Lett.* **1993**, *62*, 1097-1098.

98. Nakajima, A.; Itakura, T.; Watanabe, S.; Nakayama, N. *Appl. Phys. Lett.* **1992**, *61*, 46-48.

99. Jia, L.; Wong, S. P.; Wilson, I. H.; Hark, S. K.; Zhang, S. L.; Liu, Z. F.; Cai, S. M. *Appl. Phys. Lett.* **1997**, *71*, 1391-1393.

100. Song, J. H.; Sailor, M. J. *Inorg. Chem.* **1998**, *37*, 3355-3360.

101. Harper, T. F.; Sailor, M. J. *J. Am. Chem. Soc.* **1997**, *119*, 6943-6944.

102. Matiei, G.; Alieva, E. V.; Petrov, J. E.; Yakovlev, V. A. *Phys. Stat. Sol. (a)*, **2000**, *182*, 139-143.

103. Anglin, E. J.; Cheng, L.; Freeman, W. R.; Sailor, M. J. *Adv. Drug Deliv. Rev.* **2008**, *60*, 1266-1277.

104. Bansal, A.; Li, X.; Lauermann, I.; Lewis, N. S. *J. Am. Chem. Soc*. **1996**, *118*, 7225-7226.

105. Stewart, M. P.; Buriak, J. M. *J. Am. Chem. Soc.* **2001**, *123*, 7821-7830.

106. Schmeltzer, J. M.; Porter, L. A.; Stewart, M. P.; Buriak, J. M. *Langmuir* **2002**, *18*, 2971-1974.

107. Buriak, J. M. *Chem. Commun.* **1999**, 1051-1060.

108. Buriak, J. M. *Adv. Mater*. **1999**, *11*, 265-267.

109. Canham, L. T. In 1st Annual International IEEE-EMBS Special Topic Conference on Microtechnologies in Medicine & Biology, October 12-14, 2000, Lyon, France.

110. Li, X.; Coffer, J. L.; Chen, Y.; Pinizzotto, R. F.; Newey, J.; Canham, L. T. *J. Am. Chem. Soc.* **1998**, *120*, 11706-11709.

111. Li, X.; St. John, J. St.; Coffer, J. L.; Chen, Y.; Pinizzotto, R. F.; Newey, J.; Reeves, C.; Canham, L. T. *Biomedical Microdevices* **2000**, *2*, 265-272.

112. Canham, L. T. *Nanotechnology* **2007**, *18*, 185704.

113. Tanaka, T.; Mangala, L. S.; Vivas-Mejia, P.; Nieves-Alicea, R.; Mann, A. P.; Mora, E.; Han, H.-D.; Shahzad, M. M. K.; Liu, X.; Bhavane, R.; Gu, J.; Fakhoury, J. R.; Chiappini, C.; Lu, C.; Matsuo, K.; Godin, B.; Stone, R. L.; Nick, A. M.; Lopez-Berestein, G.; Sood, A. K.; Ferrari, M. *Cancer Res*. **2010**, *70*, 3687-3696.

114. Serda, R. E.; Chiappini, C.; Fine, D.; Tasciotti, E.; Ferrari, M. In *Nanotechnologies for the Life Sciences*, Wiley-VCH VeriagGmbh & Co. KGaA, **2007**, pp 357-398.

115. Salonen, J. S.; Kaukonen, A. M.; Hirvonen, J.; Lehto, V.-P. *J. Pharm. Sci.* **2008**, *97*, 632-653.

116. Dev Das, R.; Maji, S.; Das, S.; Roy Chaudhuri, C. *Appl. Surf. Sci.* **2010**, *256*, 5867-5875.

117. Wu, E. C.; Andrew, J. S.; Cheng, L.; Freeman, W. R.; Pearson, L.; Sailor, M. J. *Biomaterials* **2011**, *32,* 1957-1966.

118. Gu, L.; Park. J.; Duong, K. H. Ruoslahti, E.; Sailor, M. J. *Small* **2010**, *6*, 2546-2552.

119. Whitehead, M. A.; Fan, D.; Mukherjee, P.; Akkaraju, G. R.; Canham, L. T.; Coffer, J. L. *Tissue Eng.* **2008**, *14*, 195-206.

120. Fan, D.; Akkaraju, G. R.; Couch, E. F.; Canham, L. T.; Coffer, J. L. *Nanoscale* **2011**, *3*, 354-361.

121. (a) Moxon, K. A.; Hallman, S.; Aslani, A.; Kalkhoran, N. M.; Lelkes, P. I. *J. Biomater. Sci. Polymer Edn.* **2007**, *18*, 1263-1281. (b) Sapelkin, A. V.; Bayliss, S. C.; Unal, B.; Charalambou, A. *Biomaterials* **2006**, *27*, 842-846.

122. Bogue, R. W. *Biosen. Bioelectron.* **1997**, *12*, xxvii-xxviii.

123. Lin, V. S.-Y.; Motesharei, K.; Dancil, K.-P. S.; Sailor, M. J.; Ghadiri, M. R. *Science* **1997**, *278*, 840-843.

124. Stewart, M. P.; Buriak, J. M. *Adv. Mater.* **2000**, *12*, 859-869.

125. Dancil, K.-P. S.; Greiner, D. P.; Sailor, M. J. *J. Am. Chem. Soc*. **1999**, *121*, 7925-7930.

126. Veiga, M. D.; Merino, M.; Cirri, M.; Maestrelli, F.; Mura, P. *J. of Incl. Phenom. Macro. Chem.* **2005**, *53*, 77-83.

127. Coia, J. E.; Duckworth, G. J.; Edwards, D. I.; Farrington, M.; Fry, C.; Humphreys, H.; Mallaghan, C.; Tucker, D. R. *J. Hosp. Infect.* **2006**, *63*, S1-S44.

128. Nelson, J. M.; Chiller, T. M.; Powers, J. H.; Angulo, F. J. *Clin. Infec. Dis.* **2007**, *44*, 977-980.

129. Caço, A. I.; Varanda, F.; Pratas de Melo, M. J.; Dias, A. M. A.; Dohrn, R.; Marrucho, I. M. *Ind. Eng. Chem. Res.* **2008**, *47*, 8083-8089.

130. Varanda, F.; Pratas de Melo, M. J.; Caço, A. I.; Dohrn, R.; Makrydaki, F. A.; Voutsas, E.; Tassios, D.; Marrucho, I. M. *Ind. Eng. Chem. Res.* **2006**, *45*, 6368-6374.

131. Dorofeev, V. L.; Arzamastsev, A. P.; Veselova, O. M. *Pharm. Chem. J.* **2004**, *38*, 333-335.

132. Blumberg, H. M.; Rimland, D.; Carroll, P. T.; Wachsmuth, I. K. *J. Infec. Dis.* **1991**, *163*, 1279-1285.

133. (a) Zimpfer, A.; Propst, A.; Mikuz, G.; Vogel, W.; Terracciano, L.; Stadlmann, S. *Virchows Arch* **2004**, *444*, 87-89. (b) Jongen-Lavrencic, M.; Schneeberger, P. M.; van der Hoeven, J. G. *Infection* **2003**, *31*, 428-429. (c) Owens Jr., R. C.; Ambrose, P. G. *CID*, **2005**, *41*, S144-S157. (d) Mandal, B.; Steward, M.; Singh, S.; Jones, H. *Age and Ageing* **2004**, *33*, 405-406.

134. Kluytmans, J.; van Belkum, A.; Verbrugh, H. *Clin. Microbio. Rev.* **1997**, *10*, 505-520.

135. Liu, G.; Essex, A.; Buchanan, J. T.; Datta, V.; Hoffman, H. M.; Bastian, J. F.; Fierer, J.; Nizet, V. *J. Exp. Medic.* **2005**, *202*, 209-215.

136. Seifert, H.; Wisplinghoff, H.; Schnabel, P.; von Eiff, C. *Emerg. Infect. Dis.* **2003**, *9*, 1316-1318.

137. Chambers. H. F. *Emerg. Infect. Dis.* **2001**, *7*, 178-182.

138. Ibelings, M. M. S.; Bruining, H. A. *Eur. J. Surg.* **1998**, *154,* 411-418.

139. (a) Davis, W. W.; Stout, T. R. *Appl. Microbiol.* **1971**, 659-665. (b) Threlfall, E. J.; Fisher, I. S. T.; Ward, L.; Tschape, H.; Gerner-Smidt, P. *Microb. Drug Resist*. **1999**, *5*, 195-199. (c) Walker, R. D. In *Antimicrobial Therapy in Veterinary Medicine*, Prescott, J. F.; Baggot, J. D.; Walker, R. D., Eds.; Iowa State University Press: Ames, IA, **2000**, pp 12-26.

140. Stalons, D. R.; Thornsberry, C. *Antimicrob. Agents Chemother.* **1975**, *7*, 15-21.

141. Zilberman, M.; Elsner, J. J. *J. Controlled Release* **2008**, *130*, 202–215.

142. Jayanthi, B.; Manna, P. K.; Madhusudhan, S.; Mohanta, G. P.; Manavalan, R. *J. Appl. Pharm. Sci.* **2011**, *1*, 50-55.

143. Fan, D.; Loni, A.; Canham, L. T.; Coffer, J. L. *Phys. Status Solidi A* **2009**, *206*, 1322–1325.

144. Lindhe, J. *Am. J. Dent.* **1990,** *3*, 53–54.

145. Singer, H.; Müller, S.; Tixier, C.; Pillonel, L. *Environ. Sci. Technol.* **2002**, *36*, 4998–5004.

146. (a) Samyn, J. C.; Murthy, K. S. *J. Pharm. Sci.* **1974**, *63*, 370-375. (b) Muzzio, F. J.; Robinson, P.; Wightman, C.; Brone, D. *Int. J. Pharm.* **1997**, *155*, 153-178. (c) Kapil, R.; Kapoor, D. N.; Dhawan, S. *Drug Dev. Ind. Pharm.* **2010**, *36*, 45-55.

147. Caco, A. I.; Varanda, F.; Meolo, M. J. P.; Dias, A. M. A.; Dohrn, R.; Marrucho, I. M. *Ind. Eng. Chem. Res.* **2008**, *47*, 8083-8089.

148. Varanda, F.; Meolo, M. J. P.; Caco, A. I.; Dohrn, R.; Makrydaki, F. A.; Voutsas, E.; Tassios, D.; Marrucho, I. M. *Ind. Eng. Chem. Res.* **2006**, *45,* 6368-6374.

149. Ung, T.; Liz-Marzán, L. M.; Mulvaney, P. *Langmuir* **1998**, *14*, 3740-3748.

150. a) Iler, R. K. *Surf. Colloid Sci.* **1973**, *6*, 1-100. b) Iler, P. K. US Patent 2 885 366, 1959.

151. Deng, Y.; Wang, C.; Hu, J.; Yang, W. Fu, S. *Colloids Surf. A: Physicochem. Eng. Aspects* **2005,** *262*, 87–93.

152. Kasanen, J.; Suvanto, M.; Pakkanen, T. *J. Appl. Polym. Sci.* **2009**, *111*, 2597–2606.

153. Arai, T.; Ueda, T.; Sugiyama, T.; Sakurai, K. *J. Oral Rehabil.* **2009**, *36*, 902-908.

154. Liu, Q.; Xu, Z.; Finch, J. A.; Egerton, R. *Chem. Mater.* **1998**, *10*, 3936-3940.

155. Boccaccini, A. R.; Rossetti, M.; Roether, J. A.; Zein, S. H. S.; Ferraris, M.; *Constr. Build. Mater.* **2009**, *23*, 2554-2558.

VITA

Personal Background	Mengjia Wang Lanzhou, Gansu, China Daughter of Wang, Jinshun and Chai, Lanying Married Lixin Ding, January 9, 2006
Education	Bachelor of Science, Plant Science, Beijing University of Agriculture, Beijing, China, 2004 Doctor of Philosophy, Inorganic Chemistry, Texas Christian University, Fort Worth, Texas, 2012
Experience	Teaching Assistant, Texas Christian University, Fort Worth, Texas, 2007-2009 Research Assistant, Texas Christian University, Fort Worth, Texas, 2009-2012
Publications	"Sustained Antibacterial Activity from Triclosn-Loaded Nanostructured Mesoporous Silicon"; Mengjia Wang, Jeffery L. Coffer, Katrina Dorraj, Phil S. Hartman, Armando Loni and Leigh T. Canham; *Molecular Pharmaceutics*, **2010**, *7*, 2232 Manuscripts: 1) "Comparisons of triclosan loading into stain etched PSi versus anodized PSi to investigat the role of morphology"; Mengjia Wang, Jeffery L. Coffer, Phil S. Hartman, Armoando Loni and Leigh T. Canham. 2) "Incorporationof Ciprofloxacin and Ciprofloxacin HCl into different porous silicon materials"; Mengjia Wang, Jeffery L. Coffer, Phil S. Hartman, Armoando Loni and Leigh T. Canham. 3) "Investigations of triclosan release affected by PSi surface chemistry and loading methods"; Mengjia Wang, Jeffery L. Coffer, Phil S. Hartman, Armoando Loni and Leigh T. Canham.
Presentations	Student Research symposium (SRS): 1) "Inverstigation of Antibacterial Nanomaterials Based on Drug-Loaded Porous Silicon", Texas Christian University, Fort Worth, TX, 2009 2) "Functionalization of Porous Silicon Materials for Drug Delivery", Texas Christian University, Fort Worth, TX, 2010 3) "Impact of Surface Termination of the Porous Silicon Matrix on

its Antibacterial Drug Delivery Properties", Texas Christian University, Fort Worth, TX, 2011

Conferences

1) "Mesoporous silicon as an effective carrier for extended antibancterial and antifungal therapies"; Mengjia Wang, Jeffery L. Coffer, Porous Semiconductor Science and Technology Conference in Spain, 2010
2) "Nanostructured Mesoporous Silicon as an Effective Carrier for Extended antibacterial Therapy"; Mengjia Wang, Phil Hartman, Armando Loni, Leigh Canham and Jeffery L. Coffer, Materials Research Society, Symposium KK: Microbial Life on Surfaces—Biofilm-Mateiral Interactions, 2011
3) "Functionalized Mesoporous Siclion Particles for Sustained Drug Release of Antibiotics"; Mengjia Wang, Jeffery L. Coffer, Phil S. Harman, Armando Loni and Leigh T. Canham, 9th World Biomaterials Congress, 2012

ABSTRACT

CONTROLLED RELEASE OF ANTIBACTERIAL COMPOUNDS BASED ON MULTIPARAMETRIC ANALYSIS OF MESOPOROUS SILICON CARRIERS

by Mengjia Wang Ph. D. 2012

Department of Chemistry, Texas Christian University

Dissertation Advisor: Dr. Jeffery L. Coffer, Professor of Chemistry

Controlled delivery of antibacterial agents remains a topic of widespread significance, given the need for sustained release of therapeutically relevant concentrations. Porous Si (PSi), and the mesoporous form in particular, possesses useful properties relevant to its use in medical therapies such as drug delivery and tissue engineering. For drug delivery, both the biodegradability of mesoporous Si and its ability to nanostructure a given encapsulated substance present marked advantages.

In this work we have systematically investigated the influence of the properties of mesoporous silicon on both controlled release and antibacterial assay for the case of the loaded antibacterial drug triclosan and its activity versus *Staphylococcus aureus.* Specifically, the role of Si porosity, loading method, surface chemistry and particle morphology on the above outcomes are explored. For long term stabilization of the drug-loaded PSi, preliminary experiments regarding organosilicon and organotitanium surface coatings have also been carried out.

The role of PSi porosity on drug delivery has been highlighted by a comparison between the properties of triclosan loaded into porous silicon with high (81%), medium (65-75%), and low porosity (13%). The significant differences in triclosan release

behavior are demonstrated in their corresponding antibacterial disk diffusion assays. A remarkable sustained triclosan release beyond 100 days from mesoporous silicon matrices was revealed, combined with an enhanced concentration of released triclosan.

Due to the high surface area of these mesoporous materials, surface chemistry is expected to have a significant impact on drug delivery. Since freshly-etched PSi with its hydride-terminated surface possesses a relatively rapid degradation rate in aqueous media, derivatization of PSi by oxidation or chemical modification is needed. In this study, a relatively long octyl chain is covalently attached to the mesoporous silicon surface, which possesses hydrophobicity and inhibits aqueous dissolution. A combination of thermogravimetric analysis, X-ray diffraction, electron microscopy, and FT IR spectroscopy, in addition to triclosan release and antibacterial assays, are employed for this purpose.

A preliminary study involving organosilica and organotitania surface coatings on PSi was also conducted. FT IR spectroscopy, scanning electron microscopy (SEM), energy-dispersive X-ray (EDX) analyses, and subsequent antibacterial assays confirm that the coating is present.